

AN EXPERIMENTAL STUDY OF MIDDLE-EAR VIBRATIONS IN GERBILS

Department of Biomedical Engineering
McGill University
Montréal, Québec

August 2007

A thesis submitted to the Faculty of Graduate Studies and Research in partial
fulfilment of the requirements of the degree of

Master of Engineering

© Nicolas Ellaham, 2007

ABSTRACT / RÉSUMÉ

ABSTRACT

The Mongolian gerbil has become increasingly popular in middle-ear research, as it is low in cost and has easily approachable middle-ear structures. The goal of this thesis is to present vibration measurements on the gerbil eardrum. Displacement frequency responses are acquired in five gerbils at three or four points along the manubrium and at up to 8 points on the eardrum. We use a Polytec laser Doppler vibrometer to perform measurements with a sinusoidal-sweep stimulus. Displacements, normalized with respect to the sound pressure level measured near the eardrum, are presented over the frequency range from 0.15 to 10 kHz, and compared with measurements published in the literature. Spatial displacement patterns along the manubrium and on the tympanic membrane are presented. The variability and repeatability of the measurements are investigated with an emphasis on temporal effects due to the drying and rehydration of middle-ear structures.

RÉSUMÉ

Le gerbil mongolien est devenu de plus en plus populaire dans la recherche sur l'oreille moyenne, car il n'est pas trop coûteux, et les structures de l'oreille moyenne sont facilement accessibles. Le but de cette thèse est de présenter des mesures de vibration de tympan du gerbil. Des réponses fréquentielles des déplacements sont acquises dans cinq gerbils à trois ou quatre points le long du manubrium, et à autant que 8 points sur le tympan. Nous employons un vibromètre à laser Doppler de Polytec pour effectuer des mesures avec un stimulus à balayage sinusoïdal. Des déplacements, normalisés par le niveau de pression acoustique mesuré près du tympan, sont présentés sur la gamme de fréquence de 0.15 à 10 kilohertz, et comparés aux mesures publiées dans la littérature. Des motifs spatiaux de déplacement le long du manubrium et sur la membrane tympanique sont présentés. La variabilité et la répétabilité des mesures sont étudiées avec une emphase sur les effets temporels dus à la déshydratation et à la ré-humidification des structures de l'oreille moyenne.

ACKNOWLEDGEMENTS

First, I would like to thank my supervisor, Professor W. Robert J. Funnell for all his guidance as a research mentor throughout the years of my graduate education and his patience in reviewing the many drafts of this manuscript. His research ethics, professionalism, and tremendous passion for research are contagious skills which I have benefited from.

I would also like to thank my co-supervisor Dr. Sam J. Daniel, director of research for the division of Pediatric Otolaryngology at the Montréal Children's Hospital, for his support in the clinical aspects of this work and for access to the measurement equipment in his laboratory.

I would also like to thank Dr. Ross Wagner for his help with technical issues, especially in the machine shop while manufacturing the coupler used in the experiments.

I am forever grateful for the unwavering support of my loving parents Nasri and Agathe Laham, and my wonderful siblings Sami and Hiba to whom this work and all my love are dedicated. I am also thankful for all the friends and lab colleagues who have been a much needed support throughout the past years: Fadi, Nidal, Li, Shruti, Kosta, Nizar, and the many names I have no room to list here.

Above all, thanks are due to God, the creator of all wonders, and author of all knowledge. This work is the fruit of my humble efforts to make use of His many blessings.

This work was supported by the Canadian Institutes of Health Research, the Fonds de recherche en santé du Québec, the Natural Sciences and Engineering Research Council Canada, the Montréal Children's Hospital Research Institute and the McGill University Health Centre Research Institute.

TABLE OF CONTENTS

ABSTRACT / RÉSUMÉ.....	i
ACKNOWLEDGEMENTS.....	ii
TABLE OF CONTENTS.....	iii
LIST OF FIGURES.....	x
LIST OF TABLES.....	xi
CHAPTER 1: INTRODUCTION.....	1
1.1 Motivation.....	1
1.2 Thesis organization.....	2
CHAPTER 2: THE AUDITORY SYSTEM.....	3
2.1 Introduction.....	3
2.2 Overview of hearing.....	3
2.2.1 Sound generation and propagation.....	3
2.2.2 Sound perception: the auditory system.....	3
2.3 Human middle ear.....	5
2.3.1 Tympanic membrane.....	5
2.3.2 The ossicular chain.....	6
2.3.2.1 Malleus.....	6
2.3.2.2 Incus.....	7
2.3.2.3 Stapes.....	8
2.3.3 Other middle-ear structures.....	8
2.3.3.1 Middle-ear joints.....	8
2.3.3.2 Middle-ear ligaments.....	9
2.3.3.3 Middle-ear muscles.....	9
2.3.4 Middle-ear cavities.....	10
2.4 Gerbil middle ear.....	10

2.4.2 Middle-ear cavity.....	11
2.4.3 Middle-ear structures.....	11
2.5 Middle-ear mechanics.....	13
2.5.1 Axis of rotation.....	13
2.5.2 Impedance-matching mechanisms.....	14
2.5.2.1 Introduction.....	14
2.5.2.2 Surface-area ratio.....	14
2.5.2.3 Ossicular lever ratio.....	15
2.5.2.4 Tympanic-membrane curvature.....	15
CHAPTER 3: PREVIOUS STUDIES.....	16
3.1 Introduction.....	16
3.2 Non-gerbil studies.....	16
3.2.1 Introduction.....	16
3.2.2 Ossicular motion.....	17
3.2.3 Eardrum vibration patterns.....	18
3.2.4 Static eardrum deformations.....	19
3.3 Gerbil studies.....	20
3.3.1 Auditory Sensitivity.....	20
3.3.2 Static eardrum deformations.....	21
3.3.3 Vibration measurements.....	22
3.3.4 Finite-element models.....	26
3.4 Post mortem studies.....	28
3.4.1 Validity of post mortem research.....	28
3.4.2 Drying effects.....	31
3.5 Conclusion.....	33
CHAPTER 4: LASER DOPPLER VIBROMETRY.....	34
4.1 Introduction.....	34

4.2 Optical interferometry.....	34
4.2.1 Principle of operation.....	34
4.2.2 Light source.....	35
4.2.3 Laser basics.....	35
4.3 Laser Doppler vibrometry.....	36
4.3.1 The Doppler effect.....	36
4.3.2 Polytec laser Doppler vibrometers.....	37
4.3.2.1 Principle of operation.....	37
4.3.2.2 Velocity and displacement.....	38
4.3.2.3 Heterodyne interferometry.....	39
4.4 Conclusion.....	39
CHAPTER 5: MATERIALS AND METHODS.....	40
5.1 Introduction.....	40
5.2 Experimental setup.....	40
5.2.1 Specimen preparation.....	40
5.2.2 Measurement system.....	41
5.2.2.1 Acoustical system.....	43
5.2.2.2 Optical system.....	44
5.2.3 Data acquisition and analysis system.....	45
5.3 Experimental considerations.....	45
5.3.1 Electro-acoustical considerations.....	46
5.3.1.1 Noise considerations.....	46
5.3.1.2 Excitation signal.....	47
5.3.1.3 Ventilation.....	49
5.3.1.4 Coupler design.....	50
5.3.2 Optical considerations.....	52
5.4 Overview of measurements.....	54
5.4.1 Specimens studied.....	54

5.4.2 Location of measurements.....	55
5.4.3 Cosine correction factor.....	57
5.4.4 Measurement sequence.....	58
5.4.4.1 Timing of measurements.....	58
5.4.4.2 Closed-bulla experiment.....	59
5.4.5 Sound pressure level.....	60
5.5 Conclusion.....	61
CHAPTER 6: RESULTS.....	62
6.1 Introduction.....	62
6.2 Vibrations at the umbo.....	62
6.2.1 Displacement frequency response.....	62
6.2.2 Inter-specimen variability.....	64
6.2.3 Comparison with previous studies.....	65
6.3 Measurement repeatability.....	68
6.3.1 Introduction.....	68
6.3.2 Repeatability at the umbo.....	69
6.3.2.1 Low-frequency magnitude changes.....	69
6.3.2.2 High-frequency shifts.....	75
6.3.3 Open/closed bulla configurations.....	75
6.3.4 Drying and rehydration experiments.....	78
6.3.4.1 Tracking of magnitude changes at low frequencies.....	78
6.3.4.2 Tracking of frequency shifts at high frequencies.....	82
6.4 Manubrial vibrations.....	86
6.5 Tympanic-membrane vibrations.....	93
CHAPTER 7: CONCLUSION.....	98
7.1 Summary.....	98
7.1.1 Middle-ear mechanics.....	98

7.1.2 Drying and rehydration effects.....	99
7.2 Discussion.....	99
7.2.1 Comparison with previous measurements.....	99
7.2.2 Spatial vibration patterns.....	101
7.2.3 Drying and rehydration effects.....	102
7.3 Future Work.....	102

LIST OF FIGURES

Figure 2.1: Anatomy of the human ear.....	4
Figure 2.2: Human tympanic membrane.....	5
Figure 2.3: Layers of the tympanic membrane.....	6
Figure 2.4: Anatomy of the malleus.....	7
Figure 2.5: Anatomy of the incus.	7
Figure 2.6: Anatomy of the stapes.	8
Figure 2.7: Middle-ear cavities.....	10
Figure 2.8: Posterior incudal ligament connecting the incus to the middle-ear cavity wall.....	12
Figure 2.9: Four consecutive histological slices of the gerbil posterior incudal ligament.....	13
Figure 3.1: Displacements along the manubrium measured by Decraemer et al. (1991).....	18
Figure 3.2: Time-averaged holograms for six frequencies between 500 and 5000 Hz.....	19
Figure 3.3: Schematic presentation of areas of maximal displacement.....	21
Figure 3.4: Averaged peak-to-peak umbo amplitude from adult and 42-day-old gerbils.....	24
Figure 3.5: Normalized umbo responses.....	25
Figure 3.6: Simulated low-frequency vibration patterns.....	26
Figure 3.7: Simulated low-frequency vibration patterns.....	27
Figure 3.8: Umbo frequency responses from 4 post mortem and 3 in vivo studies.....	29
Figure 3.9: Post mortem and in vivo measurements of umbo velocities.....	30
Figure 3.10: Measurement stability and moistening of temporal bone preparation.....	32
Figure 4.1: Schematic diagram of the principle of operation of a laser device.....	36
Figure 4.2: Schematic diagram of the laser Doppler vibrometer.....	37
Figure 5.1: Schematic illustrations of gerbil middle ear and experimental preparation.....	40
Figure 5.2: Photographs of the experimental setup.....	42
Figure 5.3: ER-2 Tubephone, and its frequency response.....	43
Figure 5.4: ER-7C probe microphone and its frequency response curve.....	44
Figure 5.5: Polytec compact laser vibrometer (CLV) and HLV.....	45
Figure 5.6: C-24 audiometric examination room.....	46
Figure 5.7: Acoustic performance attenuation graph of Génie Audio’s sound-proof rooms.....	47

Figure 5.8:	Amplitude frequency response of the 4th order Butterworth high pass filter.....	48
Figure 5.9:	Coupler dimensions.....	50
Figure 5.10:	Experiment to determine appropriate cavity length.....	51
Figure 5.11:	Eardrum and bead placement	52
Figure 5.12:	Normalized displacements on a bead at the umbo and at an adjacent point.....	53
Figure 5.13:	Arrangement of beads in all five gerbils studied.....	56
Figure 5.14:	Estimation of the cosine correction factor.....	57
Figure 5.15:	Sound pressure level measured near the eardrum.....	61
Figure 6.1:	Normalized displacement measurements at the umbo in all five gerbils.....	63
Figure 6.2:	Normalized displacement measurements at the umbo expressed in dB.....	64
Figure 6.3:	Comparison of umbo velocities with measurements from other groups.....	66
Figure 6.4:	Assessing measurement repeatability at the umbo in Gerbil 1.....	70
Figure 6.5:	Assessing measurement repeatability at the umbo in Gerbil 2.....	71
Figure 6.6:	Assessing measurement repeatability at the umbo in Gerbil 3.....	72
Figure 6.7:	Assessing measurement repeatability at the umbo in Gerbil 4.....	73
Figure 6.8:	Assessing measurement repeatability at the umbo in Gerbil 5.....	74
Figure 6.9:	Validating the use of the ventilation tube in closed-bulla measurements.....	76
Figure 6.10:	Comparing open and closed bulla configurations.....	77
Figure 6.11:	Tracking magnitude changes over time in gerbil 2.....	80
Figure 6.12:	Tracking magnitude changes over time in gerbil 3.....	80
Figure 6.13:	Tracking magnitude changes over time in gerbil 4.....	81
Figure 6.14:	Tracking magnitude changes over time in gerbil 5.....	81
Figure 6.15:	Tracking frequency shifts over time in gerbil 2.....	84
Figure 6.16:	Tracking frequency shifts over time in gerbil 3.....	84
Figure 6.17:	Tracking frequency shifts over time in gerbil 4.....	85
Figure 6.18:	Tracking frequency shifts over time in gerbil 5.....	85
Figure 6.19:	Manubrial displacements for Gerbil 1.....	88
Figure 6.20:	Manubrial displacements for Gerbil 2.....	89
Figure 6.21:	Manubrial displacements for Gerbil 3.....	90

Figure 6.22: Manubrial displacements for Gerbil 4.....	91
Figure 6.23: Manubrial displacements for Gerbil 5.....	92
Figure 6.24: TM displacements for gerbil 1.....	94
Figure 6.25: TM displacements for gerbil 2.....	95
Figure 6.26: TM displacements for gerbil 3.....	95
Figure 6.27: TM displacements for gerbil 4.....	96
Figure 6.28: TM displacements for gerbil 5.....	97

LIST OF TABLES

Table 3.1: Strategies used by other groups to keep the middle-ear structures moist.....	31
Table 5.1: Details of specimens used in the experiments.....	55
Table 5.2: Special notes for specimens under study.....	56
Table 5.3: Timing of experimental steps.....	59
Table 6.1: Selection of measurements displayed in Figure 6.1.....	63
Table 6.2: Comparison of low-frequency umbo displacements with previous studies.....	67
Table 6.3: Summary of amplitude ratios measured at low frequencies.....	69
Table 6.4: Summary of amplitude ratios at all points along the manubrium.....	86

CHAPTER 1

INTRODUCTION

1.1 Motivation

Hearing impairment is defined as full or partial loss of the ability to detect sounds and can lead to problems with speech and language development in humans (oafccd.com). According to The Hearing Foundation of Canada, hearing impairment is the fastest growing and third leading chronic disability in Canada after arthritis and hypertension, affecting more than three million Canadians. Hearing loss is also the most common birth defect, affecting about six in every thousand newborn Canadian babies. The average age of detection of hearing loss in newborns is 2.5 to 3 years of age, well past the critical time when children are rapidly developing language, speech and social skills (thfc.ca).

The middle ear plays a major role in hearing and is the site of many infections, congenital anomalies, injuries and other diseases, such as cholesteatoma, that contribute to hearing loss. Located between the external ear and the inner ear, the middle ear consists of an air-filled space housed within the temporal bone which includes a chain of three small bones, or ossicles, connecting the eardrum to the oval window. To date, non-invasive diagnostic tools and the quality of middle-ear prostheses are often inadequate. A better understanding of middle-ear mechanics will contribute to advancements in diagnosis and treatment of hearing loss. To this end, many groups have conducted research on mammalian middle ears. In particular, gerbils have gained great popularity over the past two decades as they are low in cost and have easily approachable middle-ear structures.

The use of proven engineering methods is very helpful in studying middle-ear mechanics and diagnosing potential middle-ear problems where standard audiological tests fail, by addressing clinical issues related to conductive hearing loss. Experimental measurements and mathematical modelling complement one another when developing a quantitative understanding of middle-ear mechanics. Among many methods used for collecting experimental measurements, laser Doppler vibrometry (LDV) is a very popular tool that permits real-time velocity and displacement

measurements of the eardrum and ossicles. LDV has been used in several animal, human-temporal-bone and live-human studies. Studies by Huber et al. (2001) and Rosowski et al. (2003b) have shown possible diagnostic uses for this technology. LDV measurements also find important use in validating model simulations obtained using the finite element method.

The original intent of this research work was to characterize the mechanics of the gerbil middle ear by acquiring LDV measurements at multiple points on the eardrum with high frequency resolution. The work was later extended to include a study of the *post mortem* effects of drying and rehydration imposed by our experimental protocol. Performing measurements at multiple points on the eardrum reveals spatial details characterizing the motion of the eardrum, which are not addressed by the measurements at a single location commonly performed by other groups. The rationale for studying the effects of drying and rehydration is to track the temporal changes affecting the observed spatial patterns.

1.2 Thesis organization

This thesis begins with a general overview of the auditory system and middle-ear mechanics in Chapter 2. An extensive review of previous experimental studies relevant to this work is presented in Chapter 3, followed by a theoretical overview of laser Doppler vibrometry in Chapter 4. The methodology we used is detailed in Chapter 5. Experimental results of the study of *post mortem* effects and spatial vibration patterns on the gerbil eardrum are discussed in Chapter 6. Finally, conclusions and suggestions for future work are presented in Chapter 7.

CHAPTER 2

THE AUDITORY SYSTEM

2.1 Introduction

In this chapter we discuss the organ responsible of the faculty of hearing: the ear. We begin in section 2.2 with a discussion of the fundamentals of hearing physiology. Then, we briefly present in section 2.3 the anatomy of the human middle ear, followed by a discussion of the specifics of the gerbil middle ear in Section 2.4. Finally, middle-ear mechanics are discussed in Section 2.5.

2.2 Overview of hearing

2.2.1 Sound generation and propagation

A good understanding of hearing begins with an explanation of the physics of sound. Sound can be thought of as mechanical vibrations travelling in a material medium, most commonly air. Sound is typically generated by a vibrating object, such as the human vocal chords or the membrane of an audio speaker. As the sound source vibrates it causes a displacement of the particles of the surrounding medium, which is the basis of sound propagation. In air, for example, it is the movement of air molecules that forms waves of alternating pressure, causing local regions of compression and rarefaction. As a particle is displaced from its equilibrium position, adjacent particles are also displaced, causing these local regions (and hence the sound wave) to travel through the medium.

2.2.2 Sound perception: the auditory system

Figure 2.1 shows the general anatomy of the human ear, revealing three components:

- The **outer ear** consists of the externally visible part (auricle or pinna) and the auditory canal.
- The **middle ear** is an air-filled cavity containing the eardrum (or tympanic membrane) and a chain of three ossicles (malleus, incus and stapes) which conducts sound to the oval window, the boundary with the inner ear.
- **The inner ear** consists of the liquid-filled cochlea and the vestibular apparatus (semicircular canals and vestibule).

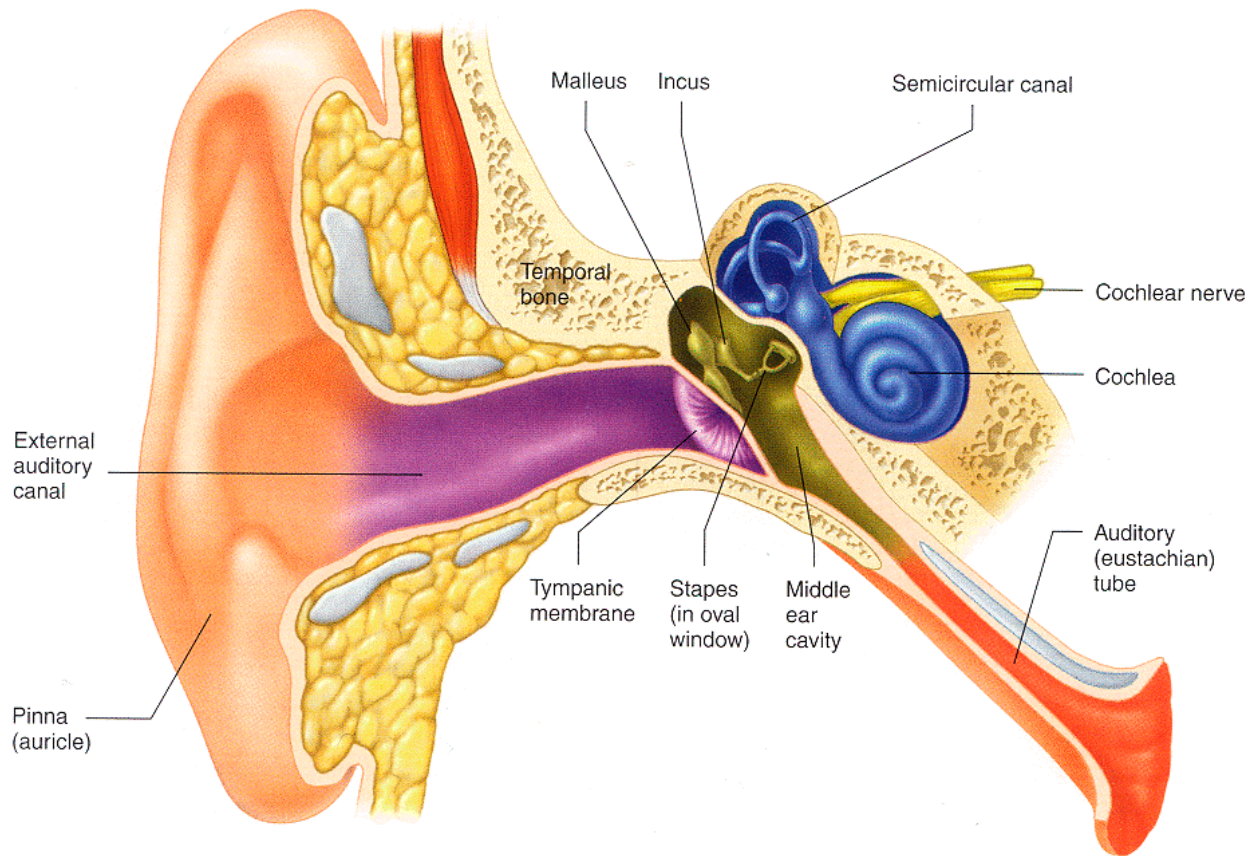


Figure 2.1: Anatomy of the human ear.
 (Source: Vander et al., 2004)

Sound perception in the ear occurs as follows: Sound waves propagating in the air reach the outer ear and are funnelled through the external auditory canal to reach the eardrum, which vibrates in response to air molecules pushing against it. The vibrations of the eardrum are mechanically transferred across the middle ear by the ossicles to reach the interface with the inner ear. The mechanics of sound transmission across the middle ear will be discussed in Section 2.5. The footplate of the stapes, the last of the chain of three ossicles, is attached to the oval window and sealed by the annular ligament. The oval window is the opening through which sound energy is transferred to the liquid contained within the cochlea. The fluid motion induces a movement of hair cells inside the cochlea. These hair cells are mechanoreceptors whose movement is accompanied by complex processes causing the generation of electrical signals in the neurons forming the cochlear nerve. These signals, also called action potentials, travel along the cochlear nerve (a component of cranial nerve VIII) to reach the brain.

2.3 Human middle ear

2.3.1 Tympanic membrane

The tympanic membrane (TM) extends across the medial end of the external auditory canal, separating it from the middle-ear cavity. As shown in Figure 2.2, the TM consists of the pars tensa and the pars flaccida. The pars tensa is the main portion of the TM; it has a generally conical shape pointing in the medial direction. The manubrium of the malleus is attached to the medial side of the TM, extending down to the umbo located at the apex of the cone. Towards its periphery the pars tensa thickens, forming a fibrocartilaginous ring known as the annulus, which anchors the TM onto the temporal bone. The pars flaccida is the smaller portion of the eardrum, located superior to the pars tensa, above the malleolar folds.

The pars tensa is a multi-layer structure with the organization shown in Figure 2.3. Three layers can be differentiated: the epidermal layer on the lateral side; the mucosal layer on the medial side; and the intermediate layer called the lamina propria (Lim 1968 & 1970). The epidermal layer is continuous with the lining of the external ear canal and the mucosal layer is continuous with the lining of the middle-ear cavity. The fibrous lamina propria consists of four layers: a layer of radial fibres which diverge away from the manubrium of the malleus; a layer of circular fibres more or less concentric around the umbo; and two layers of loose connective tissue. The pars flaccida is usually thicker than the pars tensa and does not have such an organization: fewer collagen fibrils can be observed and they have a rather irregular arrangement.

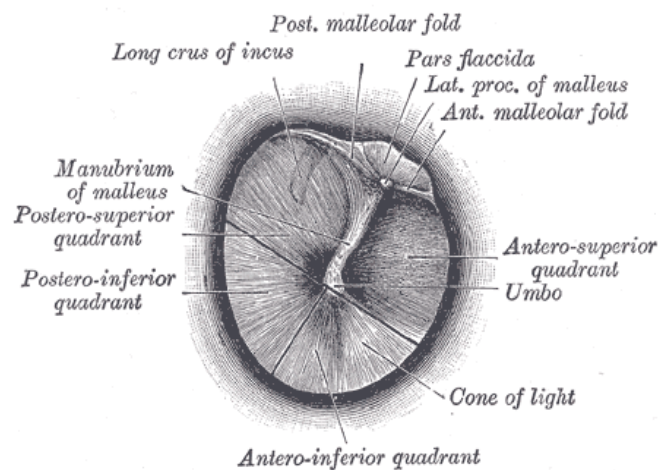


Figure 2.2: Human tympanic membrane.
(Source: Gray, 2000)

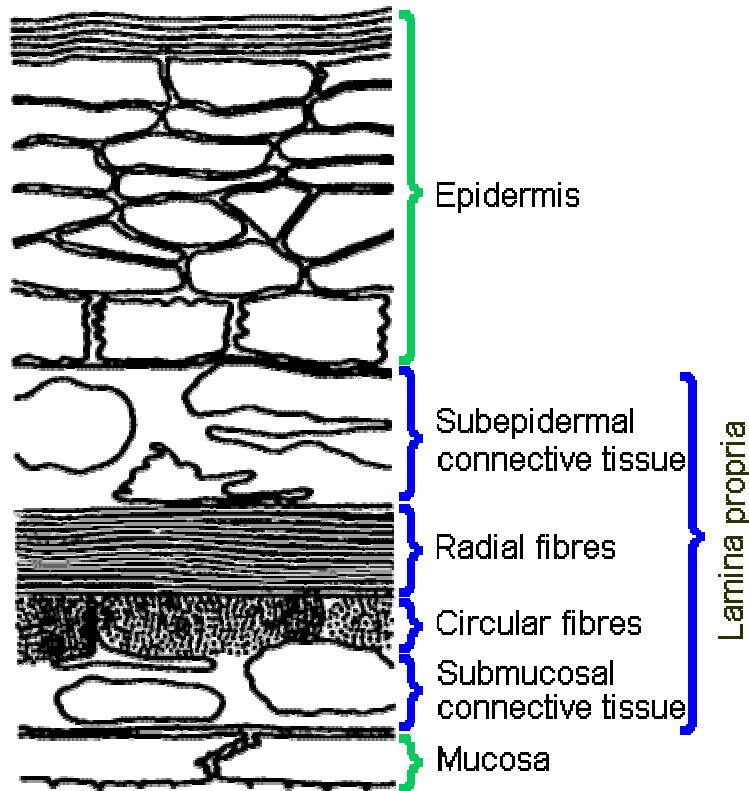


Figure 2.3: Layers of the tympanic membrane
 (Source: http://audilab.bmed.mcgill.ca/~funnell/audiLab/teach/me_saf/me_saf.html)

2.3.2 The ossicular chain

2.3.2.1 Malleus

The malleus, so named for its resemblance to a hammer, consists of a head, a neck and three processes (or crura): the manubrium, the anterior process and the lateral process (Figure 2.4). The head is roughly oval in shape and constitutes the large upper part of the bone. On its posterior surface it provides the articulation with the body of the incus. The neck is the narrow part of the bone to which the various processes attach. The manubrium is directed inferiorly, medially and posteriorly and is coupled on its lateral side to the TM. It decreases in size towards its inferior end, which is flattened transversely and slightly curved anteriorly (at the region corresponding to the umbo). The anterior process springs anteriorly from below the neck and is connected to the wall of the middle-ear cavity by the anterior malleolar ligament. The lateral process is the upper end of the manubrium.

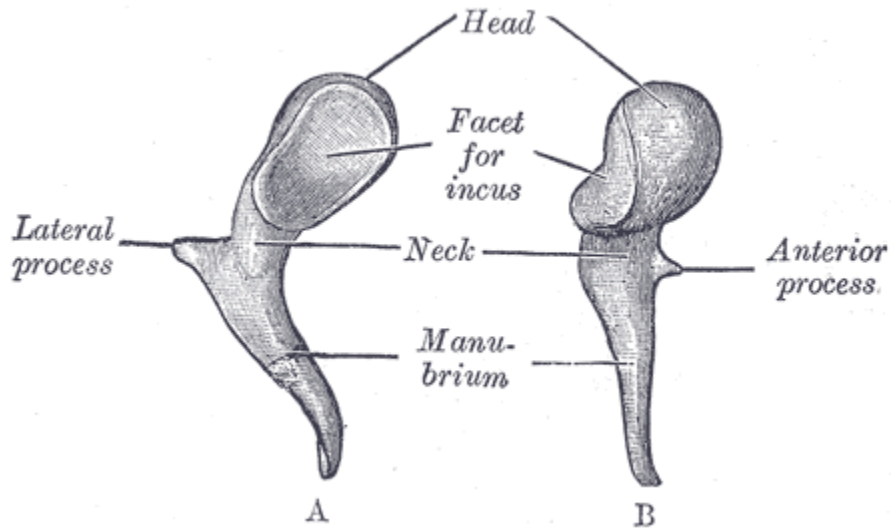


Figure 2.4: Anatomy of the malleus.
(Source: Gray, 2000)

2.3.2.2 Incus

The incus, or anvil, so called because it is acted on by the hammer, consists of a body and two processes which diverge nearly at right angles: the long process and the short process (Figure 2.5). The body of the incus has a saddle-shaped facet on its anterior surface that connects to the head of the malleus. The short process is roughly conical in shape, extends in the posterior direction and is attached to the cavity wall by the posterior incudal ligament. The long process extends inferiorly nearly parallel to the manubrium of the malleus. At its inferior end it bends medially forming a rounded projection, the lenticular process, which articulates with the head of

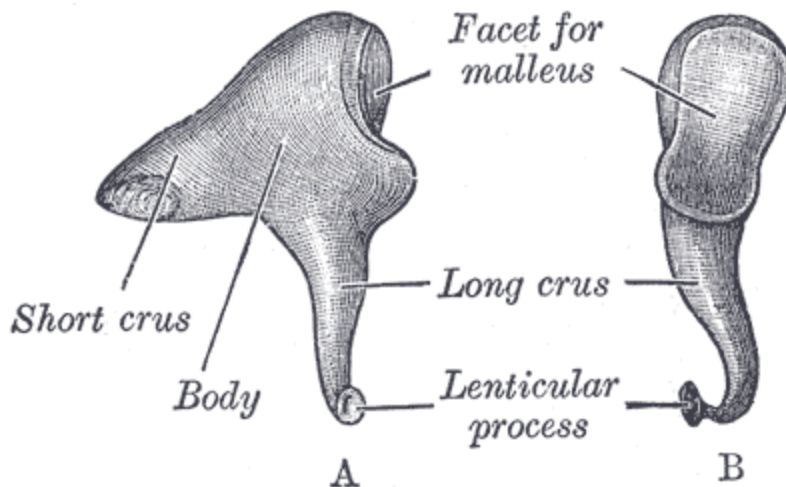


Figure 2.5: Anatomy of the incus.
(Source: Gray, 2000)

the stapes. A very thin bony connection exists between the long process and the lenticular process of the incus: the pedicle. The function of this structure has only recently been studied (Siah, 2002; Funnell et al., 2005; Elkhouri et al., 2006) and it is believed to be prone to bending.

2.3.2.3 Stapes

The stapes, so called for its resemblance to a stirrup, is the smallest bone in the human body. It consists of a head, a neck, two crura and a base (Figure 2.6). The head articulates with the lenticular process of the incus at its lateral surface, which presents a slight depression. From the neck, the part of the bone succeeding the head, diverge the anterior and posterior crura, which form a stapedia arch connected at its ends to the stapes base (or footplate). The footplate is attached within the oval window of the inner ear by a ring of fibres (the stapedia annular ligament). The shape of the footplate is generally thought of as oval, although it often has a highly asymmetrical shape (e.g., Hagr et al., 2004). The annular ligament around the footplate is also not uniform but appears to be wider and thicker on the anterior edge. These asymmetries are presumably important in determining stapes motion, which still remains controversial.

2.3.3 Other middle-ear structures

2.3.3.1 Middle-ear joints

The middle-ear ossicles are connected by two synovial joints: the saddle-shaped incudomalleolar joint connects the head of the malleus to the body of the incus; the incudostapedial joint connects the convex surface of the lenticular process and the concave surface of the head of the stapes.

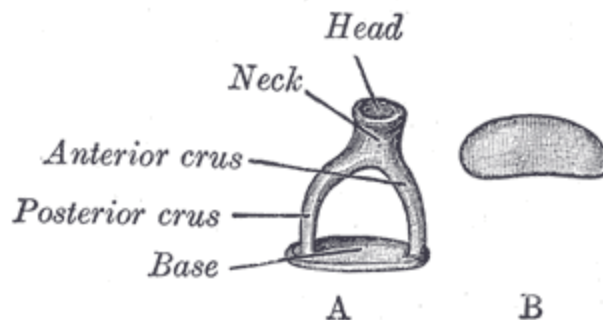


Figure 2.6: Anatomy of the stapes.
(Source: Gray, 2000)

2.3.3.2 Middle-ear ligaments

The number of ligaments in the middle ear has been disputed. Mikhael (2005) compiled a detailed review of those ligaments. In this section, we briefly summarize. One ligament extends along the entire length of the manubrium, attaching the malleus to the TM. Several malleolar ligaments have been observed, including the anterior malleolar ligament (AML) and the lateral malleolar ligament. The existence of a superior malleolar ligament is subject to disagreement (Mikhael, 2005). A number of other malleolar ligaments, controversially referred to as ‘suspensory’ ligaments, have also been described. The posterior incudal ligament (PIL) consists of two bundles of ligament connecting the short process of the incus to the posterior incudal recess in the cavity wall. Finally, the stapedial annular ligament consists of radially oriented elastin fibres and, as mentioned earlier, serves to attach the stapes footplate to the oval window.

2.3.3.3 Middle-ear muscles

Two muscles, the tensor tympani and the stapedius, anchor the ossicles to the cavity walls. The tensor tympani lies in a bony sheath in the temporal bone and emerges from the anterior wall into the middle-ear cavity. Its tendon attaches to the medial and anterior surfaces of the malleus neck and manubrium. The stapedius muscle is the smallest skeletal muscle in the human body. It emerges from the pyramidal eminence of the posterior wall of the tympanic cavity. Its tendon attaches to the neck of the stapes. These muscles contract simultaneously in response to certain stimuli, such as chewing or high-intensity sounds, thus inhibiting the movement of the ossicles: the tensor tympani muscle pulls the manubrium medially, increasing the tension on the TM and decreasing the magnitude of its vibrations, while the stapedius muscle pulls the head of the stapes backwards, inhibiting the vibrations of the footplate. The combined action of these muscles has the effect of reducing the response of the middle ear (Gulya & Schuknecht, 1995).

Smooth-muscle fibres have recently been observed in the fibrocartilaginous ring attaching the pars tensa to the annulus (Kuijpers et al., 1999; Henson & Henson, 2000; Henson et al., 2001ab; Yang & Henson, 2002). It is suggested that they play a role in regulating the tension of the eardrum.

2.3.4 Middle-ear cavities

The middle-ear structures described above are housed within the air-filled middle-ear space which resides in the petrous portion of the temporal bone. The middle-ear space can be subdivided into three openly connected compartments known as the *epitympanum*, the *mesotympanum*, and the *hypotympanum* (Figure 2.7). The epitympanum is the upper portion of the tympanic cavity and houses the head of the malleus and the body of the incus. The mesotympanum is the portion of the middle-ear space located medial to the TM, housing part of the malleus and incus, the stapes and the middle-ear muscles. The hypotympanum is the area inferior to the TM. The opening to the Eustachian tube, which opens into the nasal part of the pharynx, is located in the antero-inferior portion of the hypotympanum.

2.4 Gerbil middle ear

Mongolian gerbils (*Meriones unguiculatus*) have become increasingly popular in middle-ear research over the past decade (e.g., Olson, 1998; Rosowski et al., 1999; von Unge et al., 1999; Funnell et al., 1999 & 2000; Dirckx & Decraemer, 2001; Overstreet et al., 2003; Ravicz & Rosowski, 2004; Elkhouri et al., 2006). They belong to the Gerbillinae subfamily of the Muridae family of rodents, and live in the Asian and North African deserts (Legoux & Wisner, 1955; Lay, 1972). The middle ear is generally similar in gerbils and humans. In this section, similarities, differences and some particular characteristics will be highlighted.

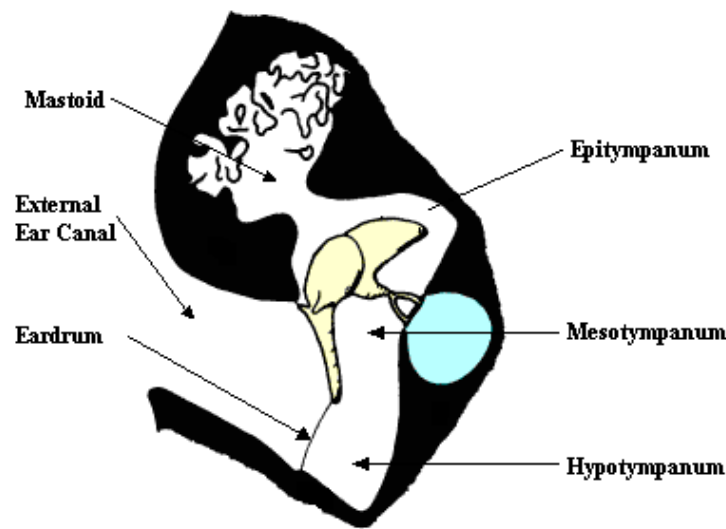


Figure 2.7: Middle-ear cavities
(After http://audilab.bmed.mcgill.ca/~funnell/AudiLab/teach/me_saf/me_saf.htm)

2.4.1 Middle-ear cavity

The gerbil middle ear has an enlarged inferior air space bounded by a bony shell known as the bulla. The human middle-ear space has a volume of approximately 2 cm^3 (Békésy, 1949). The gerbil middle-ear cavity volume is about 0.2 cm^3 , which is much smaller than the volume in humans but still quite large compared with rats and other rodents of similar size (Oaks, 1967). It has been established that the enlarged middle-ear cavity is the reason why the gerbil ear is highly sensitive to frequencies below 3000 Hz (Rosowski et al., 1999). In fact, when it comes to desert mammals, it is common to find such a small-size animal with a medium-size ear (Weber, 1927). Fleischer (1978) notes that deserts are areas with low background noise and are characterized by open space, where obstacles to locomotion are rare, thus increasing the “*biological distance*” for desert animals. The biological distance is the portion of the environment which is of interest to the animal under normal conditions. The enlarged size of the middle-ear space helps specialize the gerbil ear to perceive those frequencies produced by approaching predators (below 3 kHz), at least within its biological distance.

2.4.2 Middle-ear structures

One would of course expect the dimensions of the middle-ear structures to be smaller in gerbils than they are in humans. The human TM has a surface area of approximately 69 mm^2 (Wever & Lawrence, 1954). Lay (1972) calculated the surface of the TM to be on average 26 mm^2 in *Meriones unguiculatus* (he actually reported an “effective area” of 17 mm^2 , calculated as two thirds of the total surface area). This is a relatively large surface when compared, for example, with the rat TM (11 mm^2 according to Zimmer et al., 1994).

The ratio of the surface area of the pars flaccida to that of the pars tensa (PF/PT) is very small in humans (0.027) but quite large in gerbils (0.11) and other rodents (Kohllöffel, 1984). The pars flaccida is commonly involved in important pathologies of the middle ear, yet its actual function still remains unclear (Dirckx et al., 1998).

Both human and gerbil ears belong to what Fleischer (1978) classified as the “freely mobile

type”, where the anterior process of the malleus is fixed by means of the anterior malleolar ligament and the short process of the incus is fixed by means of the posterior incudal ligament. The malleus-incus complex is not firmly anchored in the temporal bone, hence the name “freely mobile”. The malleus and incus are not fused together in the gerbil, the articulation between the two bones being rather well developed. While the cross-section of the manubrium of the malleus is flat in humans, it is T-shaped in gerbils (Oaks, 1967).

There are fewer attachments between the ossicles and the middle-ear cavity walls in the gerbil than was described in Section 2.3.3.2 for humans. The attachments include the 2 muscles, the manubrial attachment to the TM, and only three ligaments (Oaks, 1967): the annular ligament surrounding the stapes footplate, the AML and the PIL. The superior malleolar ligament and the suspensory ligaments mentioned earlier have not been observed in the gerbil middle ear.

Finally, the PIL deserves some additional attention. The human PIL consists of two bundles connecting the short process of the incus to the posterior incudal recess laterally and medially, as illustrated in Figure 2.8A. In many rodents, including gerbils, the PIL forms one continuous ligament as shown in Figure 2.8B. To illustrate this point, we show in Figure 2.9 a set of consecutive histological slices, obtained from M. von Unge, Karolinska Hospital, Stockholm. These slices reveal the PIL as a horseshoe-shaped ligament connecting the short process of the incus, along its entire posterior extremity, to the incudal recess.

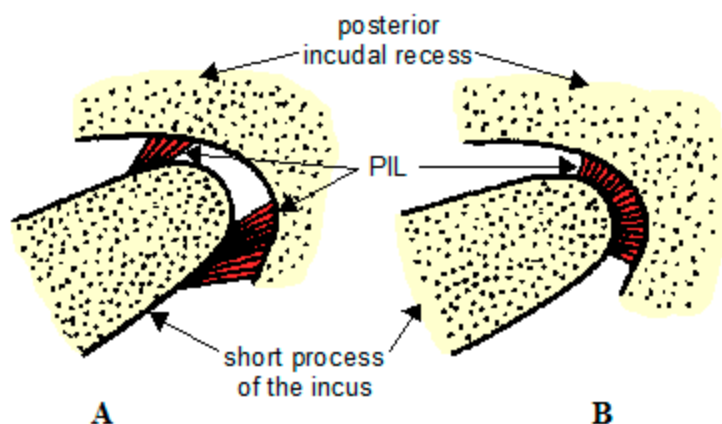


Figure 2.8: The posterior incudal ligament connecting the incus to the middle-ear cavity wall. (A) Two bundles of ligaments in humans (B) A single ligament in gerbils and other rodents. (After http://audilab.bmed.mcgill.ca/~funnell/AudiLab/teach/me_saf/me_saf.html)

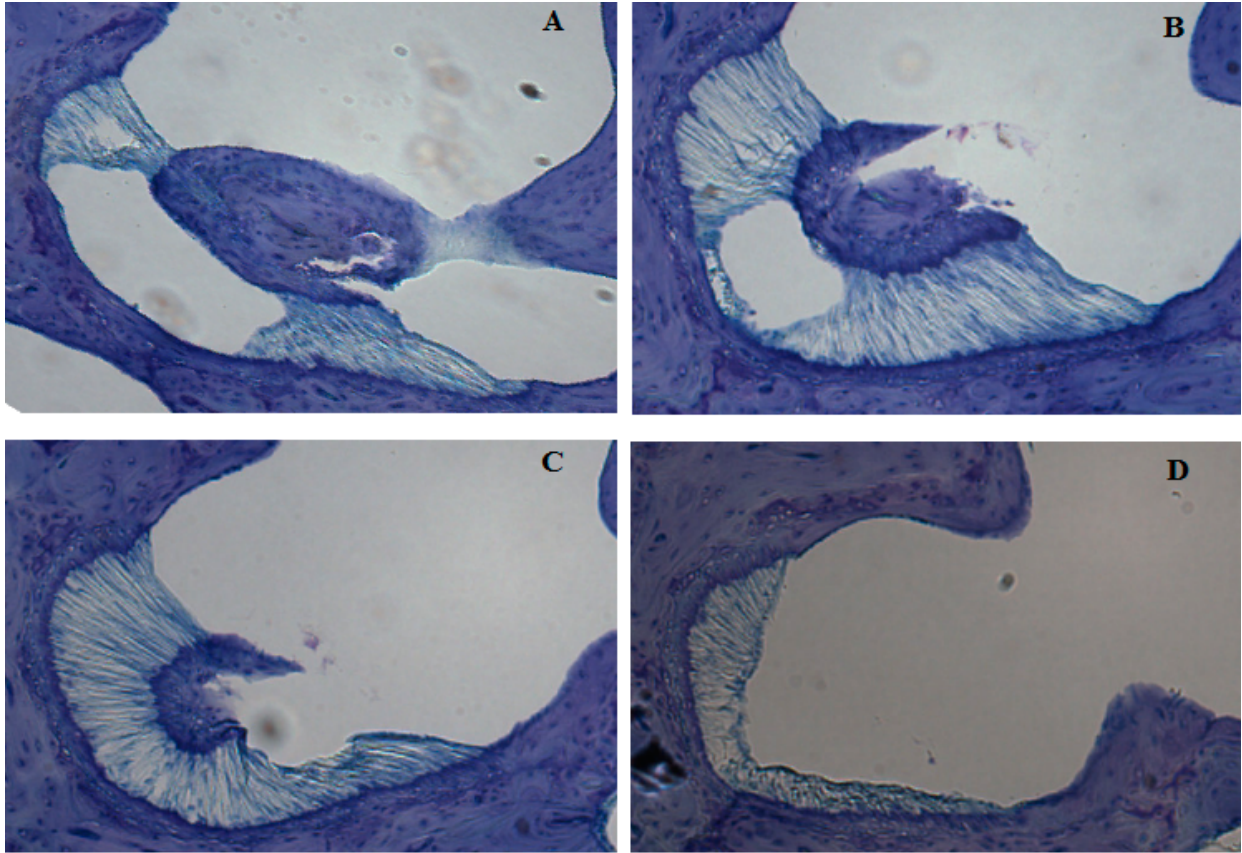


Figure 2.9: Four consecutive histological slices of the gerbil posterior incudal ligament. The short process of the incus is visible in slices A, B, and C. In slice A, there seems to be 2 bundles of ligaments but they clearly join in the following slices forming one ligament.

2.5 Middle-ear mechanics

2.5.1 Axis of rotation

Helmholtz (1869) suggested that the malleus-incus complex of the middle ear rotates around an axis defined by the AML and PIL. However, this model with a single axis of rotation is valid only for low frequencies. Studies have shown that the motion of the ossicles becomes more complicated at high frequencies (Gyo et al., 1987; Decraemer et al, 1991; Decraemer et al, 1994ab). Possible complications include shifting of the axis of rotation, bending of the manubrium, and relative motion between the malleus and incus. Ossicular motion has, therefore, been described according to frequency-dependent modes of vibrations. Research findings from several groups in this area will be presented in detail in Section 3.2.2.

2.5.2 Impedance-matching mechanisms

2.5.2.1 Introduction

The most important function of the middle ear is as an acoustical impedance-matching system. Acoustical impedance is defined as the resistance of a medium to the flow of acoustic energy. Mathematically, the acoustical impedance Z of a medium is defined as the ratio of the sound pressure P to the volume velocity U (calculated as the surface area times particle velocity):

$$Z = \frac{P}{U}$$

Sound waves travelling from one medium to another of different acoustical impedance are partially reflected. The amount of reflection depends on the ratio of the impedances of the two media. The medium of the outer and middle ear is air, while the inner ear is filled with liquid, acoustically similar to water. At an air-water interface, 99.9% of the sound energy from waves in air are reflected (Feldman & Wilber, 1976). The middle-ear is designed as a transformer mechanism to overcome part of this impedance mismatch at the air-liquid interface.

Three factors are often described as contributing to this transformer mechanism: the eardrum-to-footplate surface-area ratio, the ossicular-lever ratio, and the TM curvature. These are presented individually here, but in fact it is difficult to separate the force-transformation behaviour into these distinct factors (Funnell, 1996). As is common in the literature, the discussion of these factors is restricted here to low frequencies (below a few hundred Hz), in which range inertial and damping effects are negligible.

2.5.2.2 Surface-area ratio

This is the primary factor responsible for the middle-ear transformer mechanism. The pressure P exerted by a force F on a surface of area A is defined by the ratio:

$$P = \frac{F}{A}$$

When the same force acts on two surfaces, one larger than the other, the pressure is multiplied by the ratio of these surface areas. Due to the surface area difference of the TM relative to the small stapes footplate (or equivalently the oval window), the pressure at the footplate must be greater than at the eardrum. It is often considered that about two thirds of the area of the eardrum effectively vibrates in the transmission of sound to the inner ear, thus constituting the “effective surface area”. In humans, the ratio of the effective surface area of the eardrum to the area of the stapedial footplate is 17.2 (Wever & Lawrence, 1954). In gerbils, Lay (1972) calculated this ratio to be 27.6.

2.5.2.3 Ossicular lever ratio

At low frequencies, the malleus and incus are assumed to function as a mechanical lever system rotating around a fixed axis of rotation as described earlier. The ossicular lever ratio is obtained as the ratio of the orthogonal distance from the axis of rotation to the umbo and the orthogonal distance from the same axis to the incudo-stapedial joint. In humans this ratio is 1.31 (Wever & Lawrence, 1954). In gerbils, Lay (1972) calculated this ratio to be 3.32. This ratio adds to the effectiveness of the transformer mechanism.

2.5.2.4 Tympanic-membrane curvature

The third factor affecting the transformer mechanism is the existence of a relationship between the curvature of the eardrum and sound-pressure amplification, originally proposed by Helmholtz (1869 and 1877). Studies by Khanna & Tonndorf (1972) supported Helmholtz’ claim that such a relationship exists based on the TM radial and circular fibre organization. Using a finite-element model of the cat middle ear, Funnell (1996) found that certain regions on the TM are more effective in driving the manubrium, attributing this effectiveness to the curvature of the eardrum and not to the organization of the fibres. The contribution of the eardrum curvature to the transformer ratio is, however, less important than the other factors described.

CHAPTER 3

PREVIOUS STUDIES

3.1 Introduction

Various experimental measurement and modelling techniques are used in the study of middle-ear mechanics in live and *post mortem* ears. In this chapter we present a review of previous studies relevant to our research. In Section 3.2, we start with a review of human and non-gerbil animal studies investigating ossicular motion and eardrum vibrations. Section 3.3 presents experimental and modelling research conducted on the Mongolian gerbil. Finally, Section 3.4 presents studies that address the validity of using *post mortem* ears to study the function of live ones.

3.2 Non-gerbil studies

3.2.1 Introduction

Several groups have used laser Doppler vibrometry (LDV) to study middle-ear vibrations in various mammalian species. LDV, which will be explained in detail in Chapter 4, is an optical interferometric technique which permits dynamic vibration measurements over a wide range of audio frequencies. LDV studies have generally focused on ossicular motion, with measurements commonly performed at the umbo because it is an easily accessible and identifiable location. Such studies have been conducted on temporal bones from human cadavers (Vlaming & Feenstra, 1986; Huber et al., 1997; Nishihara & Goode, 1997; Nakajima et al., 2005), cats (Buunen & Vlaming, 1981) and rats (Doan et al., 1996; Bigelow et al., 1996 & 1998). Studies have also been conducted on live human ears, showing that LDV can be used as a clinical tool to potentially diagnose middle-ear pathologies (Goode et al., 1996; Huber et al., 2001; Rosowski et al., 2003b).

However common, measurements at the umbo alone do not completely characterize the mechanics of the middle ear. Many groups have used LDV and other techniques to more fully study ossicular motion and eardrum vibration patterns. These studies will be reviewed in the following two sections.

3.2.2 Ossicular motion

As mentioned in Section 2.5.1, the motion of the malleus-incus complex, traditionally described as a simple rigid rotation around a fixed axis (Békésy, 1960), becomes complex beyond the low frequencies. Using time-averaged holography, Gundersen and Hogmoen (1976) noted that the malleus and incus moved like a lever around a somewhat frequency-dependent axis of rotation. Using a video measuring system, Gyo et al. (1987) observed an increase in the measured lever ratio with frequency, which they attributed to a shifting of the rotational axis. Hüttenbrink (1992) suggested a gliding of the incudo-malleolar and incudo-stapedial joints resulting in a characteristic change of the ossicular movement, the imaginary axis of rotation being shifted past the ossicles. According to Hüttenbrink, "the malleus rotates around its axial ligaments, ... [the incus has a] predominant up- and downward movement, and the stapes (and the inner ear) are decoupled".

Decraemer et al. (1991) used heterodyne laser interferometry to investigate the motion of the malleus in anaesthetized cats. They measured displacements at four points along the manubrium, using glass micro beads to get good reflectivity, and reported the amplitude and phase frequency responses shown in Figure 3.1. They showed that the manubrium does not vibrate as a rigid body rotating about a fixed axis and suggested possible bending at higher frequencies. They claimed that the motion of the malleus is rotational at some frequencies, translational at others, and mixed at most frequencies, and that, even when the motion is rotational, the axis of rotation shifts with frequency. Funnell et al. (1992) incorporated realistic manubrial thickness data from serial-section histological images in a finite-element model, and their simulation results provided theoretical evidence that manubrial bending might occur. Decraemer et al. (1994a) devised an experimental setup using heterodyne interferometry to measure 3-dimensional vibrations from multiple angles at a single point at the umbo, and calculated the orthogonal components of the vibrations for different frequencies. Consistent with their earlier findings, they showed that the tip of the manubrium did not follow a straight line, as would result from a rotation around a fixed axis, but rather an elliptical path, the shape and inclination of which changed with frequency. They later performed 1-dimensional measurements at multiple points confirming that the motion of the malleus consists of a frequency-dependent combination of rotational and translational

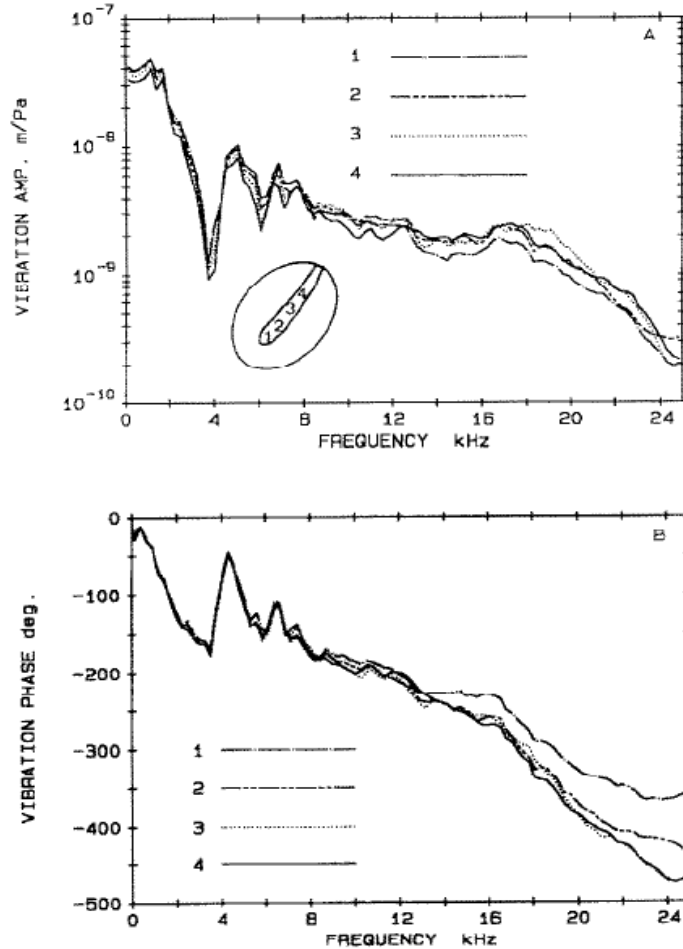


Figure 3.1: Displacements along the manubrium measured by Decraemer et al. (1991). Bead 1 (long dash dot line), bead 2 (long dash-double dot line), bead 3 (dotted line) and bead 4 (solid line). TOP: Amplitude plots. BOTTOM: Phase plots.

motion (Decraemer & Khanna, 1994). Their results again suggested manubrial bending. They investigated this further in two other specimens and showed that bending occurred at both low and high frequencies (Decraemer et al., 1994b). They continued their investigations of manubrial vibrations with 3-dimensional measurements at multiple points along the manubrium (Decraemer & Khanna, 1996 & 1997). They concluded that “the manubrium motion for a given pure tone stimulus may be compared to the motion of a ship on a stormy sea, a combination of pitch, roll and yaw on top of a translational motion, all motion components being periodic.”

3.2.3 Eardrum vibration patterns

A comprehensive review of experimental observations of eardrum vibrations dating as far back as 1874 was presented by Funnell and Laszlo (1982). Early studies used various methods ranging

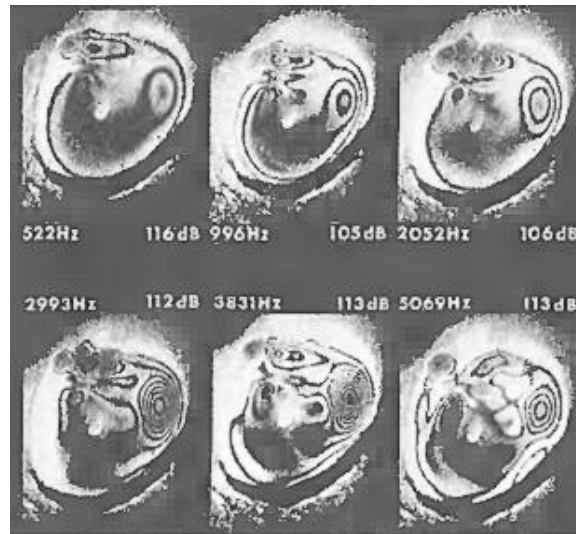


Figure 3.2: Time-averaged holograms from for six frequencies between 500 and 5000 Hz. TM of left ear. Orientation: right = posterior, left = anterior. (Source: Tonndorf and Khanna, 1972)

from visual observations and the use of mechanical and capacitive probes, to cinematographic and stroboscopic methods, leading up to interferometric techniques. Tonndorf and Khanna (1972) used time-averaged laser holography to characterize the vibration patterns of the human eardrum at different frequencies (Figure 3.2). Dark and bright lines resulting from holographic interference define contours of equal amplitudes of vibration. The contours at low frequencies show a maximum in the posterior region and another maximum of lower magnitude in the anterior region, just anterior to the manubrium. At higher frequencies, the TM seems to break up into sectional vibrations which become more complex as the frequency increases. The contours break up at about 3 kHz posteriorly and 4 kHz anteriorly. The same group reported similar holograms in a cat study (Khanna & Tonndorf, 1972) and found that the transition from simple to complex vibration patterns occurred at around the same frequencies as in humans.

Finally, LDV measurements at multiple locations on the eardrum and the manubrium in 7 rats have been reported recently by our group (Akache et al., 2007). The vibration patterns observed on the eardrum were simple up to at least 6 or 7 kHz. The responses along the manubrium had similar shapes, with exceptions in some rats revealing some frequency-dependent complexities.

3.2.4 Static eardrum deformations

Dirckx and Decraemer (1991) used phase-shift moiré topography to observe full-field shape

deformations of the human eardrum in response to static pressures. They observed two displacement maxima, one on the posterior side of the TM and a much larger one on the anterior side. (The unexpectedly large maximum in the anterior region was attributed to a possible pathology: a reduced elasticity in that region which they referred to as a “weaker spot”.) The relationship between responses to sound and these responses to static pressures are discussed in Section 3.3.2 below.

3.3 Gerbil studies

3.3.1 Auditory Sensitivity

Early gerbil studies dealt with auditory sensitivity and did not provide any measurements of middle-ear displacements. Finck and Sofouglu (1966) measured the auditory sensitivity of the Mongolian gerbil using a round-window recording of the cochlear microphonic response and observed a maximum sensitivity between 3 and 5 kHz. Above this frequency range, sensitivity decreased at a rate of 20 dB/octave, and at lower frequencies at a rate of 12 dB/octave, with the exception of a pronounced elevation in sensitivity between 1.5 and 2.5 kHz. Lay (1972) also measured the gerbil auditory sensitivity by cochlear potentials, and found similar results.

Masterton et al. (1969) argued for the existence of an inverse relationship between head size and the frequency to which an animal is sensitive, suggesting a high-frequency sensitivity for an animal with an approximate head diameter of 2 cm like the gerbil. Webster and Webster (1972) presented evidence that the enlarged middle-ear cavity of certain rodents, including the gerbil, increases low-frequency sensitivity. Consistent with both arguments, Ryan (1976) contended that the range observed by Finck and Sofouglu (and also by Lay) is not an accurate assessment of the Mongolian gerbil hearing sensitivity. Using a technique known as the double-grill avoidance response with the method of limits, he observed that gerbils respond to frequencies between 0.1 and 60 kHz, with lower audibility thresholds (higher sensitivity) for tones between 1 and 16 kHz. The author attributed discrepancies between these results and the results of Finck and Sofouglu to biases inherent in the method they used. Henry et al. (1980), while studying age-related hearing loss, measured auditory-nerve isoelectric thresholds in gerbils of different ages. They

found that younger specimens had a broad mid-frequency profile and elevated high-frequency thresholds that agreed with the findings of Ryan (1976).

In related work, Finck and Goehl (1968) measured vocal spectra and cochlear sensitivity in gerbils. Analysis of 42 vocalization recordings from 7 specimens showed 3 major peaks: a first peak in the region of 4-6 kHz, a second around 10 kHz, and a third around 15 kHz. These peaks fall within the broad mid-frequency range of high auditory sensitivity suggested by Ryan (1976).

3.3.2 Static eardrum deformations

Von Unge et al. (1993) used a real-time differential moiré interferometer to observe the displacement patterns of the gerbil eardrum in response to static (or quasi-static) pressures. They presented interferometric displacement recordings, showing two points of local maximum displacement on the pars tensa: one on the anterior side just superior to the umbo, and a larger one on the posterior side somewhat more superiorly. The maxima are situated closer to the manubrium of the malleus than to the annulus ring. Figure 3.3 shows the areas where these maxima occurred in all 18 specimens studied. Later, the same group used the same technique to

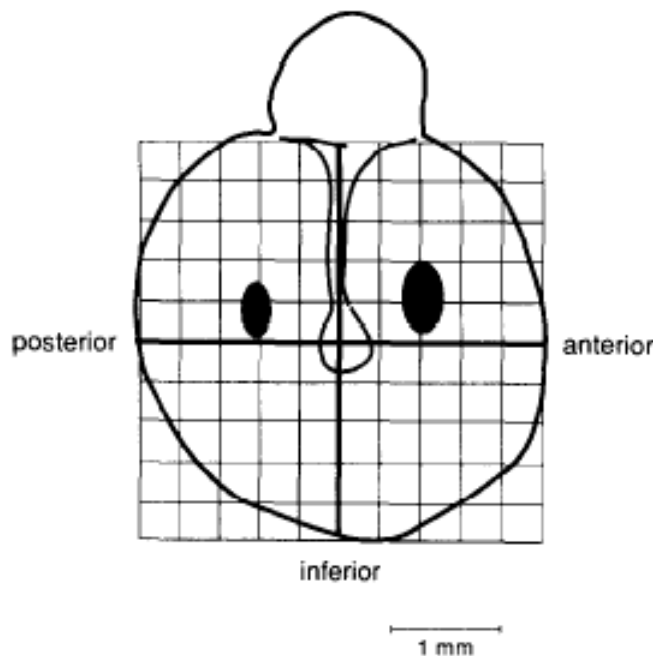


Figure 3.3: Schematic presentation of the 2 areas where the maximal displacement occur in normal ears under different positive pressures, up to + 20 cm H₂O in the external meatus. The locations of the points of maximum displacement do not vary with pressure. (Source: Von Unge et al., 1993)

investigate two experimental pathologies while using normal specimens as controls (von Unge et al., 1995 & 1999). The interferograms that they presented were consistent with those presented in 1993.

Dirckx and Decraemer (2001) used a high-resolution phase-shift projection moiré interferometer to observe the shape of the gerbil eardrum at quasi-static pressures, while studying the effects of removing middle-ear components. They measured the full-field eardrum deformations while serially removing different middle-ear components, the first measurement with the middle ear intact serving as a baseline against which the rest of the measurements are compared. By observing the eardrum shape, they measured displacements in response to static under- and over-pressures, and concluded that removing the cochlea and stapes, and cutting the tensor tympani, had no effect on static eardrum deformations. They presented shape and deformation curves across a line perpendicular to the manubrium of the malleus just inferior to the umbo. Their findings also show that maximum displacements along this line occur in the anterior and posterior regions closer to the manubrium than to the annulus ring.

Such measurements make use of high pressure levels which extend beyond the range of linear displacement of the TM. Furthermore, these pressures are maintained for some time before shape deformations are recorded. This invokes the viscoelastic characteristics of the TM (creep and stress relaxation). These measurements, even when the pressures applied are within the linear range, are thus inherently different from measurements of vibrations in response to sound, which will be presented next.

3.3.3 Vibration measurements

Many groups have produced measurements on the Mongolian gerbil using sound pressures. Ravicz et al. (1992) and Ravicz & Rosowski (1997) presented measurements of middle-ear input impedance. Rosowski et al. (1999), Olson & Cooper (2000), Overstreet & Ruggero (2002), and Ravicz & Rosowski (2004) measured the velocity of stapes vibrations over a wide range of frequencies using a laser interferometer. These studies, however, did not present measurements

of eardrum vibrations. Three studies presenting velocity measurements on the gerbil eardrum stand out in the literature and will be discussed next: Cohen et al. (1993), Rosowski et al. (1997), and the recent work of de La Rochefoucauld & Olson (2007). Displacements can be derived from velocity measurements by dividing by the frequency. A slope of 1 (or 6 dB/octave) on the velocity graph, for example, corresponds to a flat displacement curve, indicating that the system of interest is dominated by stiffness with negligible inertial and damping effects.

Cohen et al. (1993) studied the development of the umbo velocity response in live gerbils from 8 age groups: 10, 15, 20, 25, 30, 35 and 42 days after birth (DAB), and adult. Gerbils between 77 and 91 DAB were used for the adult age group. They described the velocity response at 42 DAB as a band-pass filter with a low-frequency slope of 9 dB/octave between 0.2 and 7 kHz, and a slight high-frequency roll-off of approximately 1.3 dB/octave between 7 and 40 kHz. They studied the changes in the response up to 42 DAB. They found that changes occurred mainly in the region between 0.5 and 2 kHz (the low-frequency slope increasing from 6.5 dB/octave at 15 and 30 DAB to 9 dB/octave at 42 DAB), the response remaining relatively stable in the mid- and high-frequency regions. They attributed these changes to an increased admittance due to an expanding bulla volume. The adult responses that they measured, however, were decidedly different from those at 42 DAB, showing a steeper low-frequency slope and considerable variations beyond 4 kHz: the slope of the adult response decreased at about 6 dB/octave between 4 and 20 kHz, and then increased by about 7 dB/octave from 20 to 40 kHz (Figure 3.4). The authors attributed the decrease in high-frequency sensitivity to the possible existence of additional mass elements in the adult middle-ear, such as increased ossicular mass. Furthermore, they speculated, on the one hand, that the decrease in low-frequency sensitivity could be the result of a reduction in middle-ear compliance due to a reduction in the size of the middle ear. This, they claim, could stem from a developing aural cholesteatoma prevalent in the adult gerbil (Henri et al., 1983). On the other hand, they hypothesized that changes in low-frequency sensitivity might represent an artefact of the experimental procedure, which requires drilling a 2- to-4 mm hole in the skull to position the laser beam at the tip of the umbo. Unlike the situation in younger gerbils, drilling this hole inadvertently opens the enlarged adult bullar cavity, thus

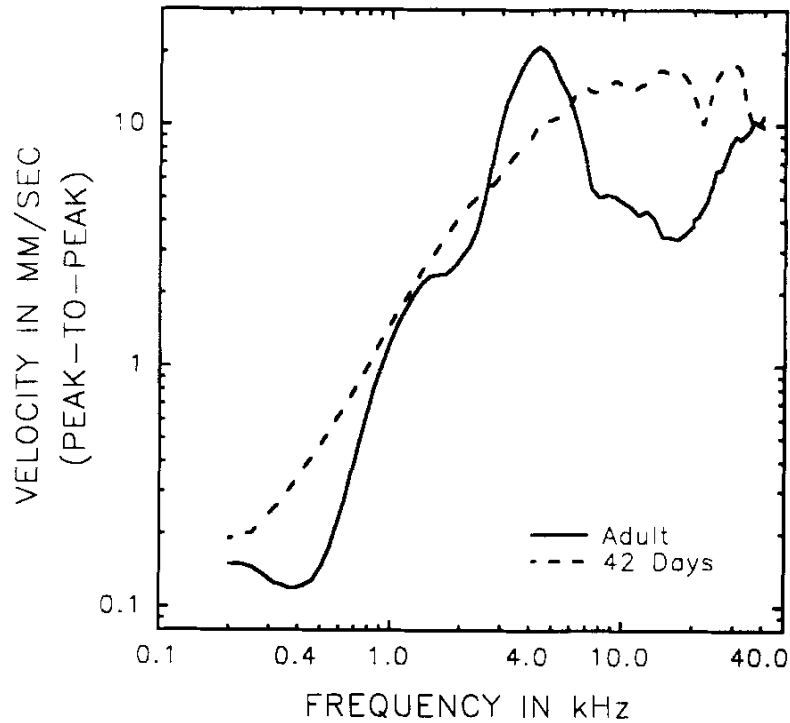


Figure 3.4: Averaged peak-to-peak umbo amplitude response from adult and 42-day-old gerbils. (Source: Cohen et al. 1993)

affecting sound transmission in the adult middle ear. They tested this hypothesis by measuring evoked-potential threshold sensitivity in one animal with an intact bulla and several animals with drilled bullae, and concluded that the opening of the bulla had minimal effects on sound transmission.

Rosowski et al. (1997) presented measurements of eardrum motion at the umbo and on the pars flaccida in live gerbils. Figure 3.5 shows their velocity measurements at the umbo with an open and a closed middle-ear cavity. The opening of the cavity consisted of a 1-mm hole drilled in the bulla which is acoustically closed with a thin tube when performing closed-cavity measurements. The open-cavity response at the umbo has a stiffness-dominated behaviour at low frequencies with a broad peak around 1.2 kHz. Beyond this frequency a roll off with a slope of -1 can be observed as the system becomes more mass-controlled. The response is complicated by a sharp drop around 3 kHz which is attributed to an anti-resonance produced by the interaction of the open bullar hole and the middle-ear cavity. Closing the bullar hole removed the effect of the anti-resonance and decreased the velocity of vibrations at low frequencies. Moreover, the broad peak

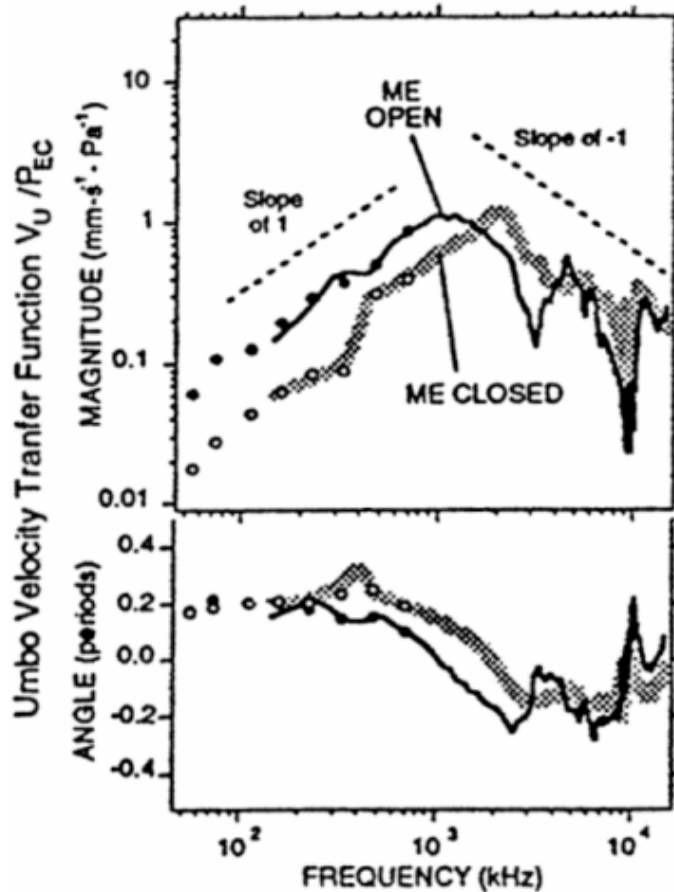


Figure 3.5: Normalized umbo response with the middle-ear cavity open (black line) and closed (grey line). Measurements were made with chirp stimuli of bandwidth 0.05 to 25 kHz (lines without markers) and with pure tones of frequencies between 0.025 and 0.8 kHz (circles). The angle between the plane of the umbo and the direction of the laser beam is $\approx 60^\circ$; this introduces an error of $\sim 15\%$ which is not corrected for in the plot. (After Rosowski et al. 1997)

observed around 1.2 kHz in the open-cavity measurement became narrower and shifted to around 2.1 kHz when the hole was closed. It is possible that this shift is a side-effect of the removal of the anti-resonance observed in the previous measurement. A sudden change in amplitude and angle occurs around 0.45 kHz in the measured umbo velocities. This is a small reflection of a very sharp resonance peak observed at this frequency in the pars flaccida velocity, which contributes to the middle-ear input admittance.

Finally, in very recent work, de La Rochefoucauld and Olson (2007) reported middle-ear velocity measurements in live gerbils in the context of an investigation of middle-ear delays and sound transmission. They performed measurements at different positions along the transmission path from the ear canal to the stapes, for a wide range of frequencies (up to 50 kHz). Their

measurements were performed using an open-field sound excitation and were normalized with respect to the sound pressure measured at the entrance of the ear canal. Acoustic resonances in the ear canal would have to be measured and corrected for in order for these measurements to be comparable to those obtained in our study or in the studies mentioned previously, where the sound pressure was measured near the eardrum.

3.3.4 Finite-element models

First introduced into middle-ear research by Funnell (1975), finite-element models have become very popular research tools in studies of middle-ear mechanics. Two 3-D finite element models of the gerbil middle ear have been developed in our lab. Simulation results from these models will be briefly presented here.

The first model was developed by Funnell et al. (1999 & 2000). The shape of the eardrum in this model is based on phase-shift moiré shape measurements from Dirckx and Decraemer. The ossicular geometry was first based on a 3-D reconstruction from a high-resolution magnetic resonance microscopy (MRM) dataset, and later improved by incorporating data from serial-section histological images. In 2000, they showed the low-frequency simulations of eardrum and ossicle displacements shown in Figure 3.6. The simulated low-frequency vibration pattern of the eardrum shows a maximum displacement in the posterior region and a less pronounced

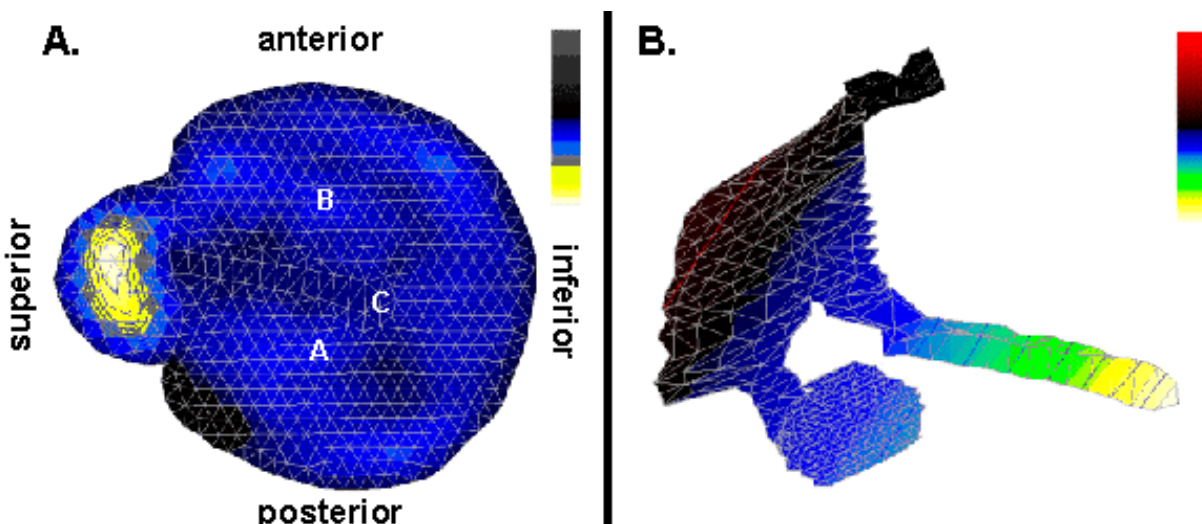


Figure 3.6: Simulated low-frequency vibration patterns of (A) the eardrum and (B) the ossicles. (After Funnell et al., 2000)

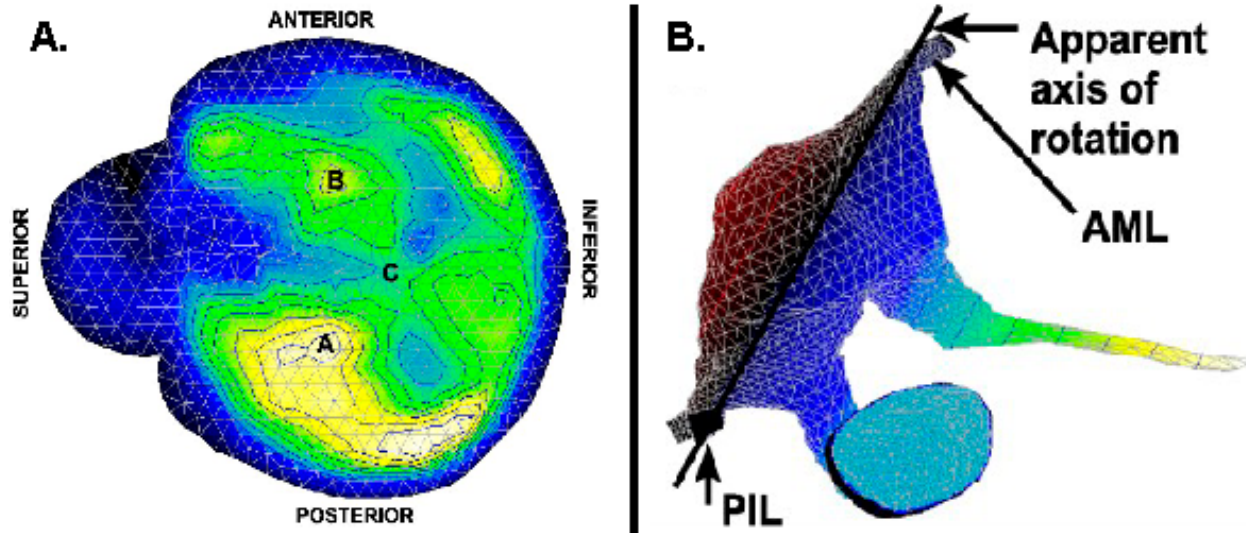


Figure 3.7: Simulated low-frequency vibration patterns of (A) the eardrum and (B) the ossicles. (After Elkhouri et al., 2006)

maximum in the anterior region closer to the manubrium than to the annulus ring (Figure 3.6A). Vibrations of the pars flaccida are much greater than those of the pars tensa for the parameters employed. The simulated ossicular motion is consistent with the classical notion of a simple rotation around a fixed axis defined by the anterior malleolar ligament and the posterior incudal ligament (Figure 3.6B). Manubrial displacements are maximal at the tip and decrease towards the lateral process.

More recently, Elkhouri et al. (2006) developed another 3-D model of the gerbil middle ear using the same MRM images and moiré data. This model also included data from a recent dataset of X-ray micro-CT images with a voxel size of $5.5 \mu\text{m}$, enabling a more precise reconstruction of the thin stapedial annular ligament. Low-frequency simulation results of eardrum and ossicle displacements are shown in Figure 3.7. These results agree with those reported by Funnell et al. (2000). The displacement patterns of the pars tensa in Figure 3.7A are very similar to those in Figure 3.6A. Displacements of the pars flaccida, however, are much smaller than those of the pars tensa in this model (the colour scale is normalized to the maximum displacement in the pars flaccida). To ease the comparison of results, maximum displacements in the posterior and anterior region, and at the umbo, have been denoted by A, B and C respectively.

3.4 Post mortem studies

3.4.1 Validity of post mortem research

Several groups have investigated the validity of using cadaver middle ears to study the function of live ones. The consensus is that the middle ear can remain relatively normal for several hours, and even days, if proper steps are taken. Khanna and Tondorf (1972) compared holograms of eardrums from live cats and from fresh cadaver specimens at 600, 950, 2000, 2900, 4000, and 5000 Hz. They concluded that “there was no difference between the vibrational patterns recorded from fresh cadaver specimens or from living animals.” Rosowski et al. (1990) compared tympanometric measurements of middle-ear input immittance from fresh and thawed human temporal bones with those from *in vivo* data from clinically normal subjects. The *post mortem* measurements compared fairly well with those taken *in vivo* for the range of 0.1 to 2 kHz. They attributed discrepancies above 2 kHz to technical differences in tympanometric measurements from different groups. To measure the effect of immediate death, they also measured the input impedance of the guinea-pig middle ear *pre* and *post mortem*. They found that the magnitude of the impedance remained relatively unchanged for 14 hours. They concluded that the middle ear maintains normal function if care is taken to keep the middle ear from drying and if the static pressures on either side of the eardrum are kept equal.

Other groups have reached similar conclusions. Goode et al. (1993 and 1996) compared umbo measurements in live and cadaver human ears. They found that the eardrum acoustic properties at low to mid frequencies are similar, and showed great similarity in the measured responses below 6 kHz. Nishihara and Goode (1997) measured eardrum vibrations in 99 human ears and noted that “human temporal bones showed very similar results to the normal [...] ears”. Similarly, Huber et al (2001) concluded that “the temporal bone is a very good model for studying middle ear mechanics” based on their findings that there were “no major differences in the results from the live human subjects and temporal bone preparations.”

This area, however, is a subject for debate in the literature. Ruggero and Temchin (2003) argued that “there are substantial differences between *in vivo* and *post mortem* measurements”. They

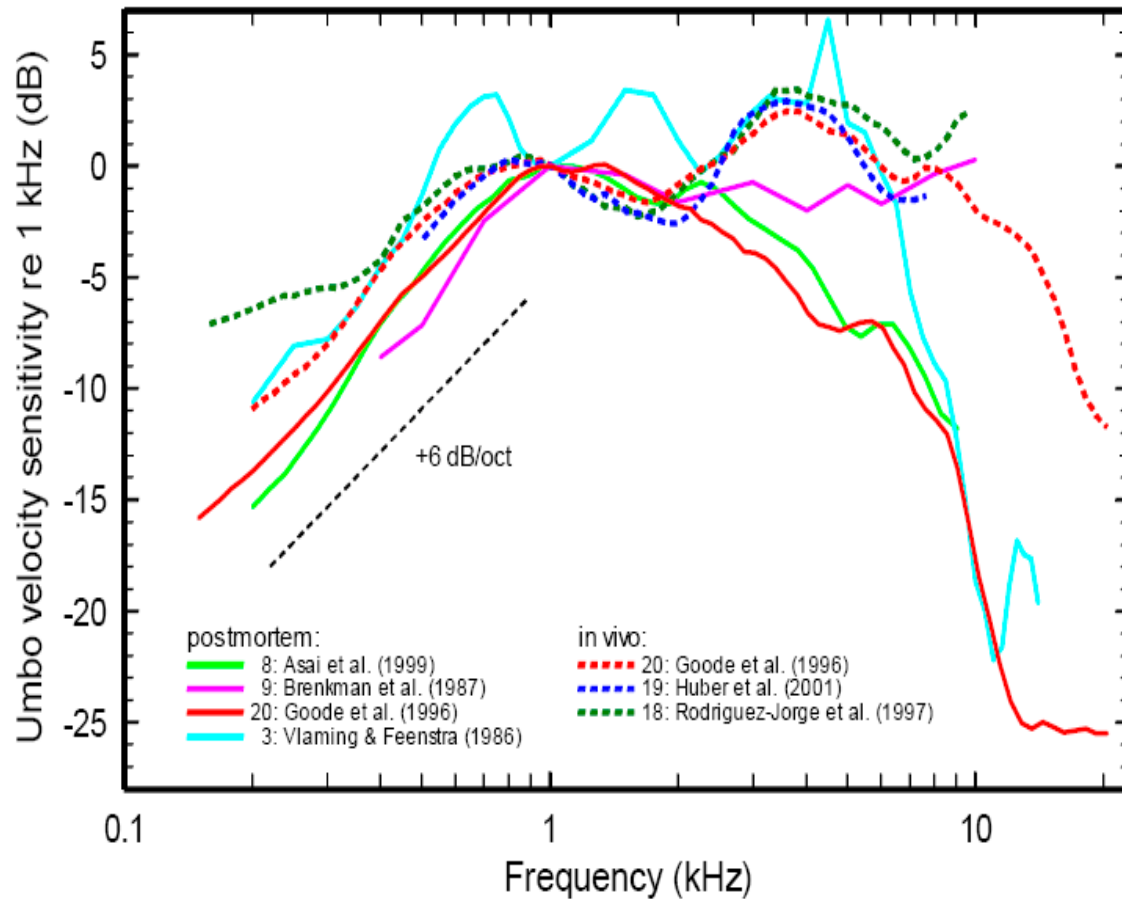


Figure 3.8: Umbo frequency responses from 4 *post mortem* and 3 *in vivo* studies normalized to 1 kHz. (Source: Ruggero & Temchin, 2003)

compared several *in vivo* and *post mortem* studies of stapes and umbo velocities from the literature. Frequency responses for umbo velocities normalized to 1 kHz are reproduced here in Figure 3.8. These plots show that the *in vivo* responses are flat for a wide range of frequencies, whereas *post mortem* responses fall beyond 2 kHz, suggesting that the dead middle ear acts as a bandpass filter. They also showed a similar comparison for stapes velocities. The authors conjecture “that most *post mortem* recordings of ossicular vibrations are flawed, and that middle-ear transmission in humans [...] does not severely limit the bandwidth of hearing.”

Rosowski et al. (2004) disputed these claims with an exhaustive survey of measurements available in the literature. They showed that all measurements from *in vivo* studies, for both umbo and stapes velocities, fell within a 95% confidence interval computed from all *post mortem* studies analysed. The comparative plot of umbo velocities is reproduced in Figure 3.9.

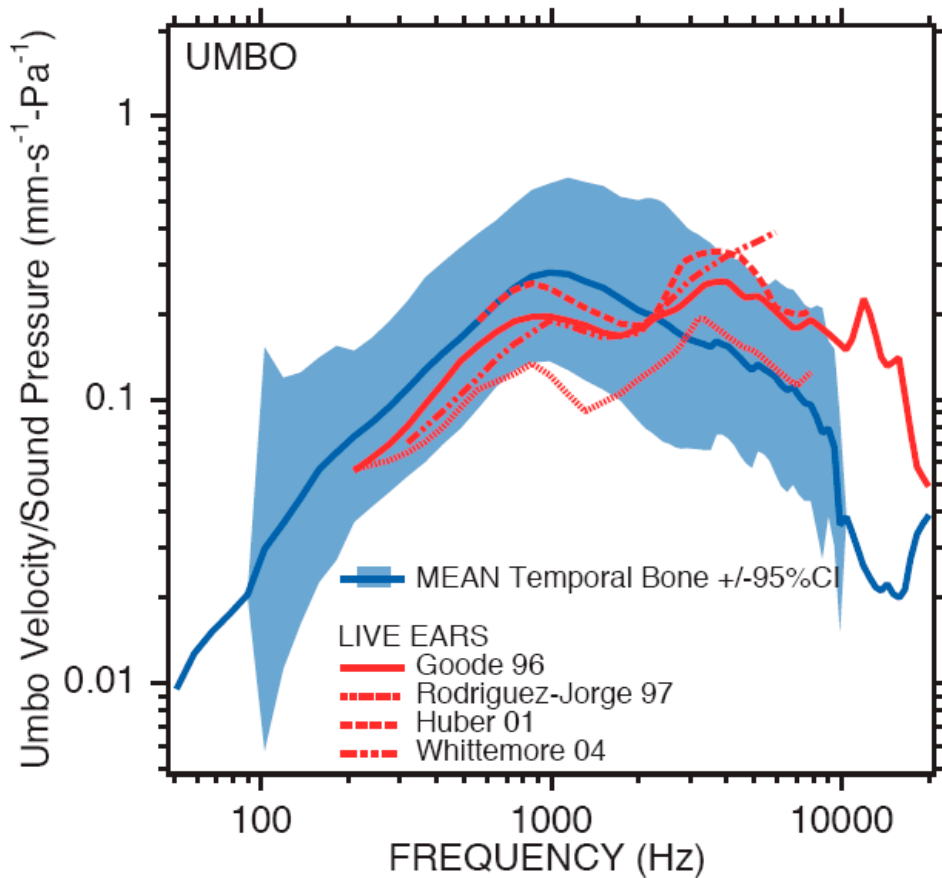


Figure 3.9: Comparison of the mean and 95% confidence intervals of *post mortem* measurements to *in vivo* measurements of umbo velocities.
(Source: Rosowski et al., 2004)

They attributed discrepancies between their results and those of Ruggero and Temchin to differences in measurement methodologies and to the loss of active mechanisms in the cochlea. Technical differences include variations in the use of reflectors, placement and calibration of microphones, methods used for stimulus generation and data acquisition, and the use of scanning laser Doppler vibrometers. According to the authors, the state of the middle-ear cavities and the role of the middle-ear muscles are also potential factors that contribute to variability in measurements from different groups.

3.4.2 Drying effects

An important *post mortem* condition that affects measurements in temporal bones is the drying of middle-ear structures. When the middle-ear is exposed to permit measurements, the eardrum and other structures dry out over time, causing changes in their material properties. Several groups have described various strategies to keep the middle ear moist, by preventing drying or by remoistening the middle-ear structures when drying occurs. A list of such methods is presented in Table 3.1.

Table 3.1: Strategies used by other groups to keep the middle-ear structures moist.

Study	Hydration method
Lynch et al. (1982)	Few drops of normal saline on stapedial annular ligament.
Rosowski et al. (1990)	Periodic rinsing of external ear canal with normal saline.
Merchant et al. (1996)	Periodic application of normal saline throughout the preparation.
Voss et al. (2000 & 2001)	Temporal bone submerged in normal saline, and gentle suction to remove excess liquid from the middle-ear cavity.
Aibara et al. (2001)	Specimen kept in a latex finger cot to keep the wet bone moist. Glass cover slips placed over the mastoid opening.
Stenfelt et al. (2003)	Temporal bone placed in a latex seal to prevent drying.
Huber et al. (2003)	Periodic remoistening with Ringer’s solution.
Songer et al. (2004)	Bulla holes plugged with “pink” when not accessing the middle-ear to prevent drying, and with moist cotton for 15 minutes when drying occurred.
Nakajima et al. (2005)	Middle ear kept moist with small pieces of moist gel foam and frequent moistening with normal saline.
Chien et al. (2006)	Temporal bone soaked with normal saline

Voss et al. (2000) observed repeated measurements of normalized stapes velocities. Their results showed a drop in magnitude which varied from ear to ear. In some preparations, the magnitude remained stable for several hours before dropping suddenly. Figure 3.10A shows an example of stable measurements. In unstable ears (Figure 3.10B), the magnitude decreased systematically in minutes. In both cases, they found that the magnitude drop was partially reversible (as illustrated in the figure) by moistening of the temporal bone with saline solution and then using gentle suction to remove the saline.

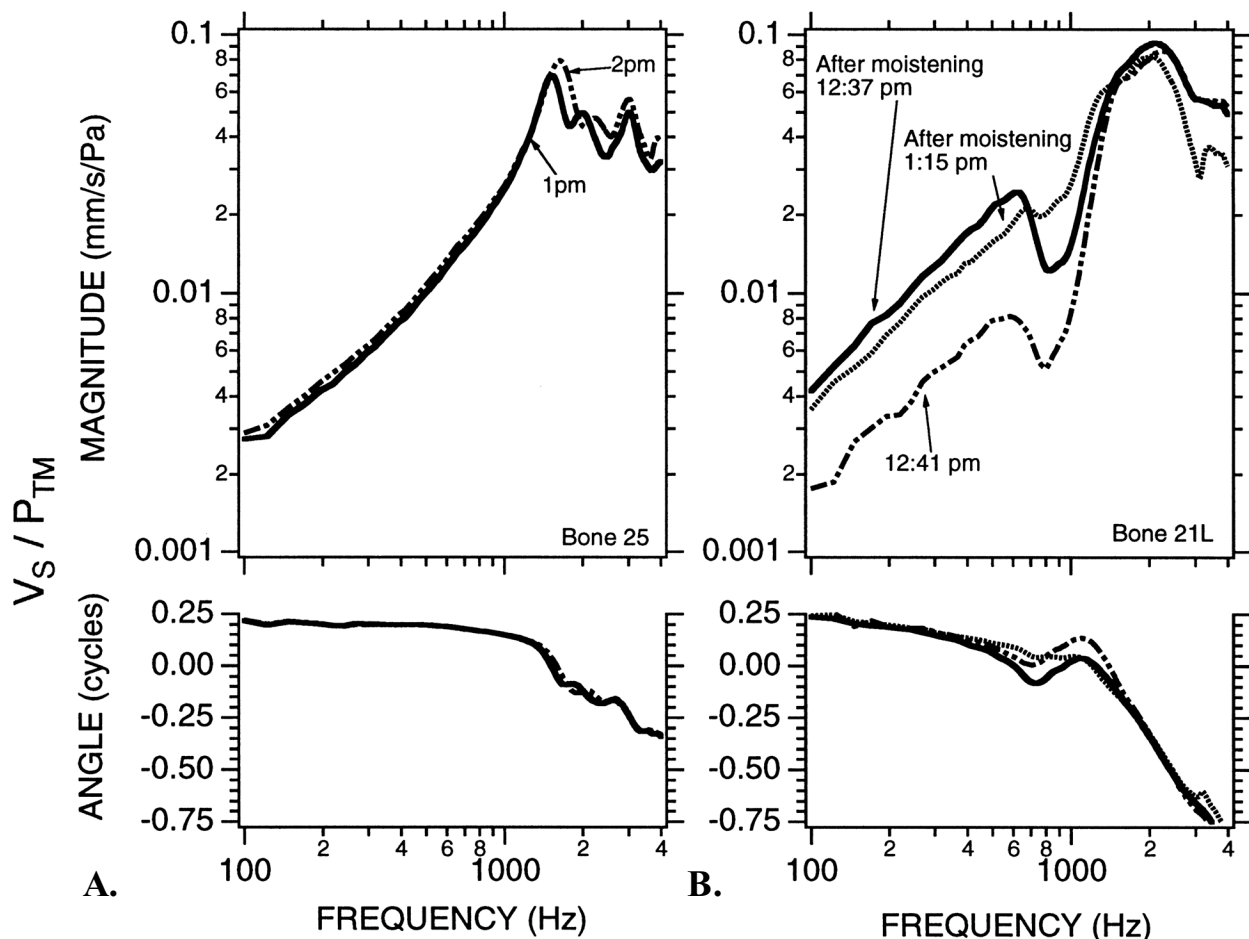


Figure 3.10: Assessment of measurement stability and moistening of temporal bone preparation. LEFT: stable measurements are nearly identical after a 1-hour time gap. RIGHT: unstable measurements show a drop in magnitude of nearly 6 dB within only 4 minutes. Remoistening the temporal bone preparation returned the response to some extent towards its original level. (Source: Voss et al., 2000)

3.5 Conclusion

We have presented a review of studies relevant to the research work presented in this thesis. Experimental measurements of eardrum vibration patterns agree about the locations of maximum displacements, and about a transition from a low-frequency mode to a high-frequency mode of vibration. The ossicular motion has been shown to be quite complex at high frequencies. In particular, the manubrium of the malleus has been shown to sometimes exhibit bending, so it cannot be assumed to vibrate rigidly. Laser Doppler vibrometry has become very common in the study of middle-ear vibrations.

For the gerbil, modelling studies have provided low-frequency simulations of eardrum and ossicular displacements. While a number of experimental measurements of stapedial motion have been reported, there is a lack of experimental data to characterize the motion of the gerbil eardrum. Such measurements at multiple points on the eardrum would be useful to validate models of the middle ear. These measurements would also help to extend our knowledge of gerbil eardrum vibrations past the low frequencies.

There is evidence supporting the use of *post mortem* ears in the study of middle-ear mechanics, provided special steps are taken to keep the middle ear moist and properly ventilated. Several studies have provided different strategies for avoiding or correcting for drying effects, but few quantitative observations of these effects have been reported.

CHAPTER 4

LASER DOPPLER VIBROMETRY

4.1 Introduction

Laser Doppler vibrometry (LDV) is a non-contact vibration-measurement technique which uses the Doppler effect to perform measurements on a surface without mass loading. In this chapter we present a theoretical overview of LDV based primarily on a comprehensive manuscript on interferometry by P. Hariharan (2007), as well as on technical information from the “Polytec Vibrometer University” Web page. Section 4.2 presents a general discussion of optical interferometry, while the details of laser Doppler vibrometry are presented in Section 4.3.

4.2 Optical interferometry

Optical interferometry is a technology that finds use in multiple disciplines, such as communications, medical imaging, astronomy and structural measurement, to name just a few. For example, interferometers enable engineers and scientists to inspect the micro-machined surfaces of semiconductors. In microscopy, spectroscopy, and coherent tomography, medical technicians employ interferometry to help physicians give more accurate diagnoses. Optical interferometers come in a variety of types, heterodyne interferometers being particularly interesting to us, as the laser Doppler vibrometer is of that type.

4.2.1 Principle of operation

Interferometry is the measurement of interference when two or more waves are superimposed. The basic principle underlying the operation of interferometers is that two waves in phase with one another reinforce each other, while two out-of-phase waves tend to cancel each other out. Light can be thought of as transverse electromagnetic waves propagating through space. Optical interference relies on the principle of superposition applied to light waves. The interference pattern typically involves alternating dark and bright fringes resulting from the phase difference between the interfering light waves. Optical interference is a common natural phenomenon that can be observed, for example, in the colours of a soap bubble, or an oil slick on a wet road.

4.2.2 Light source

Light from any source can be used to obtain interference patterns. Early interferometers used a pinhole illuminated by a mercury vapour lamp as a light source. This source, however, contains a wide spectrum of colours and produces a collection of interference patterns with a different spacing for each wavelength. It is poorly suited to producing clear interference patterns. Optical interferometry works best with a monochromatic (single colour) light source, that is, a source which emits light only at a single wavelength, or with a source emitting a narrow band of wavelengths. When filtered to produce a narrow band, a beam from a mercury vapour lamp provides only a small amount of light. The advent of the laser, a perfectly monochromatic light source, has removed many of the limitations of conventional light sources, and has made possible many new interferometric techniques. For further reading on interference patterns and light sources, we recommend Chapters 2 and 4 of the manuscript by P. Hariharan (2007).

4.2.3 Laser basics

‘Laser’ is the acronym for **l**ight **a**mplification by **s**timulated **e**mission of **r**adiation. The goal of a laser is the induced emission of photons that have identical properties, thus producing a coherent light of a single wavelength. In a laser device, the lasing material is contained within a resonant optical cavity with a reflecting mirror at one end and a partially transmitting mirror at the other. Light is repeatedly reflected between the two ends, and finally exits from the cavity through the partially transmitting mirror. An external source supplies energy to excite the atoms in the lasing material and keep the light-emission process going (Figure 4.1). The interested reader is referred to Chapter 6 of the manuscript by P. Hariharan (2007) for more information on laser technology.

There are various types of lasers with different wavelengths depending on the lasing material used for light emission. Helium-neon (He-Ne) lasers normally have a wavelength of 633 nm. They are widely used for interferometry as they are relatively inexpensive and provide a continuous visible light. Lasers are classified for safety according to their wavelength, maximum output power, and the accessibility to hazardous areas. The international laser safety standard (IEC 60825.1) of the International Electrotechnical Commission defines 7 classes of lasers (I, I

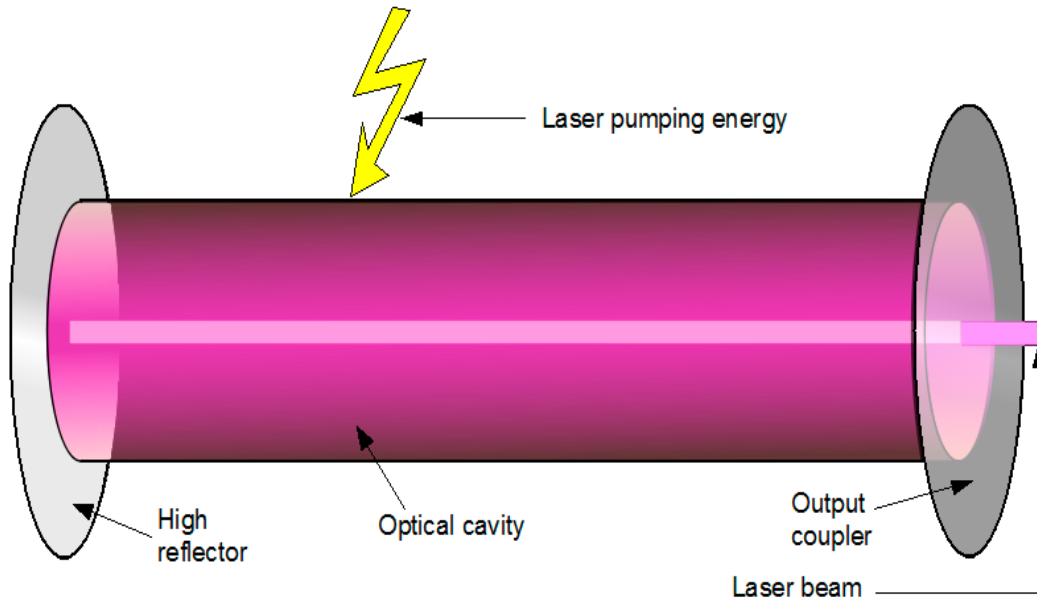


Figure 4.1: Schematic diagram of the principle of operation of a laser device.
 (After <http://en.wikipedia.org/wiki/Image:Laser.svg>)

M, II, II M, III R, III B, and IV), class I being the least and class IV the most hazardous (rp-photonics.com). The use of suitable eye protection is a strongly recommended safety precaution when operating lasers of classes IIIB and IV. The laser vibrometer that we use in our work uses an eye-safe class-II He-Ne laser source with low output power (< 1 mW).

4.3 Laser Doppler vibrometry

4.3.1 The Doppler effect

The Doppler effect is the observed change in frequency of a wave perceived by an observer moving relative to the source of the wave. This is actually a very common occurrence in daily life. One perceives the Doppler effect, for example, when the acoustical pitch of a vehicle horn changes as it passes by. The operation of the laser Doppler vibrometer is based on the Doppler principle: as a coherent laser light is reflected off the surface of a vibrating object, the measured Doppler frequency shift f_D is:

$$f_D = \frac{2 \cdot v}{\lambda} \quad (\text{equation 4.1})$$

where v is the velocity of the moving surface, and λ is the wavelength of the laser beam (633 nm

in the case of a He-Ne laser). The reflected laser beam is made to interfere with a reference beam in order to measure velocity and displacement along the axis of the reflected beam using the Doppler frequency shift. There are many ways this can be accomplished. Heterodyne interferometry presents one particular method of performing such measurements.

4.3.2 Polytec laser Doppler vibrometers

4.3.2.1 Principle of operation

Figure 4.2 shows a schematic diagram of a typical Polytec laser Doppler vibrometer, a two-beam heterodyne interferometric device. A beam splitter (BS1) splits the He-Ne laser beam into a reference beam and a measurement beam. The reference beam passes through a Bragg cell whose importance will be explained in Section 4.3.2.3. The measurement beam is passed through a second beam splitter (BS2) and pointed onto the reflective surface of the object where vibration measurements are desired. This beam is reflected with an observable Doppler frequency shift caused by the motion of the vibrating object. The reflected beam is deflected towards a third beam splitter (BS3) where it is made to interfere with the reference beam and then sent to the

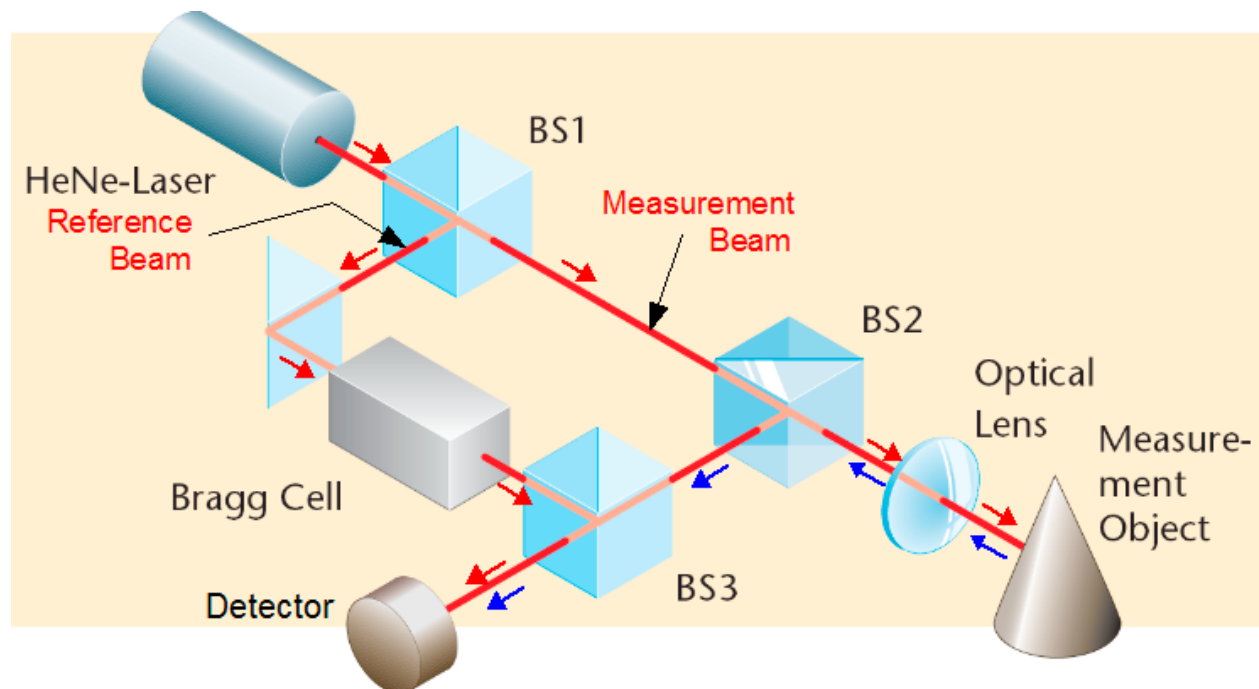


Figure 4.2: Schematic diagram of the laser Doppler vibrometer.

The He-Ne laser beam is split into a reference beam and a measurement beam. The reference beam is offset in frequency by the Bragg cell and the measurement beam is pointed onto the reflecting surface of a vibrating object. A detector picks up the resulting combined signal made up of the offset reference and the reflected beam. Three beam splitters (BS1, BS2, and BS3) are used to split, redirect, and combine the laser beams. (After polytec.com)

photodetector. The intensity of the resulting beam picked up by the detector can be calculated as:

$$I(t) = I_1 + I_2 + 2K\sqrt{I_1 I_2 R} \cos(2\pi f_D t + \Phi) \quad (\text{equation 4.2})$$

where I_1 and I_2 are the intensities of the measurement and reference beams respectively

K is a mixing-efficiency coefficient

R is the effective reflectivity coefficient of the vibrating surface

f_D is the Doppler frequency shift

Φ is the phase calculated as $\Phi = 2\pi \Delta L / \lambda$ where ΔL is the displacement of the surface.

The vibrational displacement ΔL is the difference between the path lengths of the measurement beam (time-varying) and the reference beam (constant, with the exception of negligible thermal effects). A sinusoidal vibrational displacement leads to a periodic intensity $I(t)$ on the detector, which corresponds to a dark and bright (fringe) pattern of frequency f_D .

4.3.2.2 Velocity and displacement

The velocity of the vibrating surface is directly proportional to the Doppler frequency shift (equation 4.1). Thus the vibrometer is able to perform direct measurements of velocity. Displacements can be obtained by integrating the velocity. Moreover, each dark-bright cycle on the detector corresponds to an object displacement of half the wavelength of the laser ($\lambda/2 = 316$ nm for He-Ne laser). By simply counting the number of fringes, the vibrometer is able to perform a direct measurement of displacement by increments of $\lambda/2$. The manufacturer states that “using suitable interpolation techniques, Polytec's vibrometers can attain a resolution of 2 nm, and with digital demodulation techniques down to the pm range!” They also state that “displacement demodulation is better suited for low frequency measurements and velocity demodulation is better for higher frequencies” where vibrations have higher velocities and lower displacement amplitudes. Polytec provides a variety of velocity and displacement decoders. The vibrometer that we use (the HLV-1000) is equipped with a velocity decoder and uses integration to obtain displacements.

4.3.2.3 Heterodyne interferometry

The peculiarity of heterodyne interferometry lies in the use of an acousto-optic modulator (the Bragg cell) incorporated into the interferometer arm. This enables the vibrometer to determine the direction of displacements, even though movements away from or toward the interferometer generate the same interference pattern. The Bragg cell is driven by an oscillator at frequency f_B (typically $f_B = 40$ Mhz) and generates a carrier signal at the RF drive frequency $(\Omega + 2\pi f_B)$, where $\Omega = 4.74 \times 10^{14}$ Hz is the frequency of the laser). This carrier signal is frequency modulated by the movement of the vibrating object, and the intensity picked up at the detector becomes:

$$I(t) = I_1 + I_2 + 2K\sqrt{I_1 I_2 R} \cos(2\pi(f_B - f_D)t + \Phi) \quad (\text{equation 4.3})$$

When the object is at rest a fringe pattern of frequency f_B is detected. As the object moves towards the interferometer, the detector picks up a modulation frequency below f_B . Similarly, as the objects moves away, the frequency picked up is greater than f_B .

4.4 Conclusion

Laser Doppler vibrometry is an accurate method for measuring small vibrations of a moving structure down to the nanometer level, by making use of the Doppler effect. It is an effective measurement technique for use in middle-ear research since it does not load the structure where measurements are desired. In the following chapter we shall discuss how this technology can be used to perform displacement measurements on the gerbil eardrum.

CHAPTER 5

MATERIALS AND METHODS

5.1 Introduction

Experimental measurements were made for two studies, which will be detailed in the remainder of this thesis. In this chapter we present the methodology used in our experiments. In Section 5.2 we first present the experimental setup we used to perform measurements. A discussion of experimental considerations follows in Section 5.3. An overview of the specific types of measurements made is presented in Section 5.4.

5.2 Experimental setup

5.2.1 Specimen preparation

Measurements were carried out on Mongolian gerbils (*Meriones unguiculatus*) supplied by Charles-River (St-Constant, QC). The anatomy of the gerbil middle ear was presented in Chapter 2. In Figure 5.1 are shown relevant anatomical details along with the experimental preparation. The gerbil is first sacrificed and its head is detached from the rest of its body to ease the subsequent dissection. The lower jaw is removed to expose the bulla. The external ear is

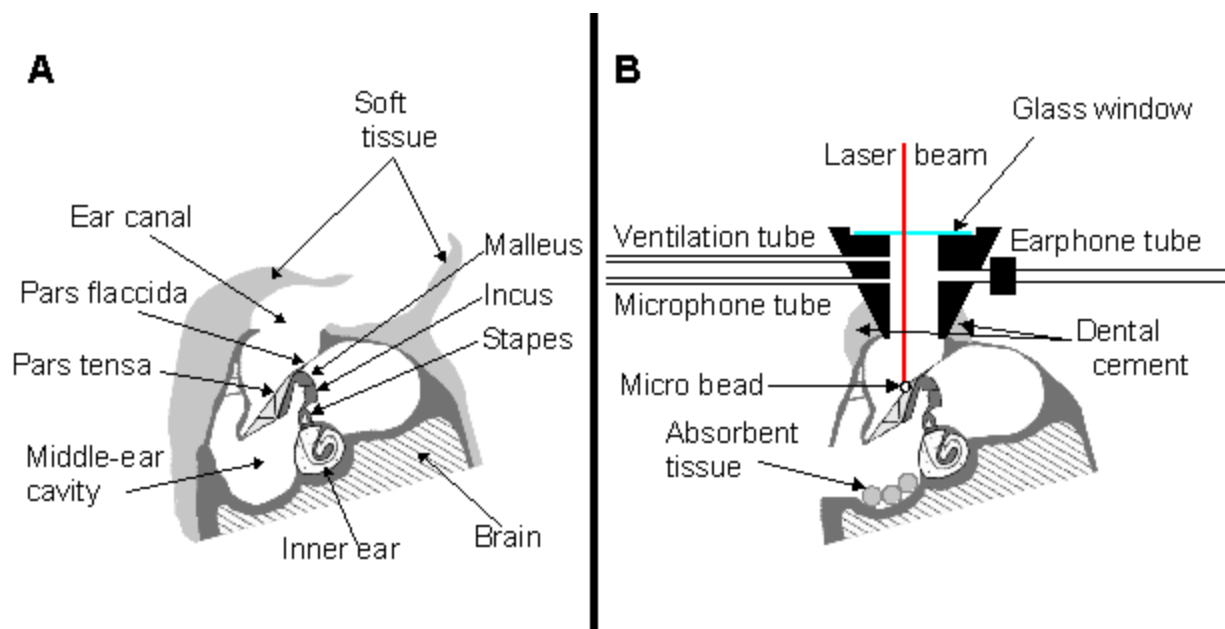


Figure 5.1: Schematic illustrations of **A.** the gerbil middle ear and **B.** the experimental preparation. Bone is drawn in dark grey and soft tissue in light grey. The laser beam is pointed through the glass window and the acoustically sealed cavity and is precisely aimed at a glass bead. (After Rosowski et al. 1999)

removed, keeping a portion of the cartilaginous part of the ear canal. Soft tissue surrounding the bulla is scraped off using a surgical scalpel. Parts of the bony ear canal are then drilled away with a surgical drill to maximize exposure of the TM and reveal the umbo, while taking care not to disrupt the fibrocartilaginous ring around the TM. During this step, the remaining cartilaginous part of the ear-canal wall is folded over the opening of the ear canal to prevent the deposit of bone chips or dust on the TM. The inferior lateral portion of the bulla is drilled away so the middle-ear cavity is widely open, to ensure pressure equalization on the two sides of the TM (as discussed in detail in Section 5.3.1.3). Small wads of absorbent tissue are placed in the inferior section of the middle-ear cavity (see Figure 5.1B). The tissue is periodically moistened with a few drops of saline during the experiment, as will be seen in Section 5.4.4.1. Very small beads are placed at locations on the TM and on the manubrium of the malleus wherever measurements are desired. The use of these beads will be discussed in Section 5.3.2.

Finally, the opening of the ear canal is affixed with dental cement to a coupler in an orientation that allows an optimal view of the TM. The coupler is a custom-designed aluminum sound chamber which will be discussed in Section 5.2.2.1. The dental cement settles within minutes and provides a solid attachment of the gerbil head to the coupler. The coupler is attached by set screws to a rigid aluminum bar which in turn is clamped in a vice. The vice is firmly mounted on the base of the microscope using a suction mechanism. The experimental preparation is placed under an operating microscope (OPMI 1-H, Zeiss) to which the vibrometer head (described in Section 5.2.2.2) is attached. This setup is shown in Figure 5.2. Care is taken to make sure that all mechanical connections in the setup are rigid, to minimize any motion of the specimen with respect to the vibrometer head.

5.2.2 Measurement system

The measurement system consists of the laser Doppler vibrometer and the attached peripherals required for its operation. Three components can be identified: an acoustical system, an optical system, and a data acquisition and analysis system.

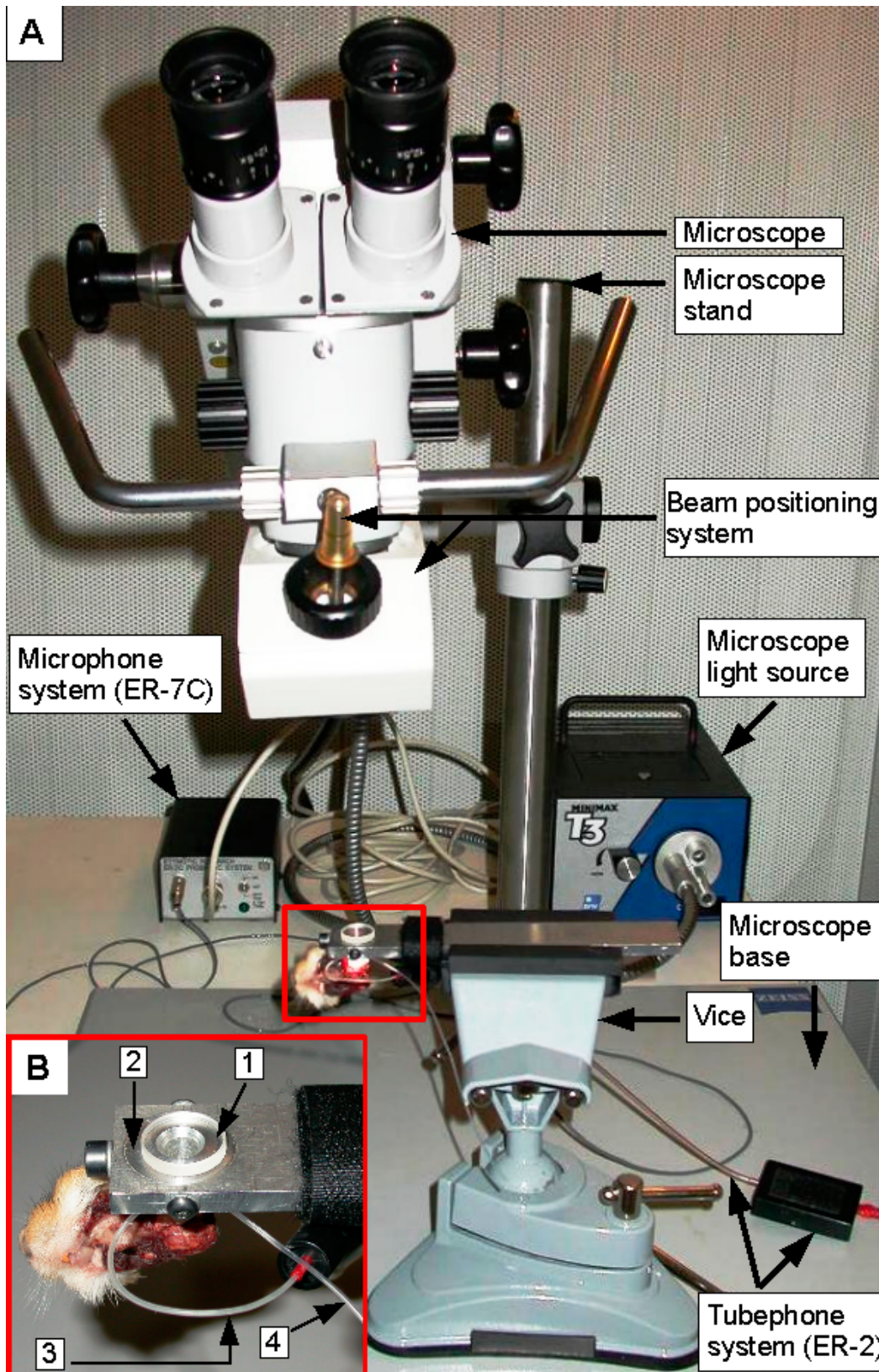


Figure 5.2: **A.** Photograph of the experimental setup. **B.** Close up of the experimental preparation.
 1. Glass window, 2. Acoustic coupler, 3. Probe microphone (ER-7C), 4. Ventilation tube.
 The ER-2 sound delivery system cannot be seen from the angle of the close up.

5.2.2.1 Acoustical system

Vibration measurements are performed in the presence of an audio stimulus exciting the eardrum. The acoustical system consists of a sound-delivery device and a sound-monitoring device coupled together in a sealed chamber (see Figure 5.1B). Sound is administered by an insert earphone (ER-2 Tubephone, Etymotic Research), and the sound pressure level (SPL) is monitored by a probe-microphone system (ER-7C, Etymotic Research) placed 2 to 3 mm from the eardrum. The specifications, frequency responses, and photos of the ER-2 Tubephone and the ER-7C probe microphone are shown in Figure 5.3 and Figure 5.4 respectively.

With such a small driver, it is important that sound administered to the middle ear be confined to a small volume. The coupler shown in Figure 5.1B is a custom-made aluminum cavity which provides a small acoustically sealed sound chamber. The coupler dimensions were designed to prevent acoustical resonances (discussed in Section 5.3.1.4). Holes are drilled in the coupler to allow the insertion of the ER-2 Tubephone and the probe microphone. A third hole is drilled to allow the insertion of a 15-cm PE-50 tube (I.D. = 0.58mm, O.D. = 0.96mm). This tube acts as a vent and will be discussed in Section 5.3.1.3. The dental cement serves not only to fix the gerbil head to the coupler but also to provide an acoustical seal at the bottom of the sound chamber.

It is important to have a clear visual field for the trajectory of the laser beam for measurements to be possible. For this purpose, the top of the cavity is covered with an antireflection-coated glass window (T47-518, Edmund Optics). The insertion of the tubes into the corresponding holes in the coupler must also be done carefully to avoid blocking the path of the laser beam.

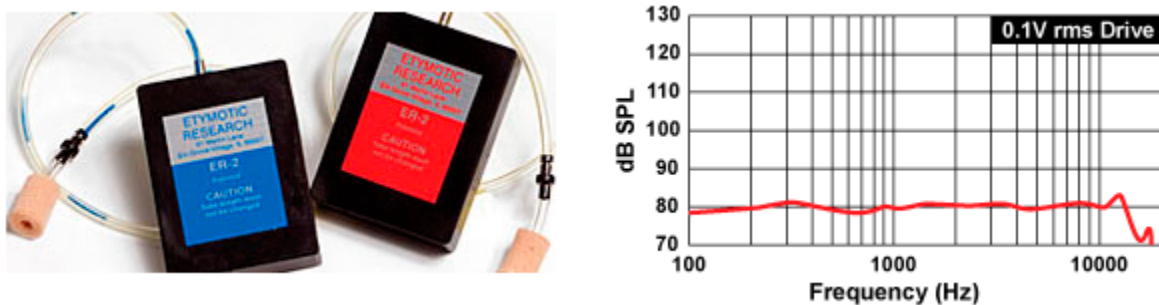


Figure 5.3: The ER-2 Tubephone, and its frequency response. Two tubephones (left and right) are shown in this figure but only one is used in our setup. (source: <http://www.etymotic.com/pro/er2-ts.aspx>)



Frequency response:
 Equalized to flat beyond 10 kHz.
 Top curve: probe tube inlet open.
 Bottom curve: probe tube inlet closed.

Probe tube (silicone):
 OD = 0.95mm, ID = 0.5mm,
 Length: 76mm

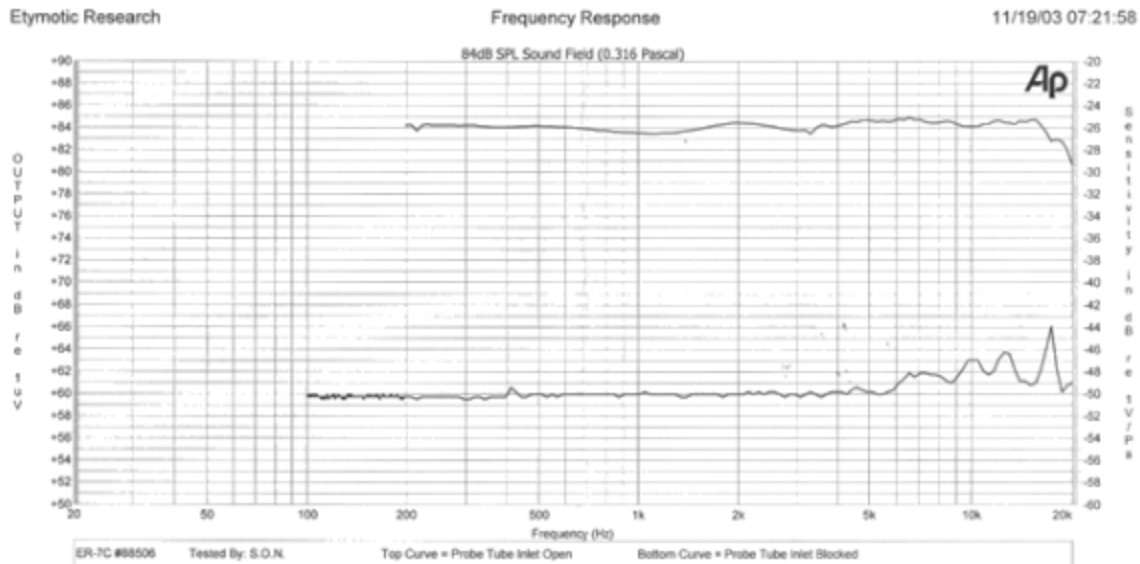


Figure 5.4: The ER-7C probe microphone and its frequency response curve provided by the manufacturer. The top curve (open probe tube inlet) corresponds to our experimental setup.

5.2.2.2 Optical system

The optical system is a type of laser Doppler vibrometer referred to as a hearing laser vibrometer (HLV-1000, Polytec). The HLV-1000 was specifically developed to measure vibrations in the middle ear and in hearing devices. It consists of a controller unit and a compact sensor head connected via a 3-meter-long fibre-optic cable (Figure 5.5A). A key property of the HLV-1000 is the insensitivity of the fibre to vibrations; this is achieved by passing both the reference and measurement beams along the full length of the fibre. The sensor head of the HLV-1000 can be mounted together with a precise beam-positioning system onto a clinical microscope (Figure 5.5B). The microscope magnifies the test surface, allowing a precise positioning of the laser beam on the desired target. The beam-positioning system houses a mirror attached to a handle which allows a user to deflect the laser beam. The sensor head attaches to the inferior end of the system, which mounts onto the microscope at its superior end. The vibrometer controller unit also connects to the acoustical system and to the data acquisition and analysis system.

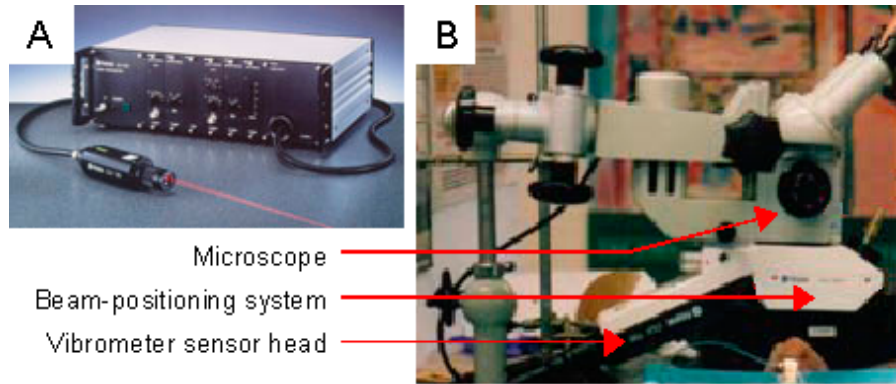


Figure 5.5: A. Picture of Polytec's compact laser vibrometer (CLV). The HLV is a special version of this type of vibrometer. B. Picture of the HLV mounted on a microscope.

5.2.3 Data acquisition and analysis system

The data acquisition and analysis system is responsible for generating the signals that drive the sound-delivery system, as well as for acquiring and processing the audio signals picked up by the microphone and the laser signal measured by the sensor head. It consists of a switch box connected to a data-acquisition board residing in an Intel-based computer with a 1.9-GHz AMD processor, 512 MB of RAM and 80 GB of hard-disk space. The software used for signal processing is VibSoft 4.1 developed by Polytec. The software allows the visualization of velocity, displacement, and SPL signals in both time and frequency domains. The hardware connections allow us to set a reference signal (for example, the SPL signal picked up by the microphone) to which the vibrometer signal can be normalized.

5.3 Experimental considerations

The range of audible frequencies extends from 0.2 to 20 kHz in humans (Vander et al., 2004) and from 0.1 to 60 kHz in gerbils (Ryan, 1976). It would be ideal if we could perform measurements over this entire range. However, some important considerations impose limitations on our measurements and affect the quality of measured signals. Noise sources range from electromagnetic fields, and mechanical vibrations picked up from the environment, to optical noise in the laser signal. These considerations will be presented in this section along with design choices we have made to improve the quality of measurements.

5.3.1 Electro-acoustical considerations

5.3.1.1 Noise considerations

In order to reduce the interference from noise picked up from the surrounding environment, measurements are carried out inside a model C-24 double-walled audiometric examination room (Génie Audio, St-Laurent, QC). Figure 5.6 shows a photograph of the room along with its dimensions. An attenuation graph provided by Génie Audio characterizing the room's acoustic performance is shown in Figure 5.7. The sound-proof room is designed to attenuate acoustical noise, but it is not very effective at blocking low-frequency vibrations.

The ER-7C probe microphone has a flat frequency response up to 10 kHz (see Figure 5.4). Its frequency response for low frequencies (below 0.2 kHz for an open inlet) cannot be assumed to be flat. The ER-2 Tubephone has a relatively flat response between 0.1 and 10 kHz (see Figure 5.3). Its frequency response is not provided for low frequencies (below 0.1 kHz). Beyond 10 kHz the Tubephone is not useful, thus limiting the bandwidth of the measurements.

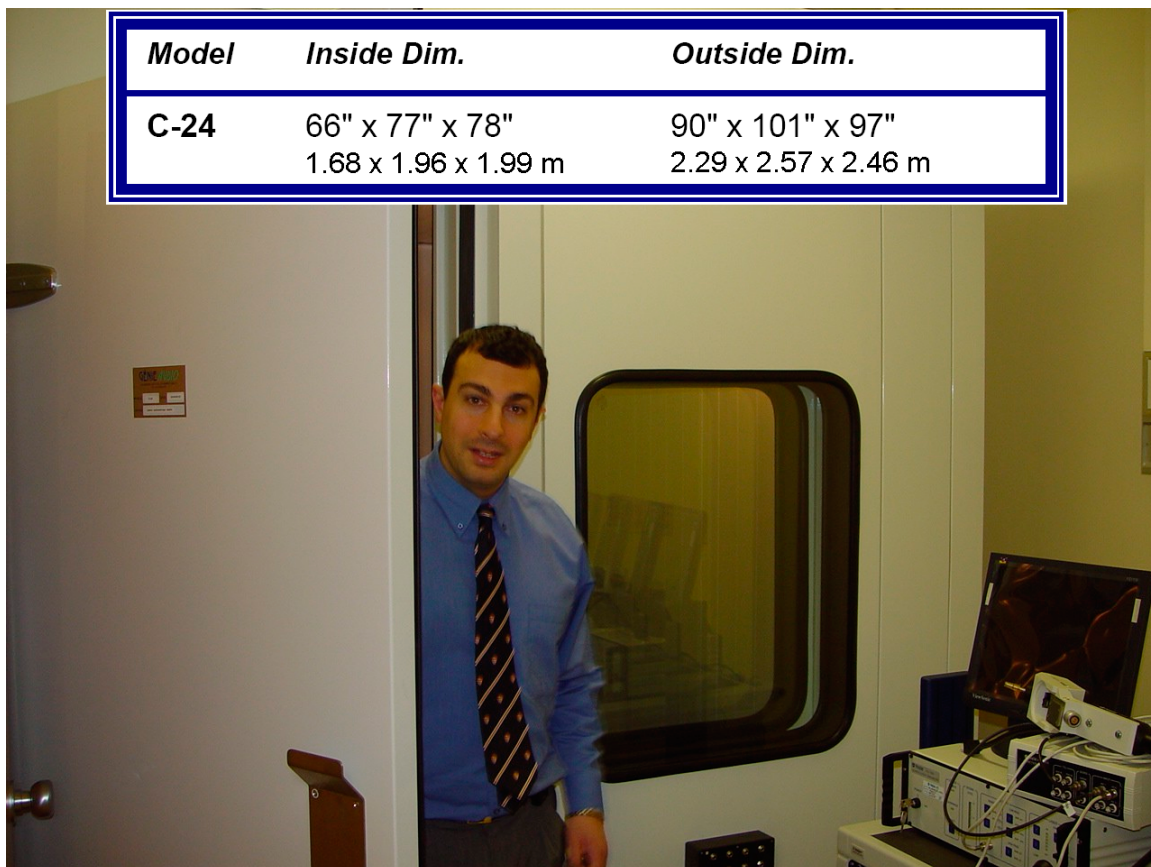


Figure 5.6: The C-24 audiometric examination room.

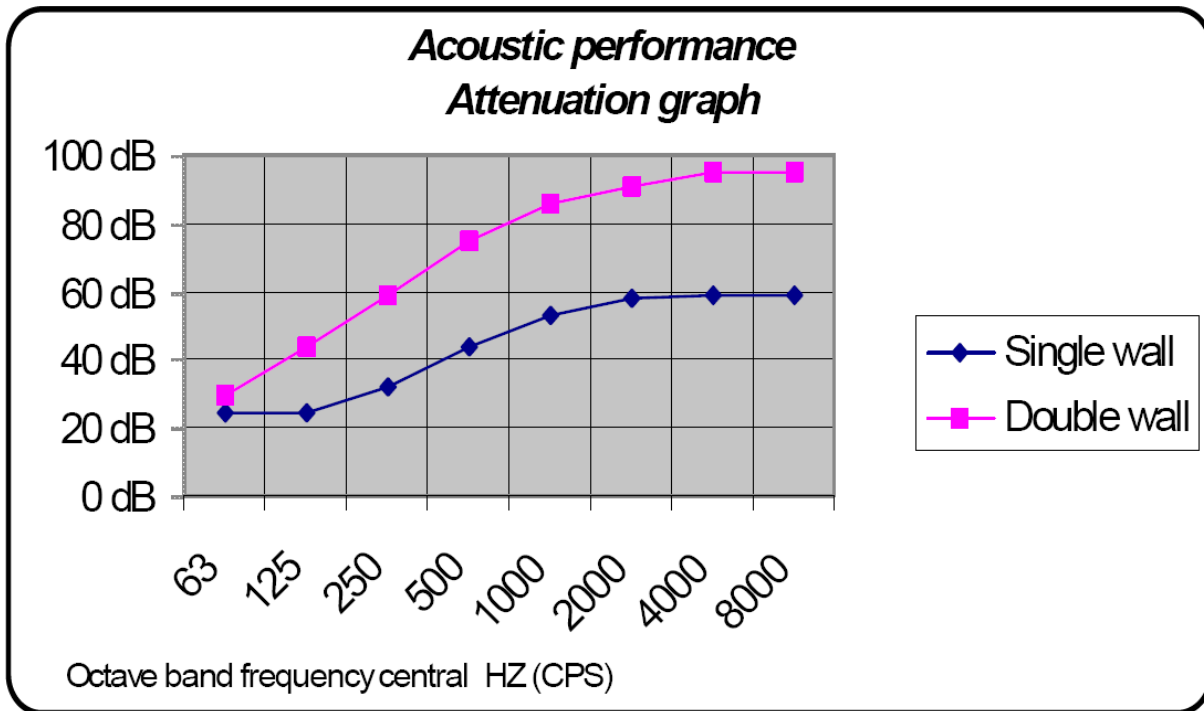


Figure 5.7: Acoustic performance attenuation graph of Génie Audio's sound-proof rooms. The C-24 room where our experiments are conducted is a double-walled room (Source: Génie Audio).

At low frequencies, the velocity of vibrations is inherently low and measurements are more vulnerable to noise. The vibrometer is equipped with a switchable high-pass hardware filter with a cut-off at 0.1 kHz. It is a fourth-order analogue Butterworth filter, with the frequency response shown in Figure 5.8. It is turned on for our measurements. Because of the low signal-to-noise ratio (SNR) observed below 0.15 kHz, the measurements we present in the next chapter will be limited to the frequency range between 0.15 and 10 kHz.

5.3.1.2 Excitation signal

The choice of an appropriate excitation stimulus (signal type and sampling rate) is important in order to achieve an acceptable frequency resolution and SNR. A sinusoidal excitation is good for measuring displacements at a particular frequency with a very high SNR. However, individual measurements at many frequencies would be very time-consuming. Achieving a high frequency resolution would be practically impossible, especially as we have to deal with time variations such as the drying effects discussed in Chapter 6. Noise (white or “coloured”) and sinusoidal sweep signals allow the investigation of a broad spectrum with a high frequency resolution in a

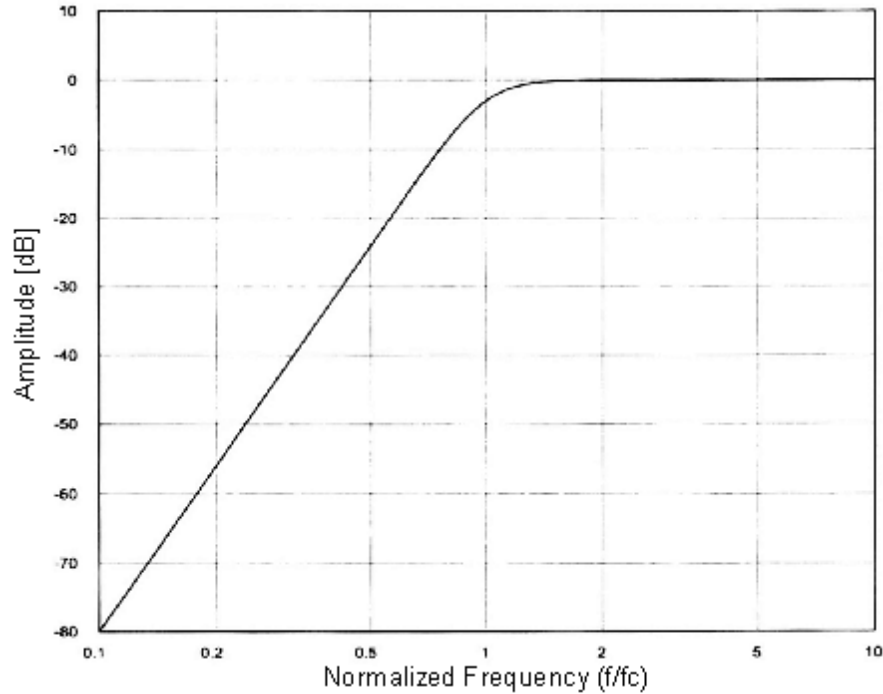


Figure 5.8: Amplitude frequency response of the 4th order Butterworth high pass filter. The frequency axis is normalized to the cut-off frequency. (Source: Polytec HLV hardware manual).

single measurement. A sinusoidal sweep signal “sweeps” through the individual frequencies in the range of interest. The most common are the linear sweep and the logarithmic sweep. The linear sweep has a linear rate of frequency change with a flat frequency spectrum similar to white noise. The logarithmic sweep has a logarithmic rate of frequency change, with a spectrum that emphasizes low frequencies, similar to pink noise. Increasing the time the stimulus spends at low frequencies improves the SNR at those frequencies that are more vulnerable to noise.

The topic of selection of audio excitation signals has been much discussed in the engineering literature. The interested reader can consult, for example, the recent works of Farina (2000), Müller & Massarani (2001) and Mateljan & Ugrinovic (2003) for more information on this subject. In our experimental setup, the selection of signals available with the vibrometer software includes sine, triangle, rectangle, ramp, linear sweep, chirp, white noise, and custom signals. We found that measurements performed with a white-noise excitation were generally noisy even after averaging over 100 samples. After unsuccessful attempts at generating custom signals, the linear sweep was used for our measurements. The use of the linear sweep excitation was previously validated in our lab, when Akache (2005) showed that measurements with individual

sinusoidal stimuli matched those performed using the sweep. We used a 128-ms linear sweep excitation signal over the range from 0.1 to 10 kHz. The closest pre-defined setting we could use for the acquisition bandwidth was 12.5 kHz with a 0.04-ms sampling interval. The vibrometer software uses a 1600-line FFT to compute the frequency-domain signal. The corresponding frequency resolution is 7.8125 Hz. For the reasons given earlier, all the frequencies outside the range 0.15 to 10 kHz are omitted from our plots.

5.3.1.3 Ventilation

For the eardrum to vibrate normally it is necessary that the air pressures in the outer ear and the middle ear be the same. If the air pressure in the middle-ear cavity is larger than the external pressure, the TM bulges outwards; conversely, if the pressure in the middle ear is less than the external pressure, the TM gets sucked inward. In both cases, the mobility of the TM and ossicles is reduced. In living (non-anaesthetized) ears, pressure mismatch is prevented naturally by the occasional opening of the Eustachian tube. For *post mortem* experiments, the pressures can be kept equal by drilling holes to vent the middle-ear cavity and the cavity of the coupler. These vents serve to prevent build up of static pressure inside the cavities. In order to preserve the acoustical properties of a cavity and minimize the effects of drilling a hole, a long thin tube can be inserted in the hole. The tube creates an acoustical open circuit in the frequency range of interest (above 100 Hz) thus preventing sound leakage at those frequencies.

Such a ventilation tube was used for the cavity of the coupler. This vent also prevents the build up of humidity inside the cavity, which could obscure the glass window and contaminate the laser signal. For the middle-ear cavity, we opted for a completely open bulla for most of our measurements. This configuration is generally used in our finite-element models of the middle ear, partly for simplicity of modelling, and partly because many groups conduct experiments with an open bulla to permit manipulation of middle-ear structures. In one specimen, however, a few measurements were performed with a closed bulla, with and without a ventilation tube. This experiment will be discussed in Section 5.4.4.2.

5.3.1.4 Coupler design

The bandwidth over which measurements are performed imposes some restrictions on the design of the coupler used as the acoustical sound chamber. A longitudinal cross section of the coupler is shown schematically in Figure 5.9. The holes for the insertion of the Tubephone, the probe microphone tube and the ventilation tube are drilled with drill-bit sizes of 45 (2.083 mm), 57 (1.092 mm) and 62 (0.965 mm) respectively. The Tubephone and ventilation tube have press fits that provide air-tight seals when inserted. The microphone tube turned out to have a slightly looser fit, but this did not affect the acoustical seal in the frequency range of interest. The outside of the cavity was made conical to increase the surface on which dental cement can be applied to make a solid fixture to hold the gerbil head. The interior of the coupler is cylindrical, with dimensions which prevent an acoustical resonance inside the sound chamber over the frequency range of our measurements. Acoustical resonance involves vibration at high amplitudes at certain “natural” frequencies with little or no energy input. In the case of an air-filled tube with one end closed, when damping is small, the n^{th} longitudinal resonance frequency is related to the length L of the tube according to the equation

$$f = \frac{n \cdot v}{4 \cdot L}$$

where v is the speed of sound in air (340 m/s at 20 C). By setting the first ($n = 1$) resonance frequency to 10 kHz to make sure that it does not fall within our range of excitation, the maximum tube length appropriate for our setup would be:

$$L \leq \frac{340}{4 \cdot 10} = 8.5 \text{ mm}$$

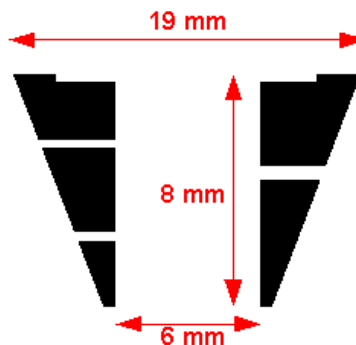


Figure 5.9: Coupler dimensions.

Ideally, we would design the coupler to have a much smaller tube length to make sure the resonance frequency falls far beyond 10 kHz. However, due to constraints on the length of the tube, we designed the coupler with an 8-mm-long cylindrical shape on the inside. (This allows 4 mm for the screws mounting the coupler to the aluminum bar, 4 mm for the holes for tube insertion, and enough room to apply dental cement.) The inside diameter is 6 mm, large enough to allow a full view of the opening of the ear canal. Any transverse resonances due to the diameter of the tube would occur beyond 10 kHz.

These calculations were verified with experimental trials: using a 3-cc syringe, with a hole for inserting the probe microphone and the front end sealed with the TubePhone, we collected several measurements of the SPL within the cavity, each time increasing the volume (and length) of the cavity by pulling the plunger outwards. The SPL curves measured are shown in Figure 5.10. (The ripples in the pressure curves at low frequencies are presumably due to resonances in the probe tube.) As the length of the cavity increases beyond 8.5 mm ($V = 0.5$ ml) we start observing a dip in the SPL indicating a resonance at a frequency below 10 kHz. As expected, the

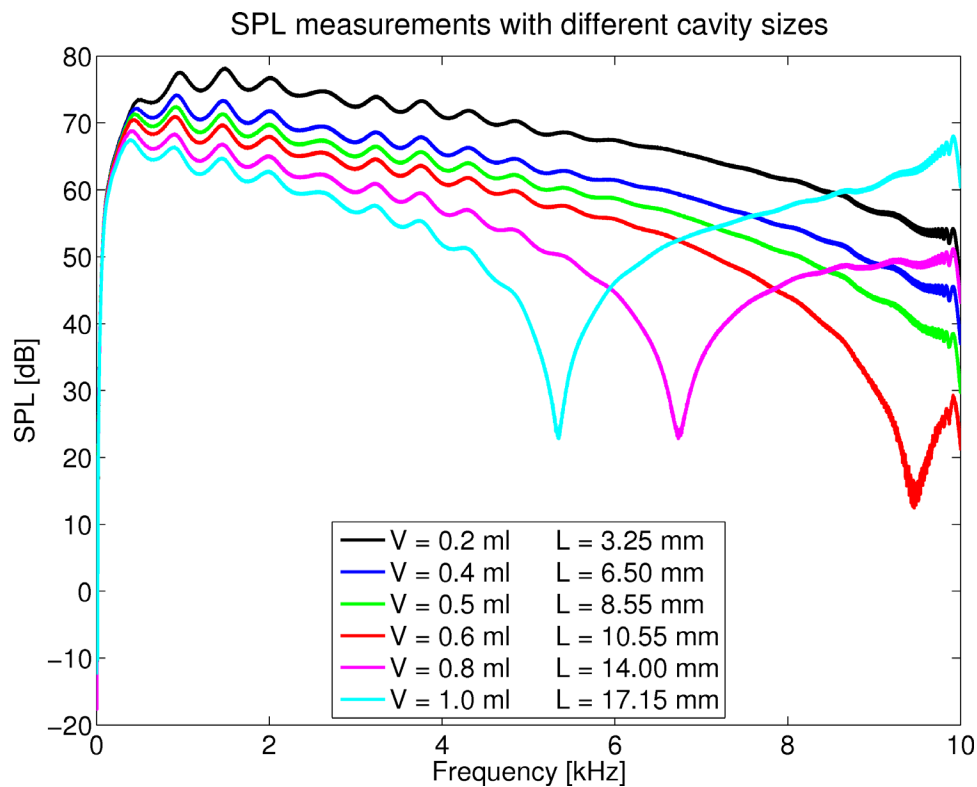


Figure 5.10: Experiment to determine appropriate cavity length.

V denotes the volume of the cavity read on the syringe, and L the length measured with a digital calliper.

resonance shifts to lower frequencies as we continue to increase the size of the cavity. The surface of the plunger of the syringe is not flat. It has a conical shape of height $h = 1.6$ mm. The resonance frequencies observed in Figure 5.10 match the frequencies calculated using the equation above if the height h is subtracted from the values of L indicated on the figure.

5.3.2 Optical considerations

The operation of the vibrometer requires a sufficient amount of light reflecting off the surface of the eardrum. However, the high anisotropy coefficients of biological tissues (between 0.9 and 0.99) cause much light to be lost to forward scattering (Vogel et al., 1996). The slope of the surface of the tympanic membrane relative to the incident laser beam further reduces the amount of back-scattered light. To compensate, we place glass-coated plastic microcarrier beads (Sigma-Aldrich, model G4519, diameter 90–150 μm) at the points of measurement to increase the amount of back-scattered light in the direction of the incident beam and improve the SNR in the measured signal. These micro beads adhere to the moist tympanic membrane by simple capillary force.

Figure 5.11 shows the eardrum observed under the microscope and gives a visual impression of the dimensions of middle-ear structures and the micro beads. It represents one example of the arrangement of micro beads whereby measurements are made across the width of the visible portion of the pars tensa and along the length of the manubrium. The

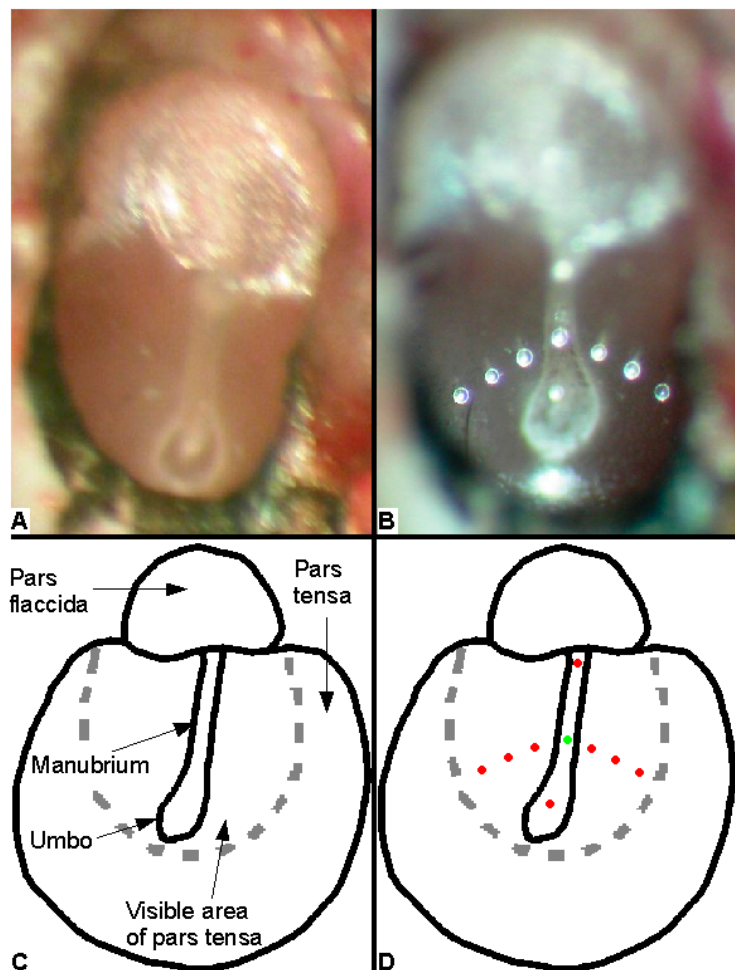


Figure 5.11: A. Photograph of the eardrum under microscope. B. With beads placed at measurement locations. Corresponding schematic diagrams are shown in C and D respectively.

different arrangements realized in the 5 gerbils are presented later in Section 5.4.2.

Decraemer et al. (1989) validated the use of such beads, showing that the bead tends to closely follow the vibrations of the surface it adheres to. They compared frequency responses measured on a bead at the tip of the manubrium and on a brightly reflective spot on the malleus adjacent to the bead. Between 0.13 and 25 kHz, they found that the ratio of amplitudes remained between 0.85 and 1.15 (-1.41 and $+1.21$ dB) and the phase difference remained between -10° and $+25^\circ$.

We performed a similar set of measurements on a bead placed near the tip of the manubrium, and at a naturally reflective spot on the malleus just inferior to the bead. The measured responses are shown in Figure 5.12 along with the noise-floor measured in the absence of the audio stimulus. In this particular case the measurement on the bead is unusually noisy. These measurements were actually taken at a preliminary stage in our experimental work prior to adopting some important measures that have improved our experiments. A comparison with the frequency responses presented in the next chapter would be misleading. Nevertheless, over the frequency

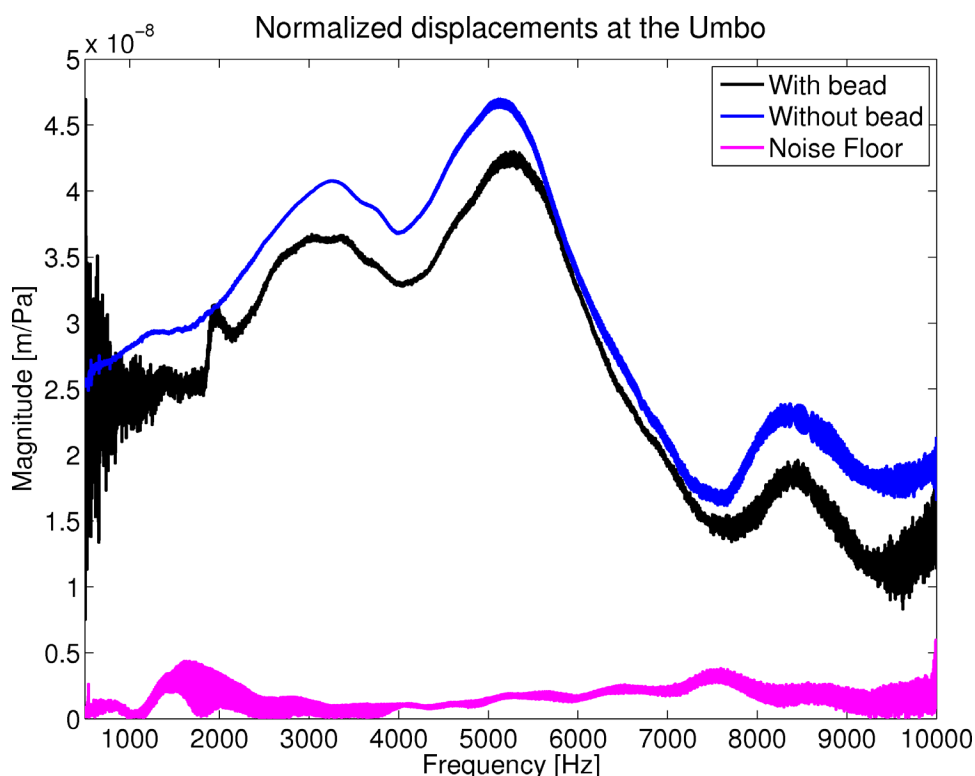


Figure 5.12: Normalized displacements measured on a bead at the umbo and an adjacent point.

range where the signal has an acceptable SNR (between 2 and 9 kHz) the difference between the two curves is less than 2 dB.

There are a few factors that could be contributing to the observed difference. The location of the measurement on the manubrium just inferior to the bead places it further away from the axis of rotation. The distance between the measurement locations is, however, too small to make a significant contribution. Furthermore, the measurement without the bead was taken 5 minutes before the one on the bead. Drying effects (discussed in Chapter 7) could, therefore, make a small contribution to the amplitude difference. A third factor could be that the bead does not exactly follow the movement of the underlying surface. However, the small size of the measured difference provides evidence justifying the use of these beads in our experiments.

Despite the use of reflective micro beads, the strength of the measured laser signal sometimes tended to fluctuate in early experiments, yielding very noisy signals. A real-time, non-averaged observation of the time-domain signal revealed an unstable envelope when this happened. The magnitude of the envelope appeared to fluctuate by about 10 to 20% over a time period on the order of 2 seconds. A small fuzzy glare surrounding the laser beam could be observed through the microscope when fluctuations occurred. The problem was resolved by using the antireflection-coated glass window to cover the sound chamber, instead of the microscope slide used previously. Prior to conducting experiments, the glass window was thoroughly cleaned by removing dust particles with compressed air first, then gently applying a special lens-cleaning solution. These measures drastically improved the stability and quality of measurements.

5.4 Overview of measurements

5.4.1 Specimens studied

Five Mongolian gerbils (*Meriones unguiculatus*) were used in our experiments. Their details are summarized in Table 5.1. Generally, we performed measurements on the left ear to maintain consistency. However, when defects were observed in the left ear after the dissection, the right ear was used instead. Vibration measurements were collected for two studies: the first study is an

investigation of the displacement patterns of the eardrum and the manubrium; the second study is an investigation of *post mortem* time effects due to the drying of middle-ear structures. All five gerbils were used in the vibration-pattern study, and the number of points at which measurements were performed for each gerbil are indicated in the table below. Gerbil 1 was not included in the study of drying effects.

Table 5.1: Details of specimens used in the experiments. The fifth column presents the number of points where measurements were performed. Four out of the five gerbils were used for the study of drying effects.

#	Gender	Weight (g)	Ear	Number of points	Drying-effects study
1	Male	82	Left	8	No
2	Male	63	Left	8	Yes
3	Male	72	Left	9	Yes
4	Male	89	Right	11	Yes
5	Male	69	Left	9	Yes

5.4.2 Location of measurements

Measurements were performed on the gerbil eardrum at multiple points where glass micro beads were placed. Different arrangements were used in different specimens, and are shown schematically in Figure 5.13. In gerbils 1 and 2 measurements were taken along the manubrium and in the inferior and superior portions of the pars tensa. In gerbils 3, 4 and 5 measurements were taken along the manubrium and along a line on the TM orthogonal to the manubrium. In gerbil 4, measurements were taken along both an inferior line and a posterior line. A micro bead was also placed on the pars flaccida in each specimen, but measurements were unsuccessful due to an unusually weak SNR. The bead on the pars flaccida was not easy to locate under the microscope with the laser, and a sufficient amount of reflected light was not obtained. To help explain any unexpected patterns in the measured frequency responses, visible abnormalities in the ear and any foreign objects observed on the eardrum after dissection are documented in Table 5.2. The table also includes special notes about the measurements where needed.

Table 5.2: Special notes for specimens under study.

Gerbil Notes

- 1 Blood clot observed behind the pars flaccida.
Inner end of cochlea broken during dissection.
Measurement at point 2 (lower mid-manubrium) was unsuccessful due to weak SNR.
 - 2 Small bone chip observed on the medial side of the TM close to point 5.
 - 3 Blood clot observed behind the pars flaccida and the manubrium.
Small hair observed on lateral side of the TM adjacent to the bead at point 4.
 - 4 Measurement at point 12 (short process) was unsuccessful due to weak SNR.
 - 5 Measurements were taken before and after opening the bulla.
-

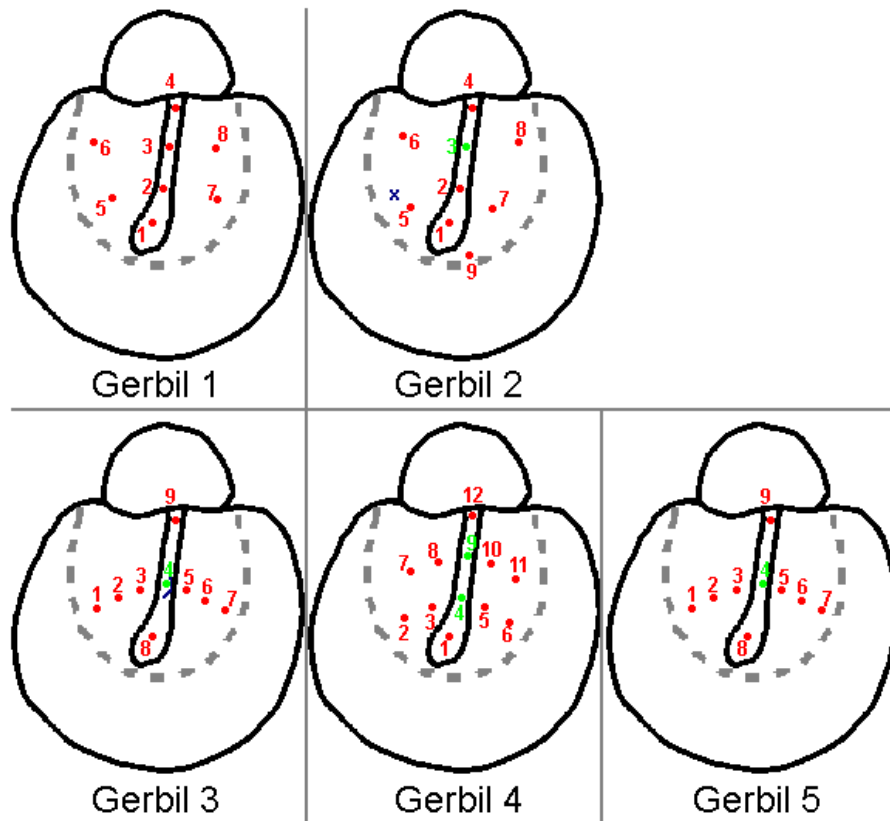


Figure 5.13: Arrangement of beads in all five gerbils studied.
Green points correspond to measurements taken for the study of drying effects.

5.4.3 Cosine correction factor

Displacements recorded by the vibrometer are measured along the direction of the laser beam. To obtain the component of the displacement normal to the plane of the TM (i.e. the plane of the tympanic ring), a cosine factor is used to correct for the angle between the laser beam and the plane of the tympanic ring. In the absence of a goniometer, an instrument capable of accurately measuring this angle at the time of the experiments, a crude estimate was obtained using a 3-D finite-element model of the gerbil middle-ear, as shown in Figure 5.14. The model was rotated so that the ring delimiting the pars flaccida is roughly horizontal, corresponding to what we observe under the microscope (see Figure 5.11). Figure 5.14 shows the plane of the tympanic ring to be roughly parallel to that of the umbo. The angle was calculated as shown in the figure, and the correction factor applied to obtain the normal component of the displacement was:

$$1/\cos(35^\circ) \approx 1.22$$

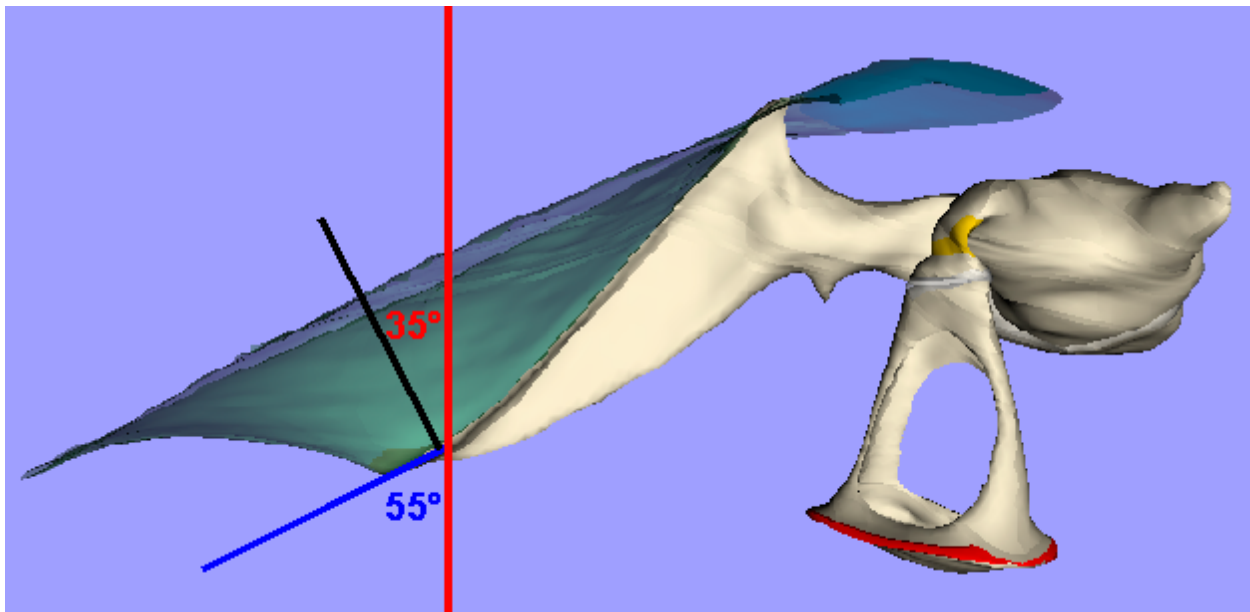


Figure 5.14: Estimation of the cosine correction factor.

Red line designates the laser beam. Blue and black lines are the tangent and normal to the manubrium at the umbo respectively. The plane of the umbo will be considered to be parallel to the plane of the tympanic ring.

5.4.4 Measurement sequence

5.4.4.1 Timing of measurements

Measurements were taken starting between 80 minutes and 4 hours after the animal was sacrificed. This is the time required to prepare the specimen and set up the experiment. Individual measurements were carried out using signal averaging over 100 samples, which takes about 15 seconds to complete. Measurements were carried out at all points repeatedly, in the following sequence:

- Step 1: Two sets of measurements (A & B) were acquired at all points on the eardrum and along the manubrium according to a pre-assigned sequence for each specimen.
- Step 2: Single-point measurements were acquired midway along the manubrium (green points in Figure 5.13) at 5-minute intervals to track the amplitude response for approximately 3 hours. The absorbent tissue was re-moistened one or more times during this step.
- Step 3: Two sets of measurements (C & D) were acquired once again at all points according to the same sequence as in step 1.
- Step 4: One final measurement (E) was acquired at the point midway along the manubrium to provide one last sample for tracking the drying effects.

Table 5.3 summarizes the timing of measurements according to the sequence outlined above. Measurements A and B were usually performed at the beginning of the experiment. Measurements C and D were performed after a series of measurements with 1, 2, 3 or 4 rehydration steps. Since gerbil 1 was not included in the study of drying effects, step 2 consisted of simply re-moistening the absorbent tissue and waiting a few minutes before performing the measurements in step 3, while step 4 was completely omitted. The starting time of an experiment is an important factor when analysing frequency responses, as we shall see in the next chapter. Significant delays were experienced with gerbils 1 and 4 (marked with asterisks in the table). In the first case, we had problems with a dirty glass window which took a considerable amount of time to clean. The absorbent tissue was moistened twice before the experiments were started; the time of initial hydration indicated in the table is the time of the last hydration before

measurement A was recorded. In the case of gerbil 4, the fixture of dental cement broke and the gerbil head fell off the coupler before we began our measurement sequence. Mixing more dental cement and attaching the head onto the coupler again were time consuming.

Table 5.3: Timing of experimental steps (sacrificing, hydration, and measurements) for the 5 gerbils under study. Measurement A is set as the point of reference ($t = 0$ min).

Timing [min]	Gerbil 1	Gerbil 2	Gerbil 3	Gerbil 4	Gerbil 5
Time of death	-210*	-80	-164	-230*	-180
Initial hydration of tissue	-30	-5	-24	-110	-
Measurement A	0	0	0	0	0
Measurement B	6	12	11	23	15
First rehydration of tissue	66	24	30	45	88
Second rehydration of tissue	-	53	102	108	150
Third rehydration of tissue	-	98	162	-	210
Fourth rehydration of tissue	-	174	-	-	-
Measurement C	73	183	198	180	235
Measurement D	94	195	210	199	244
Measurement E	-	203	221	208	260

5.4.4.2 Closed-bulla experiment

A special modification of the measurement sequence presented above was performed in gerbil 5 in order to assess the effect of opening the bulla. In this specimen, measurements A and B, along with 8 consecutive measurements on the mid-manubrium over a period of 19 minutes, were performed with a closed bulla. A small hole (diameter ~ 1 mm) was drilled in the inferior portion of the bulla and a 15-cm PE-50 tube was inserted into the hole (press-fit) for ventilation as explained in Section 5.3.1.3. Other groups have used this method to perform closed-bulla measurements of middle-ear input impedance (cf. Ravicz et al., 1992; Lynch et al., 1994;

Rosowski et al., 2003a). The series of measurements collected during this time tracked possible effects of drying in the closed bulla. While collecting closed-bulla measurements, access to the middle-ear cavity was not possible and the absorbent tissue was not placed until after the bulla was opened.

With the setup kept as stable as possible under the microscope, we turned off signal averaging and proceeded to monitor, in real time, the changes in the frequency response as we opened the bulla. This was a difficult task as even minute vibrations of the setup due to experimental manipulations reduced the SNR. A repositioning of the laser beam was often required. Nevertheless, the frequency response was monitored without averaging at different steps while gradually chipping off parts of the bulla. Opening the bulla increases the effective volume of the middle-ear cavity, thereby leading to a decrease in the load impedance faced by the TM and, consequently, an increase in displacements. This will be further discussed in Section 6.3.3. The rest of the measurements after the first rehydration of the absorbent tissue (including measurements C, D and E) were performed with a completely open bulla.

5.4.5 Sound pressure level

Figure 5.15 shows the sound pressure level (SPL) measured with the ER-7C probe microphone near the eardrum in response to a sinusoidal sweep excitation signal over the frequency range between 0.1 and 10 kHz. 20 recordings (from four sets of repeat measurements on all five specimens) are shown in the figure along with the average. The shape of the curve is consistent among all 20 measurements, and the magnitudes fall within ± 4 dB of the calculated average.

Over the frequency range of excitation, the SPL varies between 45 and 78 dB SPL, remaining above 50 dB SPL up to 9.9 kHz (The dB SPL reference is 0 dB = 20 μ Pa). The shape of the curve is generally smooth. This is important as all vibration measurements will be normalized by dividing the amplitudes of displacements by the SPL. The resulting frequency response will behave predictably if the pressure frequency response is smooth, and the high SPL favours a good SNR in the normalized response.

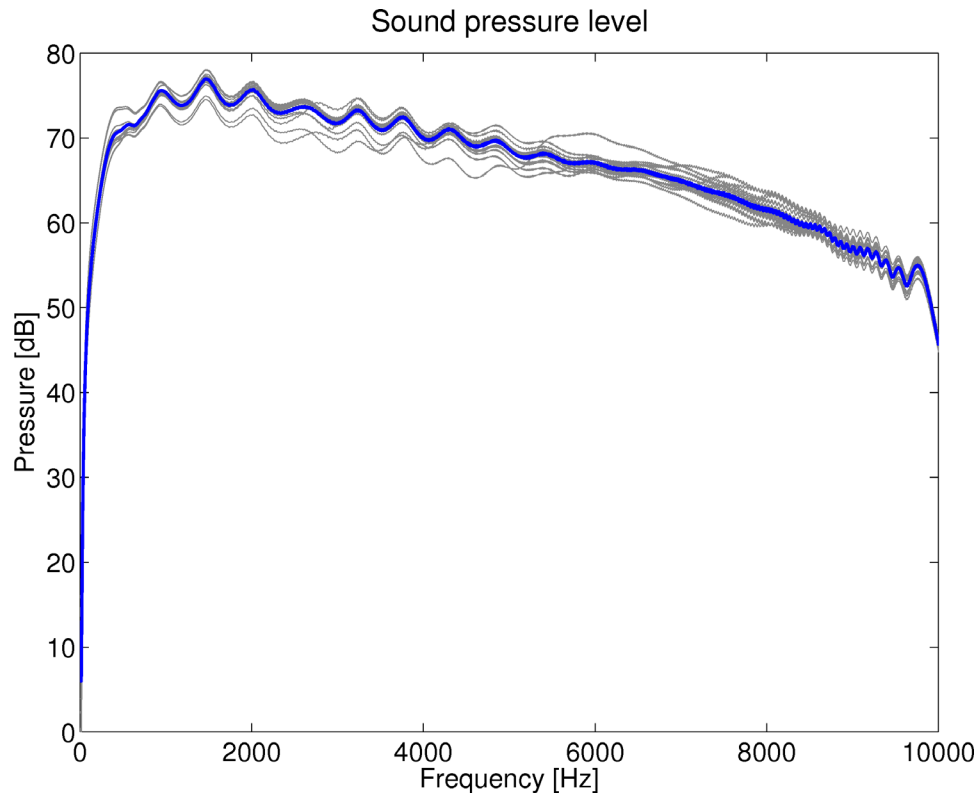


Figure 5.15: Sound pressure level measured near the eardrum. 20 individual measurements (in grey) from 5 specimens are shown with the average (in blue).

5.5 Conclusion

Our experimental protocol employs laser Doppler vibrometry in order to perform displacements measurements on middle-ear structures. The experimental setup that we are using accounts for several electro-acoustical and optical considerations which might compromise the quality of the measurements. In the following chapter we will examine the measurements performed at multiple points on the pars tensa of the tympanic membrane, and track the progression of *post mortem* drying effects by analysing repeated measurements at fixed time intervals.

CHAPTER 6

RESULTS

6.1 Introduction

In this chapter we present measurements performed at multiple locations on the gerbil eardrum. In Section 6.2 we discuss the frequency responses measured at the umbo, address variability between specimens, and provide a comparison with previously reported results. We proceed with a discussion of repeatability in Section 6.3, with an emphasis on the state of the bulla (open/closed) and the effects of drying and rehydration. Spatial vibration patterns along the manubrium and on the TM are presented in Sections 6.4 and 6.5 respectively. The frequency responses presented throughout this chapter are normalized with respect to the sound pressure level (SPL) as described in Section 5.4.5. Unless otherwise indicated, all measurements are plotted on logarithmic axes over the frequency range from 0.15 to 10 kHz.

6.2 Vibrations at the umbo

6.2.1 Displacement frequency response

In this section we present the normalized displacement frequency responses measured at the umbo, the measurement location common to all specimens studied (Figure 6.1). Measurements were selected as explained in Table 6.1 in order to show a consistent pattern suitable for an overall description. Some frequency responses were different in some gerbils, but the discussion of repeatability will be left until Section 6.3. The displacement curves show a flat response at low frequencies, suggesting that the eardrum behaves as a stiffness-dominated system up to at least 0.7 kHz. A slight elevation can be observed between 0.7 and 2 kHz. As mass terms become more significant, displacements increase beyond 2 kHz with 2 peaks observed at mid and high frequencies: a peak between 5.7 and 6.6 kHz and a larger peak between 8.2 and 9.7 kHz.

Although efforts were made to improve the quality of measurements, the signal-to-noise ratio remained low at frequencies below 300 Hz, especially for gerbils 1 and 4. However, examining the curves where low-frequency noise is relatively low, we can say with confidence that the frequency response remains flat below 300 Hz.

Normalized displacements at the umbo

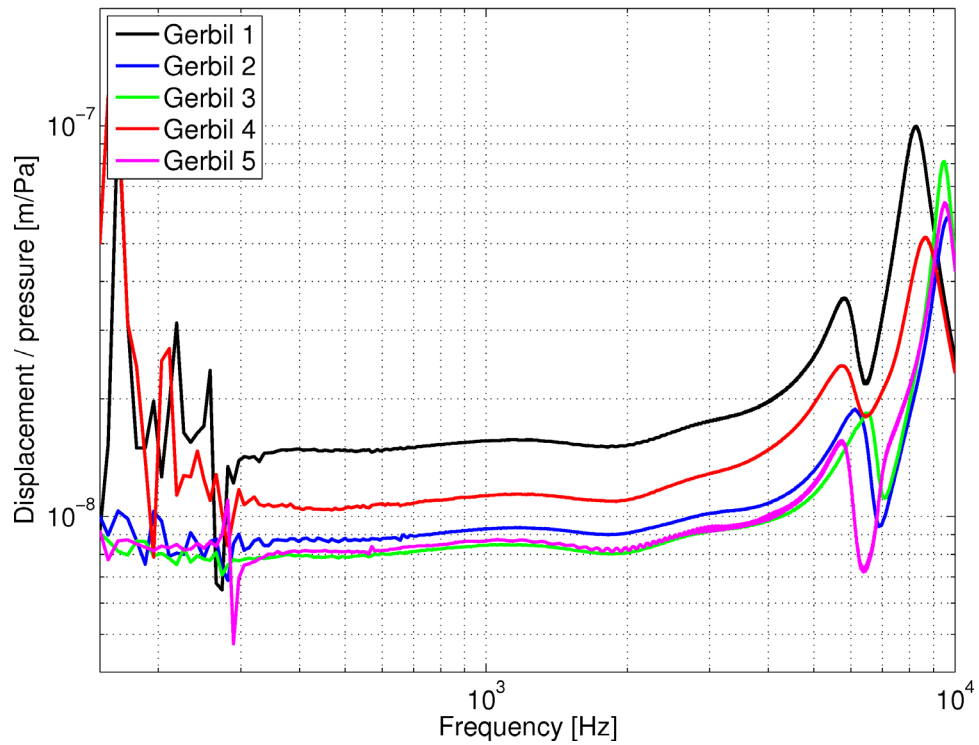


Figure 6.1: Normalized displacement measurements at the umbo in all five gerbils.

Table 6.1: Selection of measurements displayed in Figure 6.1. Generally, the first two measurements (A & B) for each specimen were consistent and measurement A was selected for display.

Gerbil Measurement Comments

1	B	Measurement A had peaks at a lower frequency.
2	A	Measurements A & B were consistent.
3	A	Measurements A & B were consistent.
4	A	Measurements A & B were consistent.
5	C	Measurements A & B were performed with a closed bulla.

6.2.2 Inter-specimen variability

Inter-specimen variability is always a concern when attempting to make a generalized conclusion from experimental measurements. In Figure 6.2 we reproduce the same amplitude frequency responses shown in Figure 6.1 using decibel units for comparison. Ignoring low-frequency noise, the responses in all 5 gerbils fall within a range of 5 dB for frequencies below 5 kHz. The magnitude difference is about 10 dB over the frequency range from 5 to 7.2 kHz where the mid-frequency peak occurs, and about 13 dB for frequencies above 7.2 kHz where the high-frequency peak occurs.

This variability falls within the range found in other studies. Cohen et al. (1993) presented averaged measurements from 5 or 6 gerbils in each age group. The 95 % confidence interval estimated from the standard error bars they presented is between 6 and 16 dB. They describe the error as being ‘relatively constant at all test frequencies’ and as being ‘comparable’ in all age groups. Rosowski et al. (1997) did not specify a measure of variability. They presented measurements from 1 gerbil and stated that “similar results were found in five others”. In humans, the measurements of Goode et al. (1993) from 15 temporal bones and those of Voss et

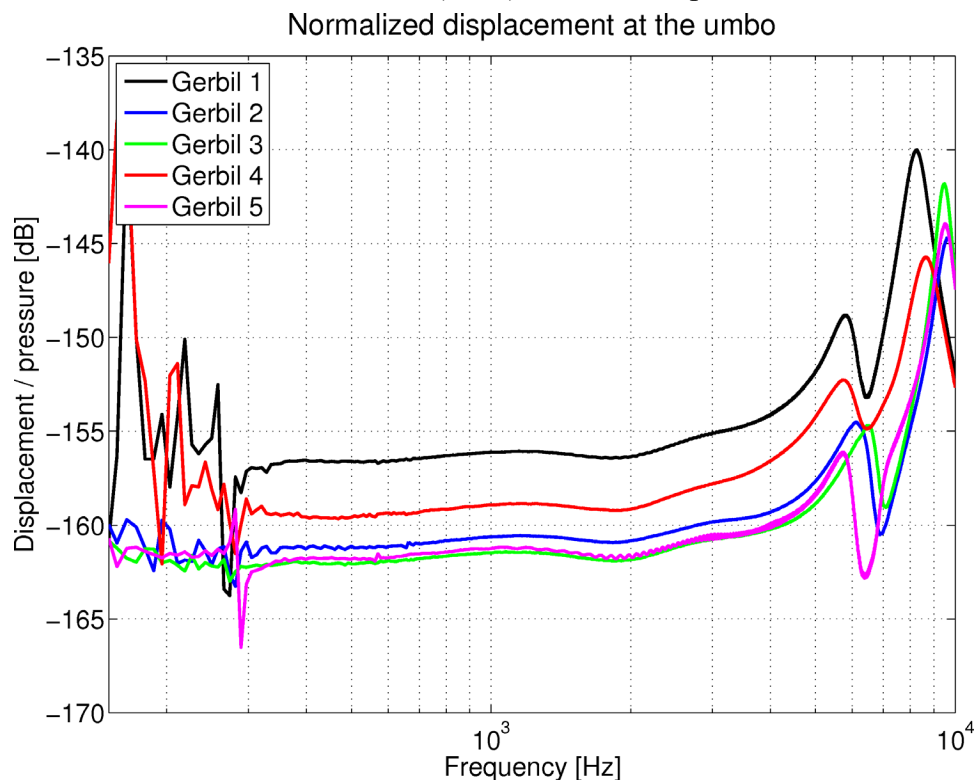


Figure 6.2: Normalized displacement measurements at the umbo expressed in dB.

al. (2000) from 18 temporal bones had a variability of approximately 20 dB. Finally, the 95% confidence interval reported by Rosowski et al. (2004), from 9 LDV studies by other groups, shows a variability of about 20 dB.

6.2.3 Comparison with previous studies

In this section, we compare our umbo displacements with two of the vibration studies presented in Section 3.3.3, namely the measurements of Cohen et al. (1993) and Rosowski et al. (1997), along with the simulation results of Elkhouri et al. (2006). The recent velocity measurements reported by de La Rochefoucauld and Olson (2007) will not be included in the comparison as they present an inherently different acoustical situation (cf. Section 3.3.3).

Figure 6.3 presents a comparison of normalized velocity measurements at the umbo. It was obtained by superimposing our results on those reported by Cohen et al. (1993), for the 42-day-old and adult gerbils, and by Rosowski et al. (1997) with the middle-ear cavity open and closed. The velocities for our measurements were obtained by multiplying the displacements by the frequency (in radians/sec). The measurements presented by Cohen et al. (1993) are peak-to-peak velocity responses to a 100 dB SPL stimulus. For this figure they have been divided by $4\sqrt{2}$ to obtain the appropriately normalized velocity response (a factor of 2 to normalize the response to 1 Pa, a factor of 2 to obtain a zero-to-peak response, and a factor of $\sqrt{2}$ to obtain a RMS response). While the two other groups both found a band-pass behaviour over the frequency range of interest with the same high-frequency roll-off of -1 (or -6 dB/octave), the shapes of their responses show some significant discrepancies: the adult response measured by Cohen et al. has a lower magnitude and steeper slope at low frequencies, and a peak which occurs at a higher frequency than in the response measured by Rosowski et al..

The shape of our responses at low frequencies (linear increase with a slope of 1) is similar to what Rosowski et al. observed in both open and closed measurements. However, the magnitude of our responses is smaller at these frequencies. The measurements of Cohen et al. seem to be of the same order of magnitude as our responses at low frequencies, but have a steeper slope which

NORMALIZED VELOCITIES AT THE UMBO

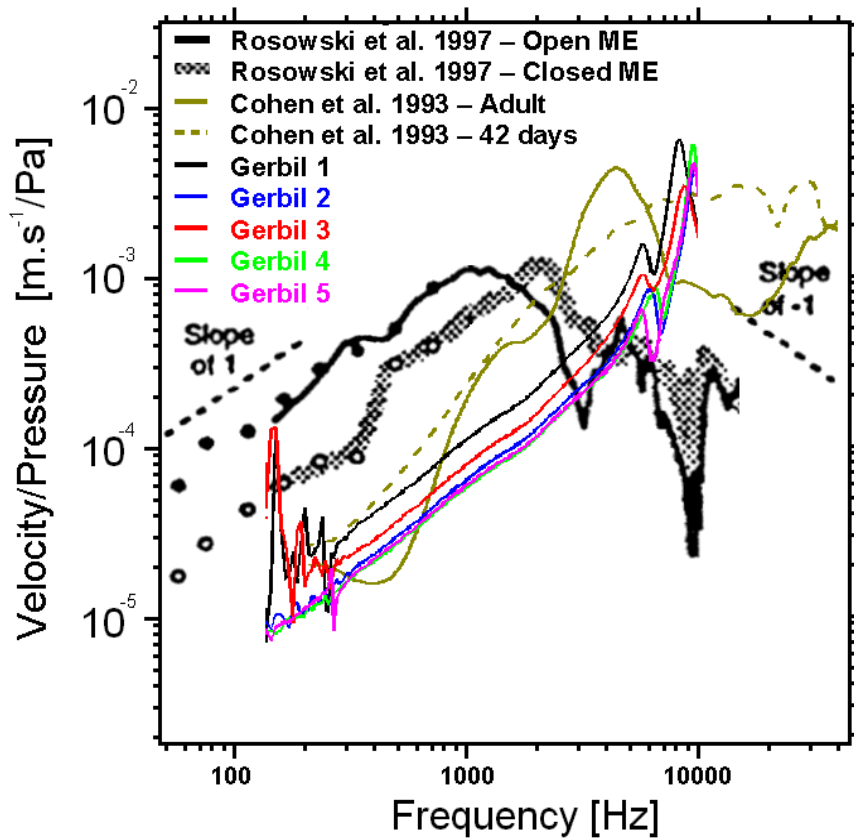


Figure 6.3: Comparison of velocities measured at the umbo in our study with measurements from other groups.

is not characteristic of a stiffness-dominated system. Beyond the low frequencies, our responses exhibit a rapid increase with two pronounced peaks around 6 and 9 kHz. Both other groups observed a single, and relatively wider, peak in their responses at a lower frequency (between 1 and 2 kHz for Rosowski et al., and around 4 kHz for Cohen et al.) followed by a high-frequency roll-off of -1 . Our results may have a minute upward bulge between 0.7 and 2 kHz. This may be equivalent to what we observe around 0.45 kHz in the measurements of Rosowski et al., which they claim is a reflection of a resonance observed in the pars flaccida response (cf. Section 3.3.3). The adult umbo response presented by Cohen et al. may also have a similar behaviour between 1 and 2 kHz.

Table 6.2 compares our low-frequency displacements with those of Cohen et al. and Rosowski et al., as well as with the simulated displacements of Elkhouri et al. (2006). For our measurements,

the displacements were averaged over the frequency range between 300 and 700 Hz, thus avoiding low-frequency noise. The adult response of Cohen et al. does not have flat displacements at low frequencies. The value in the table is the displacement at the lowest frequency, i.e., 200 Hz, obtained from the velocity graph by dividing by the frequency (in radians/sec). For the results of Rosowski et al., displacements were obtained from their open-cavity velocity measurements. A factor of 15% was used to compensate for the 60° angle between their laser beam and the plane of the umbo, which is not corrected for in their published frequency responses (cf. Section 3.3.3). The average reported in the table was calculated from samples obtained with pure-tone excitations between 55 and 700 Hz (marked with black circles in Figure 6.3). The simulation results from Elkhouri et al. were obtained using a uniform low-frequency sound pressure of 1 Pa. Our low-frequency displacements are about 1.5 to 3 times smaller than those reported by Cohen et al., 15 to 28 times smaller than those of Rosowski et al., and 7 to 13 times smaller than the results of Elkhouri et al.

Table 6.2: Comparison of low-frequency displacements at the umbo with results from previous studies.

Gerbil studies	Displacements [nm/Pa]
Gerbil 1	14.8
Gerbil 2	8.7
Gerbil 3	7.9
Gerbil 4	10.6
Gerbil 5	8.1
Cohen et al. (1993)	22.5
Rosowski et al. (1997)	219.8
Elkhouri et al. (2006)	104.5

Several factors could be contributing to the discrepancies described above, including differences in methodology and measurement conditions. Our measurements were performed on *post mortem* gerbils, with the middle-ear cavity completely open. The results from Cohen et al. and Rosowski et al. were obtained from live anaesthetized gerbils with slightly open middle-ear cavities (cf. Section 3.3.3). *Post mortem* effects on stiffness are presumably the main factor contributing to the mismatch in the the magnitude of the response and the frequencies of the peaks. The opening of the bulla could also affect these measurements. While there may also be other factors contributing to the differences observed, *post mortem* effects and the effect of the opening of the bulla will both be further analysed in the remainder of this work.

6.3 Measurement repeatability

6.3.1 Introduction

Since the response of the middle ear changes over time, it is important to investigate the repeatability of measurements. In Chapter 3, drying effects were introduced as an important consideration that affects the stability of *post mortem* measurements (cf. Section 3.4.2). Here, we re-iterate the following findings from Voss et al. (2000):

- In their experiments, the stability of measurements varied from ear to ear, leading them to a distinction between “stable” and “unstable” ears.
- A magnitude drop can be observed in the frequency response over time, and can be attributed to the drying of the TM and other middle-ear structures.
- The effects of drying are partially reversible by moistening of the middle ear with saline.

In the last chapter we introduced the measurement sequence we followed to collect responses at repeated intervals of time (cf. Section 5.4.4.1). In this section, we analyse the repeatability of these responses, addressing issues related to the findings of Voss et al.. After we look at repeated measurements at the umbo, we assess the effect of the state of the bulla (open or closed) on the recorded frequency responses. Finally, we investigate the effects of drying and rehydration by tracking the changes in the measured responses at low and high frequencies.

6.3.2 Repeatability at the umbo

Figures 6.4 to 6.8 show the repeated measurements performed at the umbo in all 5 gerbils. Each figure shows four normalized displacements (measurements A, B, C, and D) along with the ratio of each measurement to measurement A, expressed in dB. The amplitude ratios are useful for quantifying the repeatability only at low frequencies, since the frequency shifts of the peaks make a simple amplitude comparison irrelevant at high frequencies. These figures are best interpreted with reference to Table 5.3 presented in Section 5.4.4.1. In most cases, the pair of measurements C–D, taken after rehydration steps, exhibits larger differences (at least at low frequencies) than the initial pair of measurements A–B.

6.3.2.1 Low-frequency magnitude changes

Ignoring the high level of low-frequency noise in some measurements, we summarize the amplitude ratios at low frequencies for each gerbil in Table 6.3. These ratios are grouped by pairs with similar measurement conditions (B/A and D/C). The values in the table were calculated over the lower frequency range, before the peaks occur. Except for gerbil 1, all the ratios in the table fall within 2 dB. The large ratio between measurements A and B in gerbil 1 can be attributed to drying effects, which are particularly significant in this specimen due to the long time that had elapsed before measurements were started. The large ratio D/C is mainly due to the erratic behaviour of measurement C, which is not representative because a drop of saline was accidentally deposited on the infero-posterior side of the TM while moistening the absorbent tissue. The somewhat erratic behaviour was also observed in other measurements taken around that time close to that region of the TM, and decreased as the TM dried. For gerbil 3, measurements A and B are almost overlapping, with B slightly larger than A, resulting in a positive amplitude ratio.

Table 6.3: Summary of amplitude ratios measured at low frequencies in all 5 gerbils.

Ratio [dB]	Gerbil 1	Gerbil 2	Gerbil 3	Gerbil 4	Gerbil 5
Measurements B / A	–5	–2	+0.3	–2	–0.5
Measurements D / C	–8	–0.5	–0.3	–2	–1

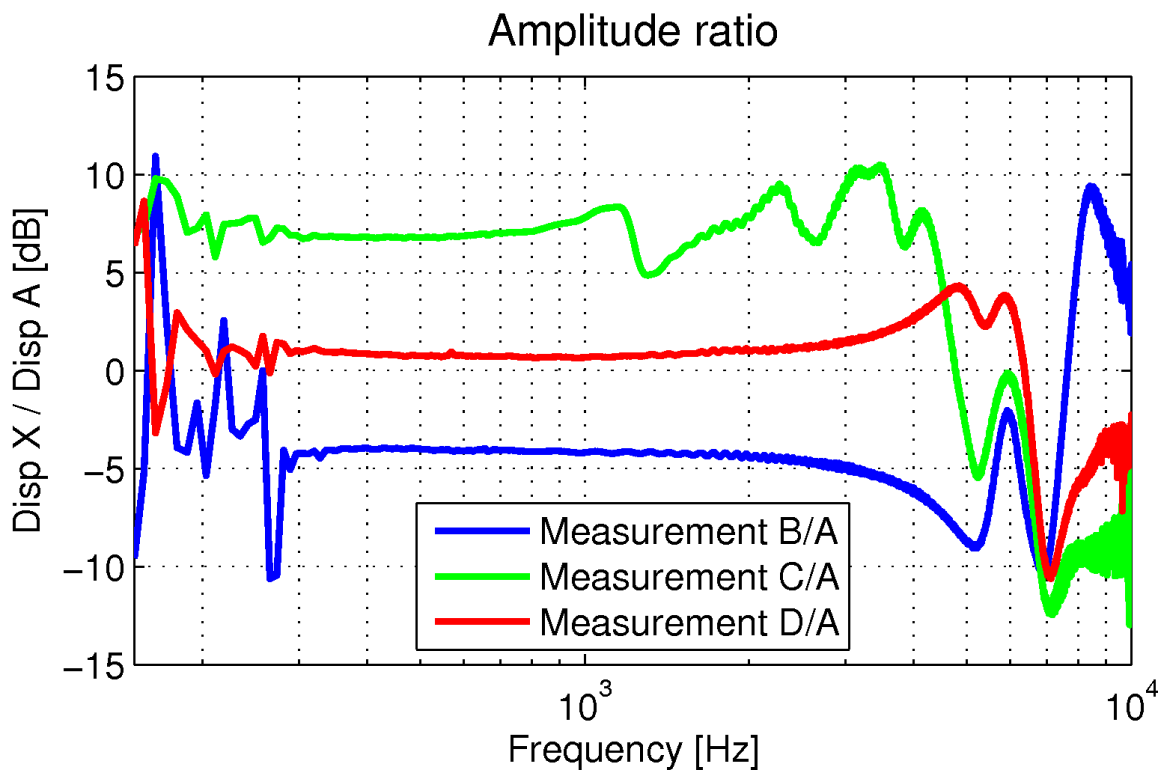
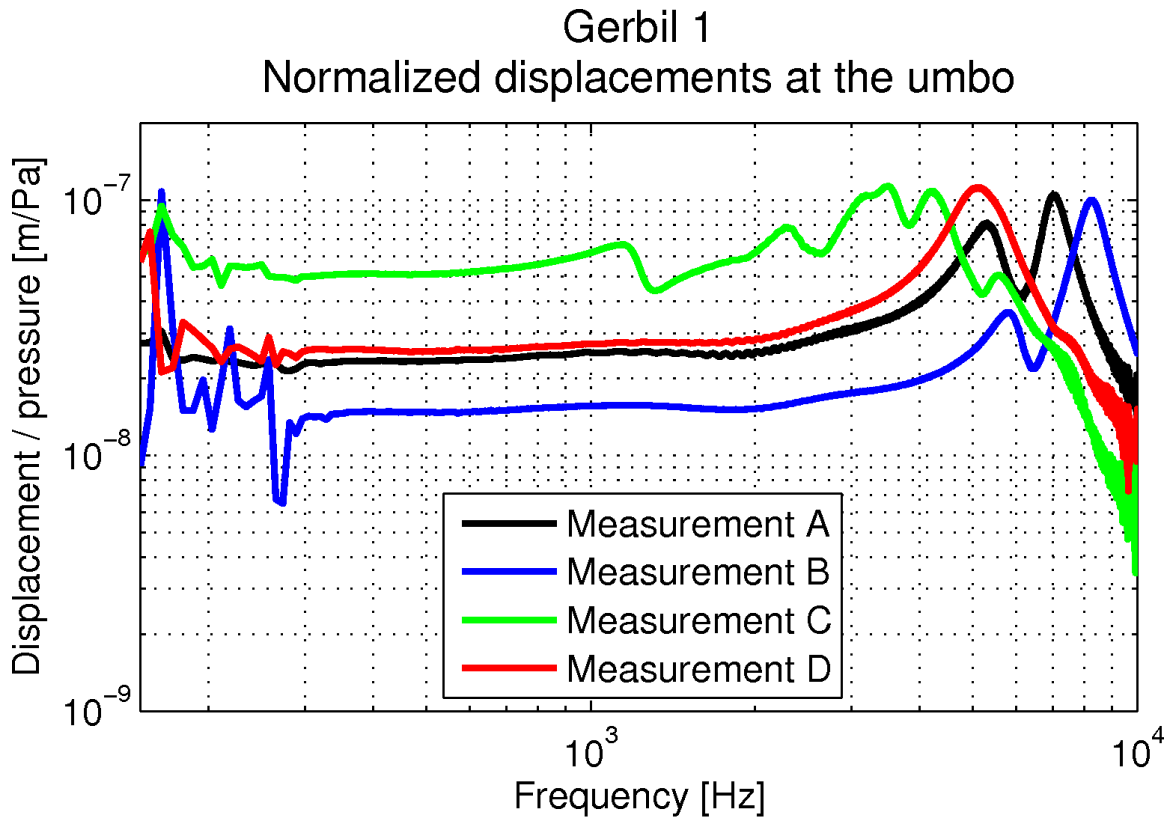
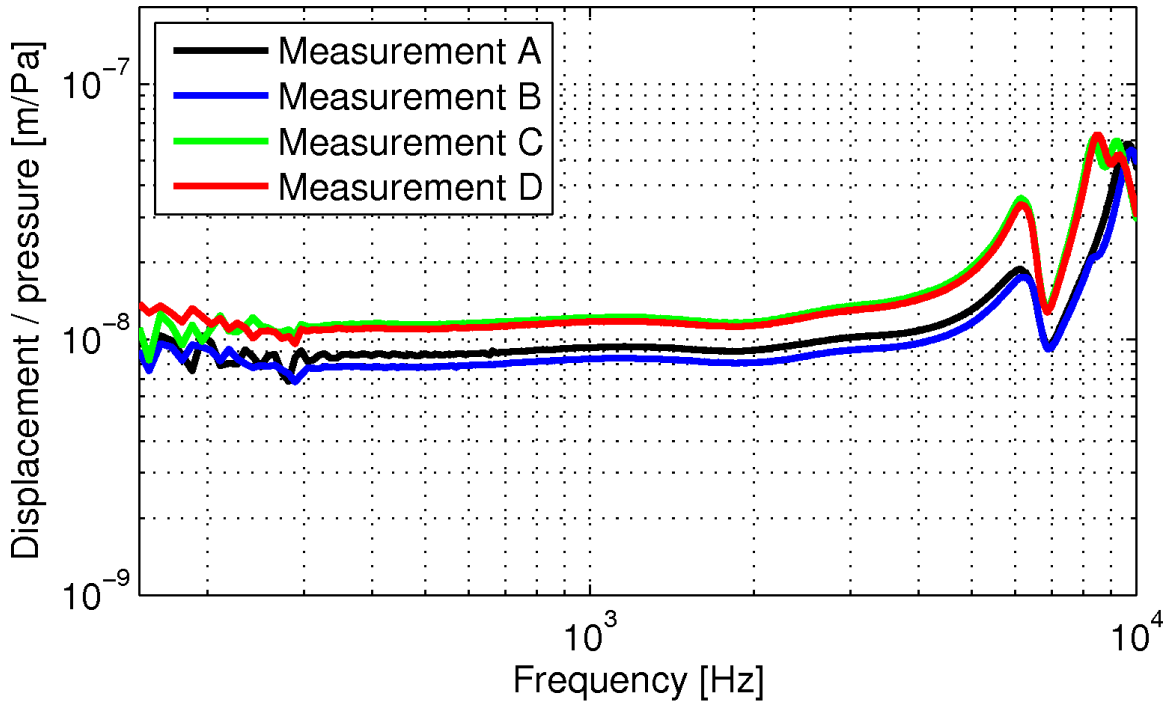


Figure 6.4: Assessing measurement repeatability at the umbo in Gerbil 1.
TOP: Normalized displacements. Bottom: Amplitude ratios with respect to Measurement A.

Gerbil 2 Normalized displacements at the umbo



Amplitude ratio

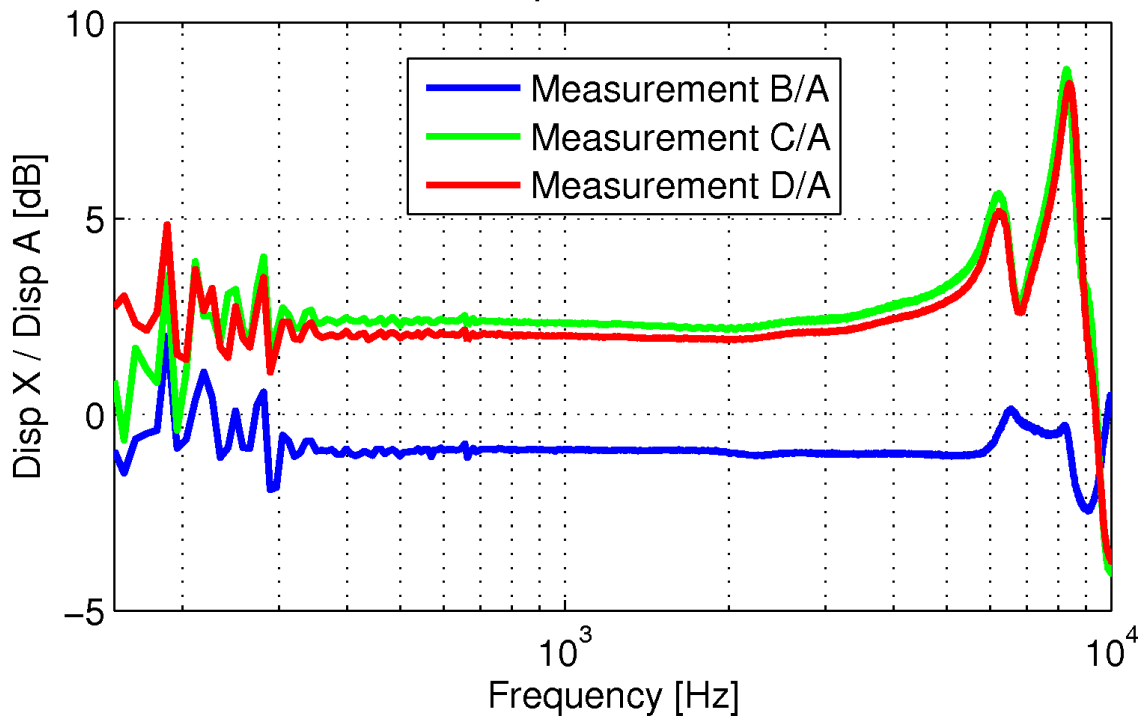
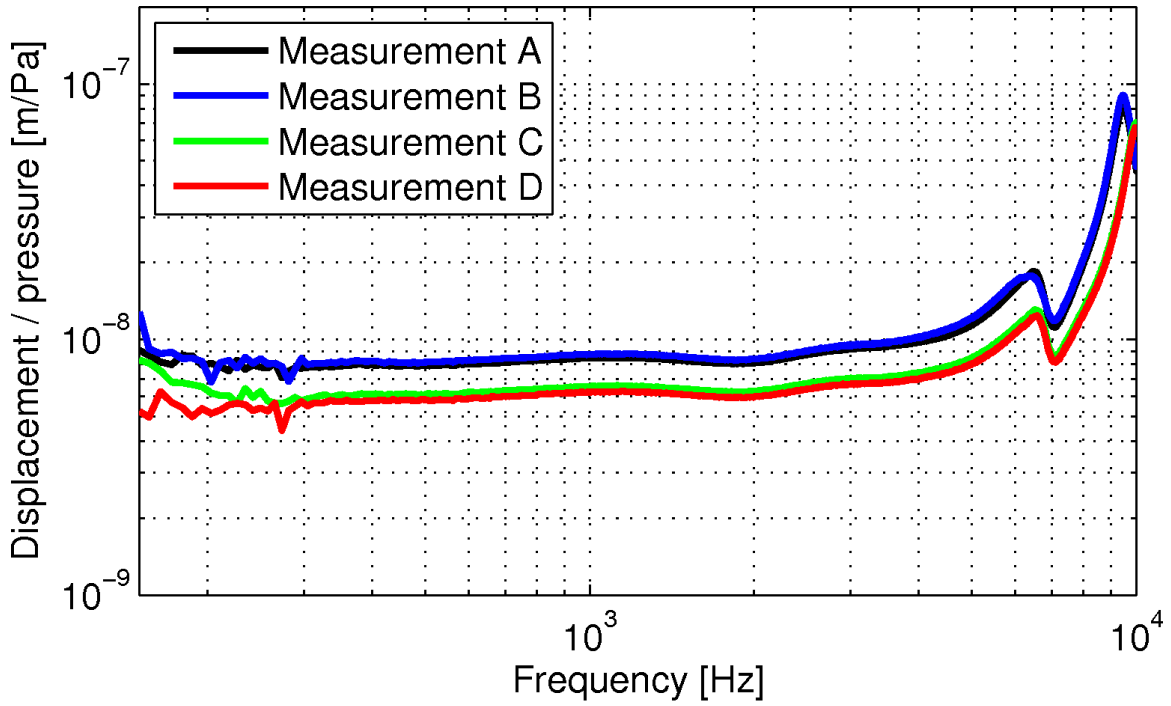


Figure 6.5: Assessing measurement repeatability at the umbo in Gerbil 2.
TOP: Normalized displacements. Bottom: Amplitude ratios with respect to Measurement A.

Gerbil 3 Normalized displacements at the umbo



Amplitude ratio

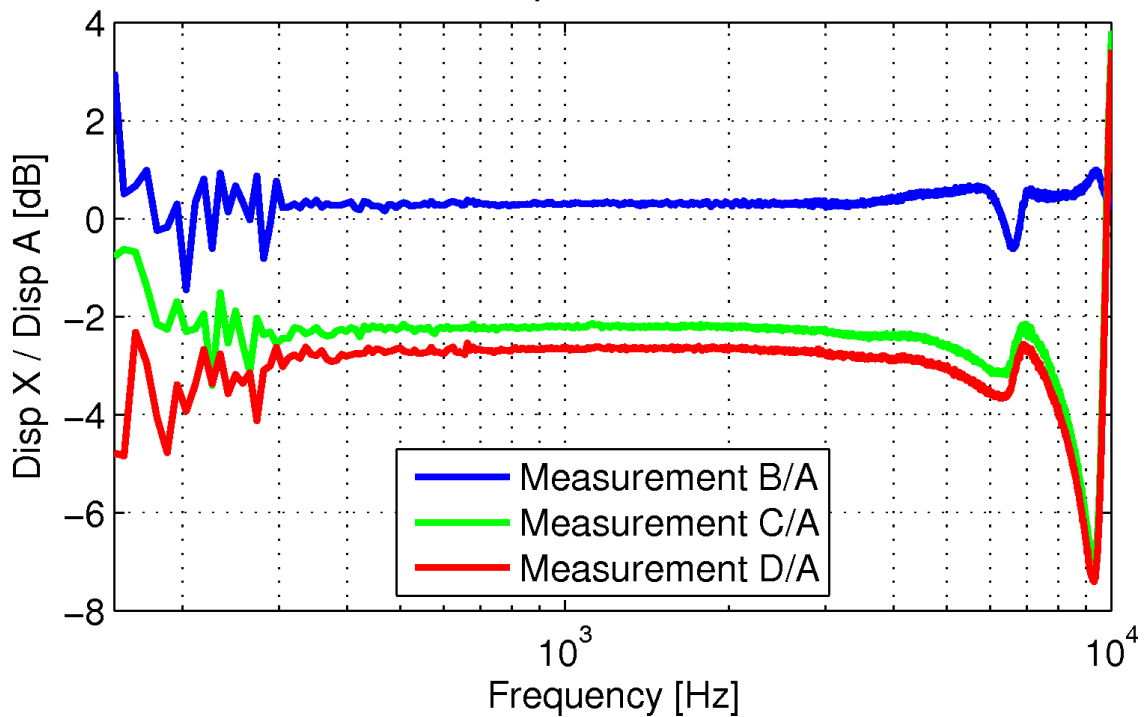
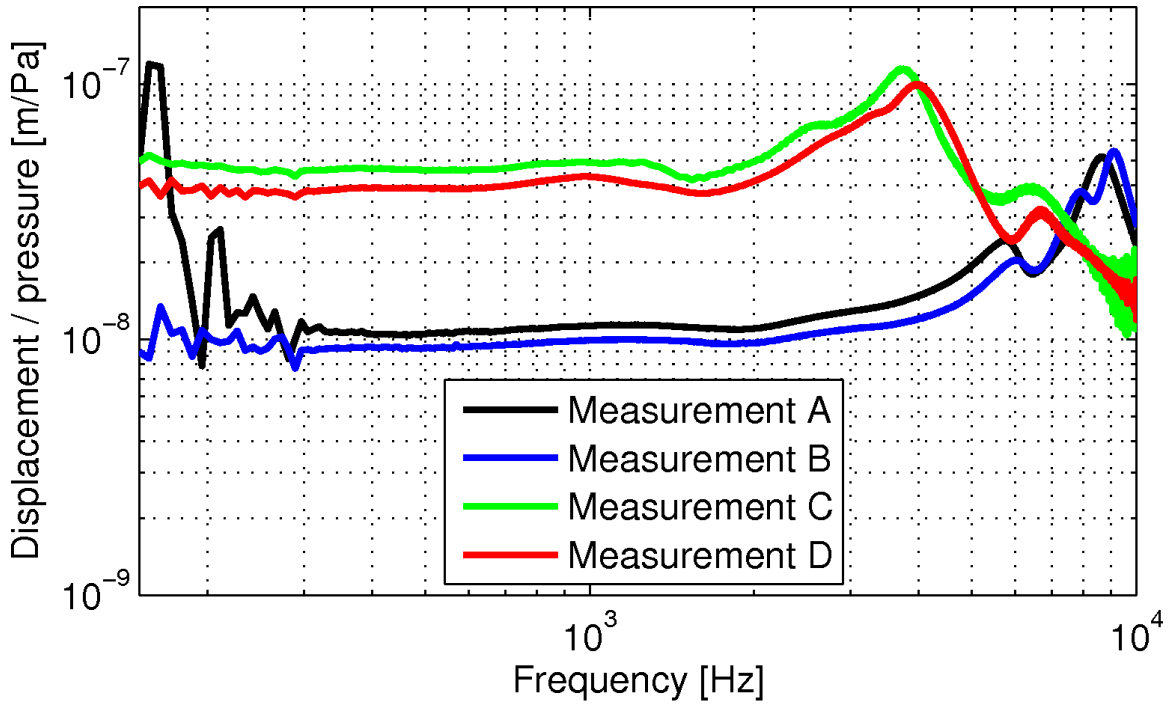


Figure 6.6: Assessing measurement repeatability at the umbo in Gerbil 3.
TOP: Normalized displacements. Bottom: Amplitude ratios with respect to Measurement A.

Gerbil 4 Normalized displacements at the umbo



Amplitude ratio

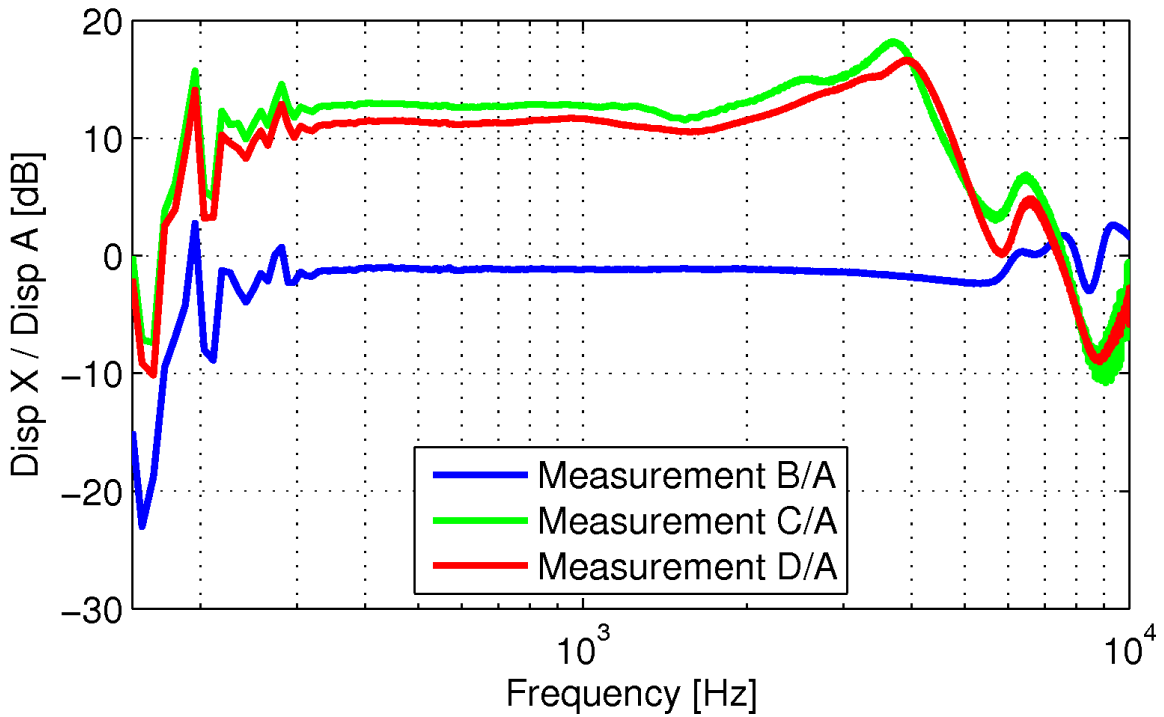
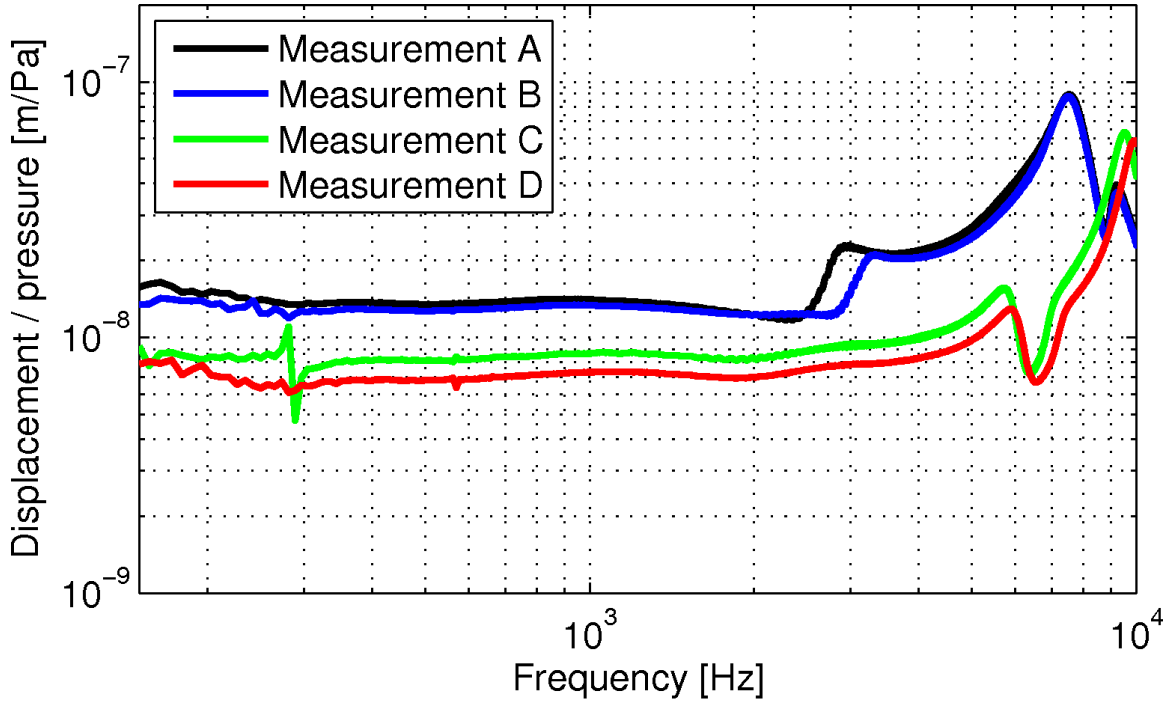


Figure 6.7: Assessing measurement repeatability at the umbo in Gerbil 4.
TOP: Normalized displacements. Bottom: Amplitude ratios with respect to Measurement A.

Gerbil 5 Normalized displacements at the umbo



Amplitude ratio

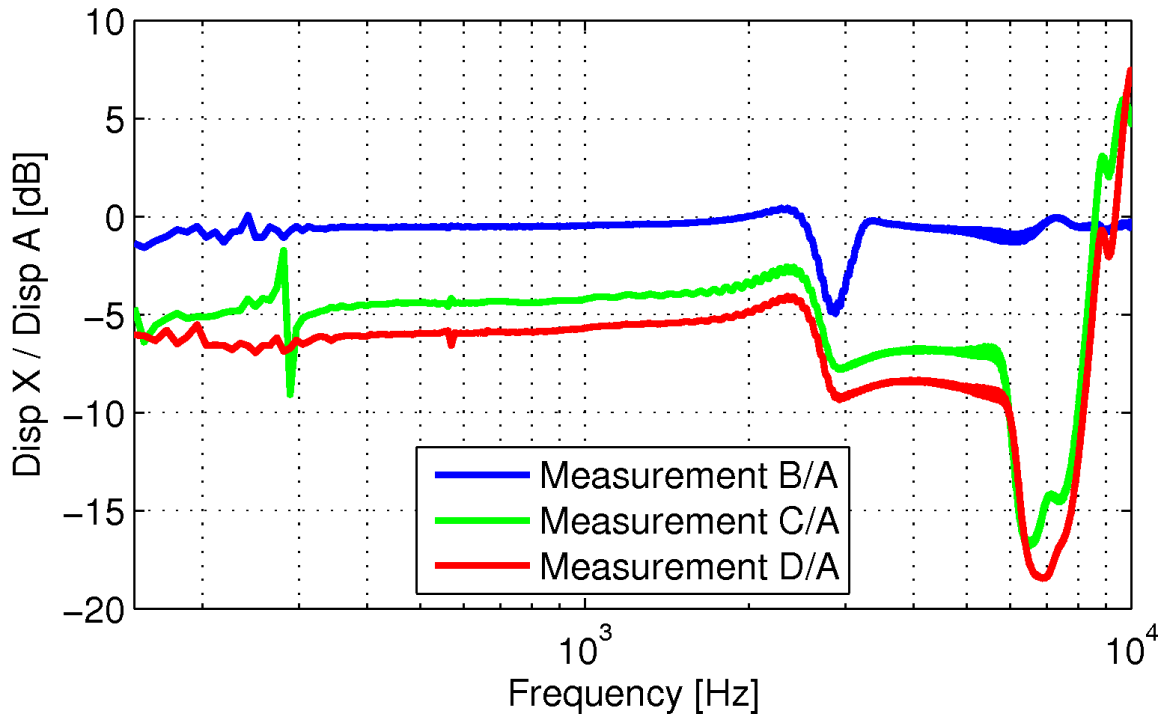


Figure 6.8: Assessing measurement repeatability at the umbo in Gerbil 5.
TOP: Normalized displacements. Bottom: Amplitude ratios with respect to Measurement A.

6.3.2.2 High-frequency shifts

At high frequencies the assessment becomes more complicated. There is generally a positive frequency shift of the peaks with time. This can be observed in the plots of normalized displacements between each pair of measurements (A–B and C–D) in all five gerbils (excluding the erratic measurement C in gerbil 1). We attribute this change to the drying of the TM, as rehydration tends to shift the peaks back to lower frequencies. This will be discussed further in Section 6.3.4, but here we note two particular observations. In some measurements, the two peaks seem to merge into one after rehydration (see measurement D in gerbil 1, and to some extent measurements C and D in gerbil 4). This might be due to remoistening the absorbent tissue with more saline than usual in these specimens. The resulting peak occurs around 5 kHz in gerbil 1 and 4 kHz in gerbil 4. This single peak has shifted closer to the ones observed by Cohen et al. (1993) and by Rosowski et al. (1997) in live ears, which could suggest that an increased rehydration makes the *post mortem* middle ear behave more like a live one. In some other measurements, the peak around 9 kHz seems to break up into two distinct peaks over time (see measurements C, D and to some extent B in gerbil 2, and measurement B in gerbil 4). It is impossible to decide whether this is a measurement artefact or an effect of further drying of the middle ear, as these effects are highly variable from ear to ear.

Finally, the changes in the frequency response in gerbil 5 are related to the opening of the bulla. In this specimen, measurements A and B were performed with a closed bulla while C and D were performed with an open bulla. This will be further discussed in the next section.

6.3.3 Open/closed bulla configurations

The experiment to compare the open-bulla and closed-bulla configurations was described in Section 5.4.4.2. We re-iterate that the closed-bulla setup featured a small hole in the inferior portion of the bulla in which a ventilation tube was inserted. Without the tube, the hole drilled in the bulla would introduce an anti-resonance in the mid-frequency range, like the one observed by Rosowski et al. (1997). To study the effect of the ventilation tube we performed two consecutive measurements, with and without the tube, at a point midway along the manubrium, within a 1

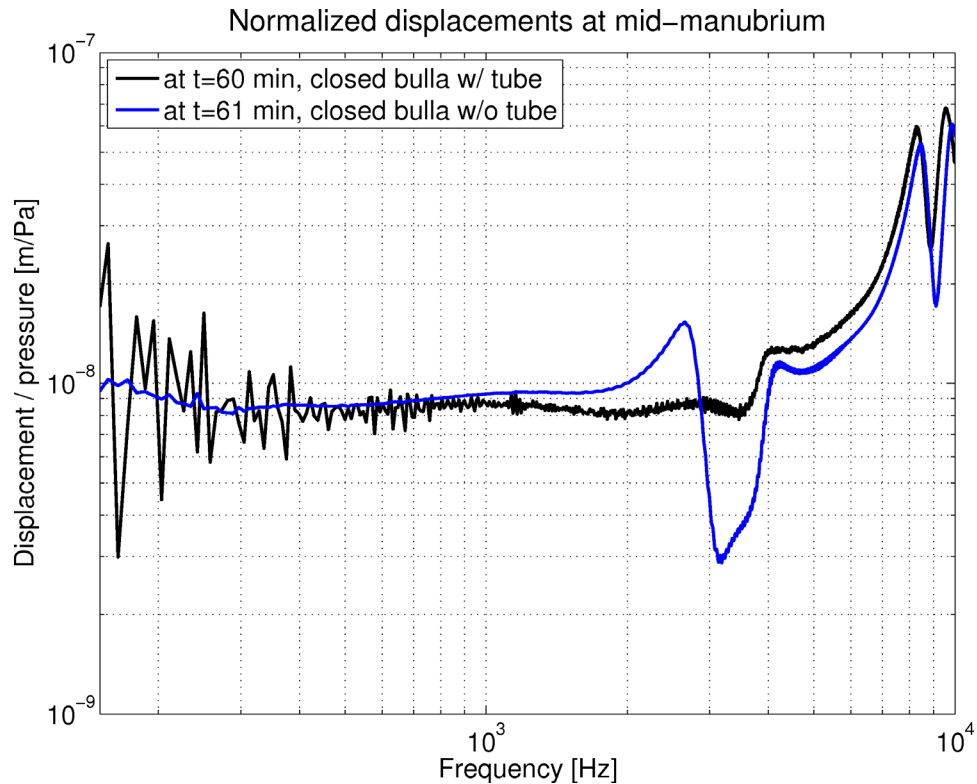


Figure 6.9: Validating the use of the ventilation tube in closed-bulla measurements.

minute interval. The recorded frequency responses are shown in Figure 6.9. The responses are similar up to around 1 kHz. The response in the second measurement (without the tube) increases over the mid-frequency range beyond 1 kHz until an anti-resonance is reached around 3 kHz, where a quick drop towards a local minimum is observed. Beyond this frequency the two responses converge to a similar shape, the second response remaining slightly below the first. The frequency at which the anti-resonance occurs and the relative behaviour of the two responses are similar to what Rosowski et al. (1997) observed in their measurements (cf. Figure 6.3).

After the measurement without the tube (at $t = 61$ min) we proceeded with real-time monitoring of the frequency response as we gradually opened the bulla. Since we could not monitor the real-time changes and record the measurements at the same time, only a qualitative description of the changes is presented here. The next recorded measurement was performed after the bulla was opened completely and the hydrated absorbent tissue was placed in the middle-ear cavity (at $t = 88$ min). Since no measurement was recorded with the open bulla prior to initial rehydration, the effects of drying and rehydration (discussed in the next section) were probably combined

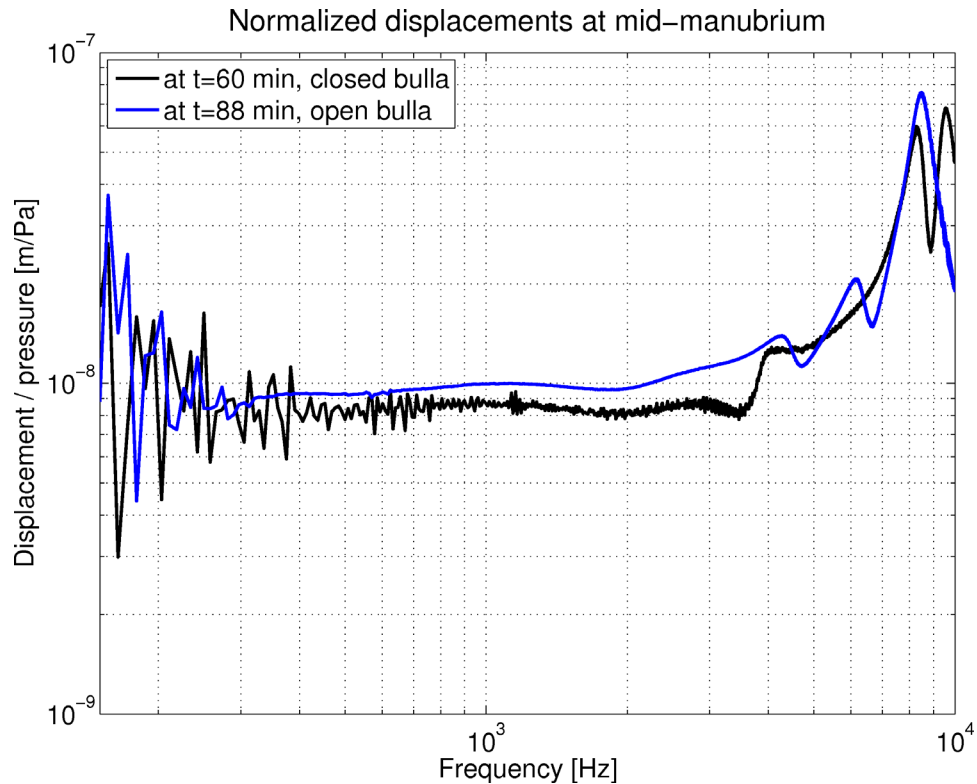


Figure 6.10: Comparing open and closed bulla configurations.

with the effects of opening the bulla. The comparison will therefore be limited to the shape of the frequency response. In Figure 6.10 we present the last closed-bulla measurement (with the ventilation tube) and the first recorded open-bulla measurement. Tracking of changes in the frequency response before and after these measurements will be shown in Section 6.3.4.

The closed-bulla measurement shows a flat response up to approximately 3.5 kHz, a sudden magnitude increase around 4 kHz and 2 large peaks at 8.2 kHz and 9.5 kHz. The open-bulla measurement features a flat low-frequency response, a gradual increase with frequency beyond 2 kHz, 2 small local maxima around 4.2 kHz and 6 kHz, and a large peak around 8.5 kHz. Between those measurements, we noted an immediate positive frequency shift as soon as the bulla was opened, the peak at the highest frequency going beyond the measurement range. Magnitude changes were difficult to quantify due to a low SNR caused by motion due to experimental manipulations. However, a small overall magnitude drop was observed as the bulla was opened even though an increase was expected (cf. Section 5.4.4.2).

6.3.4 Drying and rehydration experiments

The experiments presented in this section were designed to track the effects of drying of the middle ear, which we observed first in the frequency responses recorded in gerbil 1. The protocol, which was carried out in all subsequent specimens, also aims to quantify the effect of rehydrating the middle ear. As described in Section 5.4.4.1, we performed a large number of measurements at short time intervals as the middle ear dried out, and periodically rehydrated the middle ear by remoistening the absorbent tissue with drops of saline. We present here a tracking of the changes in the frequency responses recorded over time, in the form of magnitude changes at low frequencies and frequency shifts at high frequencies. In gerbils 2, 3 and 5, all the measurements were performed at the same point midway along the manubrium (cf. Figure 5.13 in Section 5.4.2) without moving the laser beam. In gerbil 4, measurements were alternated between two points along the manubrium, but only the responses at the lower point will be presented because both points behaved essentially the same.

6.3.4.1 Tracking of magnitude changes at low frequencies

Figures 6.11 to 6.14 present a low-frequency tracking of magnitude changes in gerbils 2 to 5 respectively, at four discrete frequencies (1.0, 1.5, 2.0, and 2.5 kHz). Measurements A, B, C, D, and E are indicated by labels along the time axis, and the times of rehydration by red triangles. At first glance, we note that in each plot the four curves behave similarly (except for two special instances at 2.5 kHz in gerbils 4 and 5, that will be addressed later), affirming that these plots are representative of low-frequency behaviour.

There is an overall trend of decreasing magnitude over time between rehydration steps that is common to all the gerbils. The trend is a more or less exponential decay with small amplitude fluctuations. Moreover, the slope of the decay is variable among specimens and between different rehydration steps within the same specimen. At the time of the next measurement following a rehydration (5 minutes after rehydration) we observe an increase in magnitude. The size of the magnitude increase is not the same at each rehydration step, and may depend on (1) how dry the middle ear was before remoistening the absorbent tissue, and (2) how much

saline was used during the rehydration step. Exceptions and specific observations for each specimen are presented next.

- In gerbil 2, the local minimum observed at measurement C (at $t = 183$ min) is very likely to be an artefact. This was confirmed by observing the amplitude responses measured at the other 8 beads during that step. These responses remained slightly greater than or equal to the ones measured in the next step (measurement D). Many factors could affect a single measurement, such as an imperfect laser signal or sound pressure, or mis-aiming the laser beam.
- In gerbil 3, the response for measurement B (at $t = 11$ min), is larger than the one for measurement A (at $t = 0$), contrary to what is expected due to drying effects. This is also consistent with the responses observed at the umbo during these steps (cf. Figure 6.5). The next measurement taken after rehydration, however, has an amplitude which is lower than B but, as expected, higher than A.
- In gerbil 4, the large maximum observed after the second rehydration (at $t = 108$ min) is more pronounced around 2.5 kHz. This is a result of a large frequency shift that occurred in this specimen, and will be discussed further in the next section.
- In gerbil 5, measurements up to $t = 61$ min were performed to track magnitude changes before opening the bulla. During this period a decrease in magnitude is observed at low frequencies, just as in the case of open-bulla measurements. The sudden jump in magnitude observed at $t = 61$ (labelled with a blue triangle), especially around 2.5 kHz, is the effect of removing the ventilation tube as discussed earlier in Section 6.3.3.

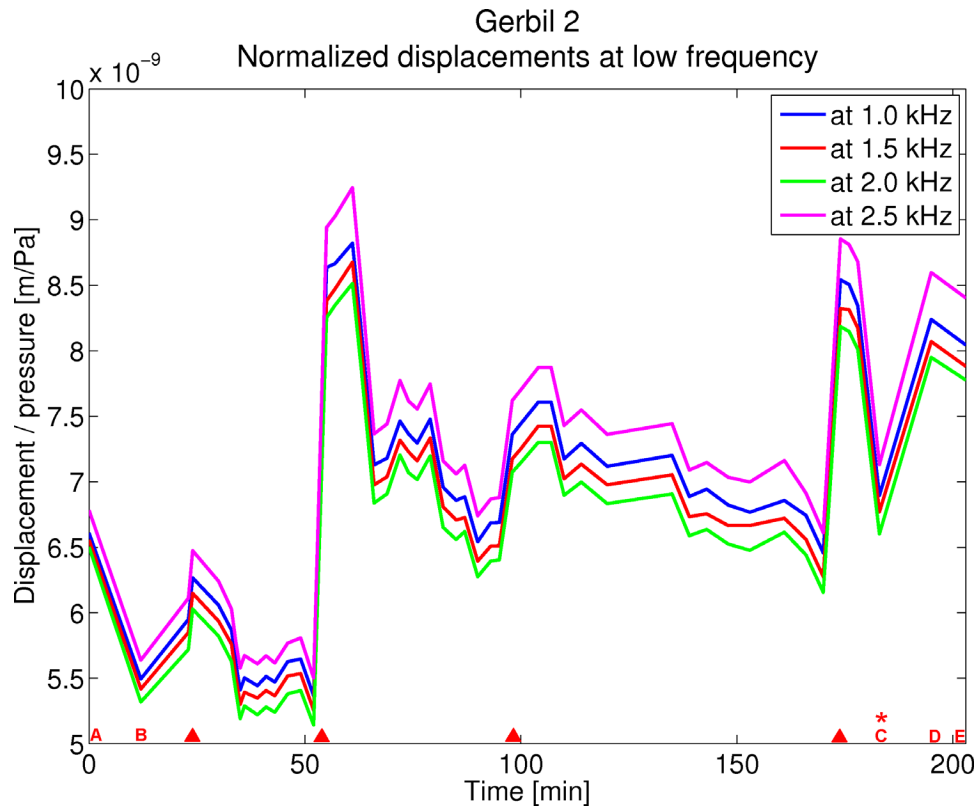


Figure 6.11: Tracking magnitude changes over time in gerbil 2, at 1.0, 1.5, 2.0 and 2.5 kHz. Times of rehydration indicated by \blacktriangle . Exceptions marked with (*) are explained in the text.

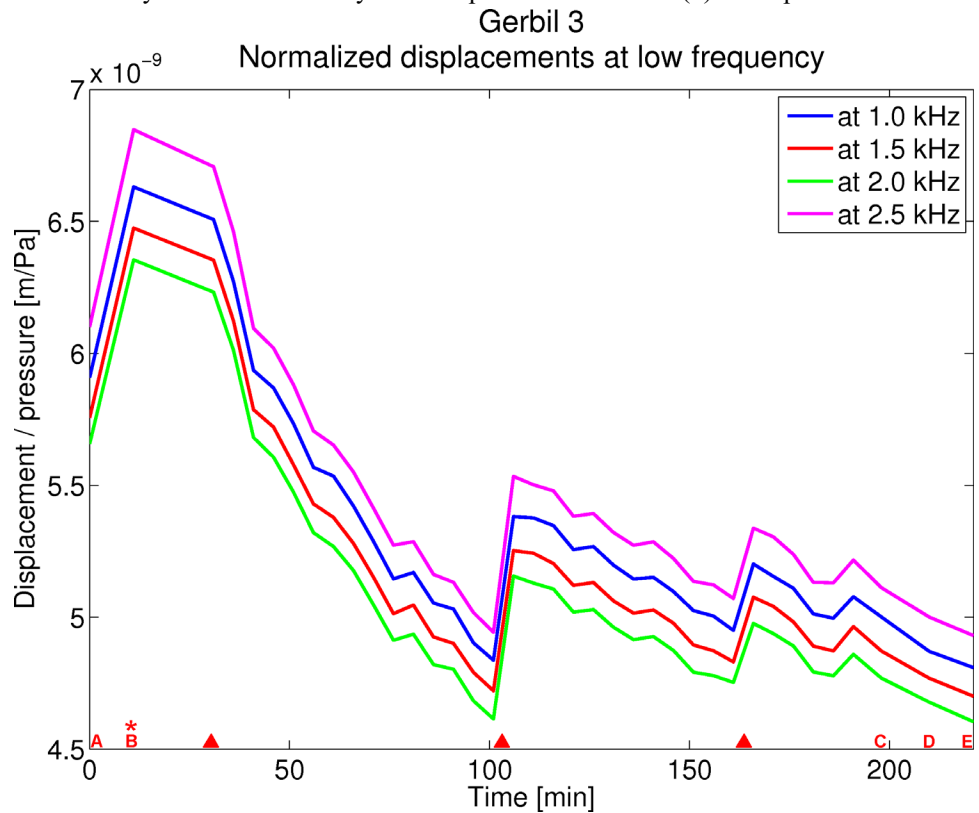


Figure 6.12: Tracking magnitude changes over time in gerbil 3, at 1.0, 1.5, 2.0 and 2.5 kHz. Times of rehydration indicated by \blacktriangle . Exceptions marked with (*) are explained in the text.

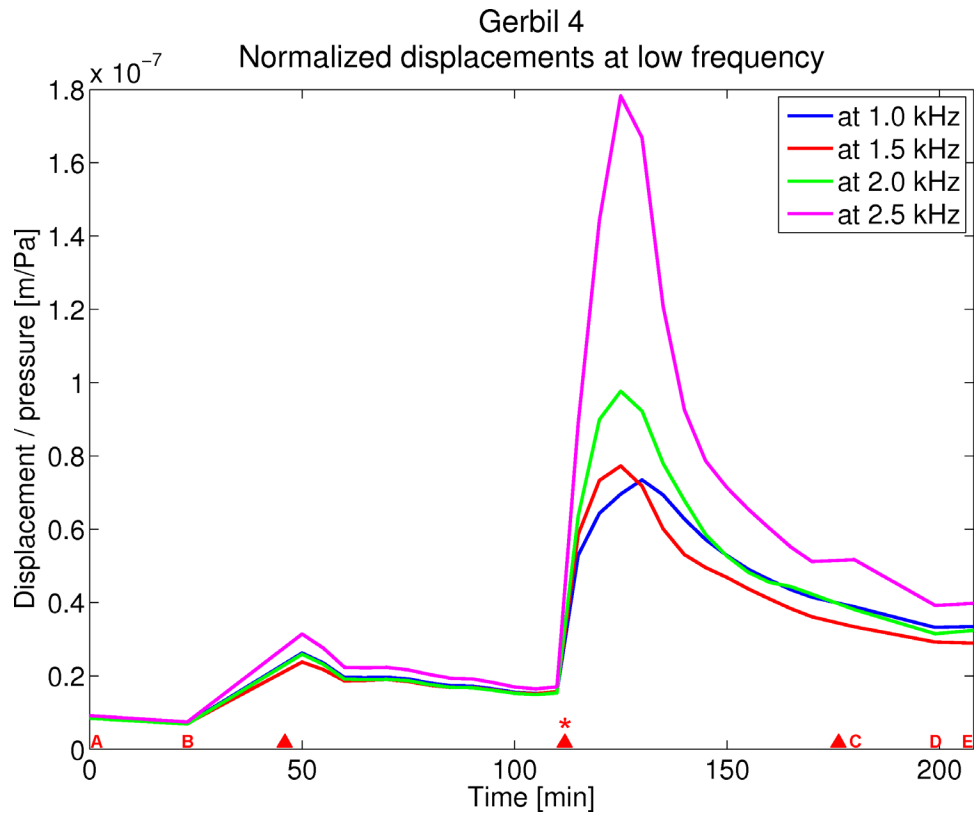


Figure 6.13: Tracking magnitude changes over time in gerbil 4, at 1.0, 1.5, 2.0 and 2.5 kHz. Times of rehydration indicated by \blacktriangle . Exceptions marked with (*) are explained in the text.

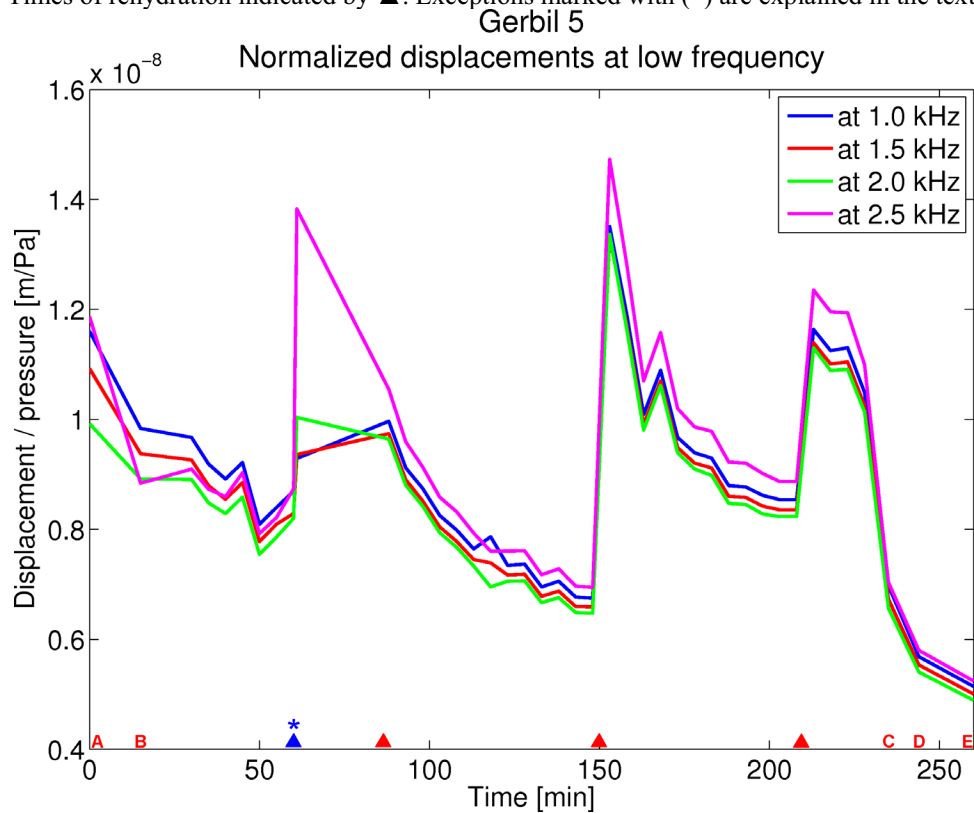


Figure 6.14: Tracking magnitude changes over time in gerbil 5, at 1.0, 1.5, 2.0 and 2.5 kHz. Times of rehydration indicated by \blacktriangle . Exceptions marked with (*) are explained in the text.

6.3.4.2 Tracking of frequency shifts at high frequencies

Figures 6.15 to 6.18 show the progression of the frequency responses over the duration of the experiments for gerbils 2 to 5 respectively. The format of a spectrogram is used for these graphs, using a linear vertical axis to represent time, and a logarithmic horizontal axis to represent frequencies. Magnitudes are expressed using a logarithmic colour scale normalized to an estimated value of the maximum displacement. To better reveal the frequency shifts at the peaks, low frequencies (below 4 kHz for gerbils 2, 3 and 5, and below 1 kHz for gerbil 4) are dropped from the displays, as they do not contain pertinent information. As in Figures 6.11 to 6.14, measurements A, B, C and D and times of rehydration are labelled next to the plots.

Over time, there is an overall trend of positive frequency shifts of the peaks between rehydration steps. The trend is more pronounced for the peak around 9 kHz. At the time of rehydration, we observe an immediate negative shift which brings the peak closer to its frequency at the previous rehydration, and in some instances even beyond that point. The spectrograms show that the frequencies of the peaks increase at a variable rate, more or less exponentially after most rehydration steps. In the following paragraphs the results for individual gerbils are described.

- In gerbil 2, the spectrogram shows a rather irregular pattern, with amplitude fluctuations consistent with those observed at low frequencies in Figure 6.15. Nonetheless, the overall trend between rehydration steps is a positive frequency shift of the peaks. After the third and fourth (and less obviously the second) rehydration steps, a new high-frequency peak seems to appear beyond 8 kHz. This could be a breaking up of the peak around 9 kHz as discussed in Section 6.3.2.2, or another peak, originally outside the measurement range (i.e., above 10 kHz), which shifted to lower frequencies after rehydration.
- In gerbil 3, the spectrogram shows a smooth visual pattern revealing the positive frequency shift of both peaks. In some measurements, the peak around 9 kHz shifts beyond the limits of the display (10 kHz). The observation noted earlier for measurement B (Section 6.3.4.1) can be seen here by the slightly brighter colour intensity (larger magnitude) compared with measurement A.

- In gerbil 4, measurements A and B were performed about 4 hours after the specimen was sacrificed and about 2 hours after the initial moistening of the absorbent tissue (cf. Section 5.4.4.1). By this time, drying and *post mortem* effects would be significant. Subsequent measurements after the first and second rehydration steps show a very large frequency shift at the peaks (approximately -3 kHz, and -4.5 kHz respectively). This is possibly due to the large amount of saline used in the rehydration steps for this specimen. Moreover, after the second rehydration step the two peaks seem to gradually come closer to form a single peak extending over a broad range of frequencies (as of $t = 120$ min). This helps explain the large maximum observed earlier in the low frequency plots, especially at 2.5 kHz. The frequency of the single peak in these responses was as low as 2.8 kHz, much closer to the frequency of the peak observed by Cohen et al. (1993) and Rosowski et al. (1997) in live ears (cf. Section 6.2.3).
- In gerbil 5, measurements taken up to $t = 61$ min correspond to a closed bulla setup. During this period the frequency shift observed at high frequencies is consistent with the one observed in open-bulla measurements. The effect of the first rehydration cannot be quantified as no measurement was recorded with an open bulla just before rehydration (at $t = 88$ min). The effects of drying and rehydration after that point are quite consistent with the general behaviour described so far, except for a sudden positive frequency shift (approximately 0.75 kHz) at the measurement at $t = 233$ min and in subsequent measurements C, D and E.

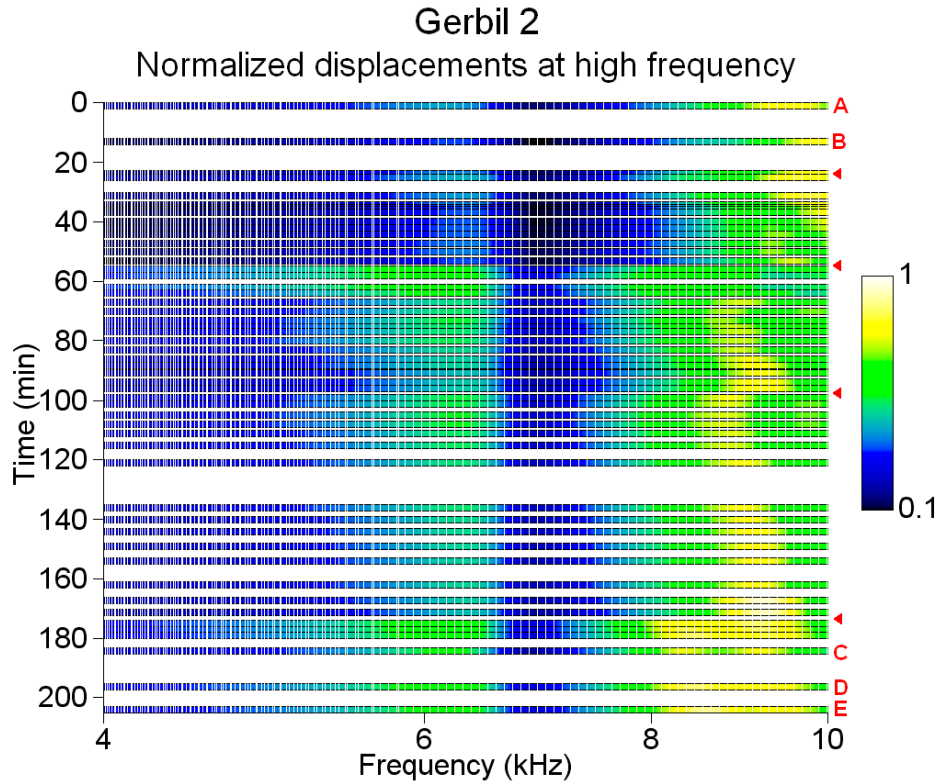


Figure 6.15: Tracking frequency shifts over time in gerbil 2 between 4 and 10 kHz. The colour scale is normalized to 60 nm/Pa.

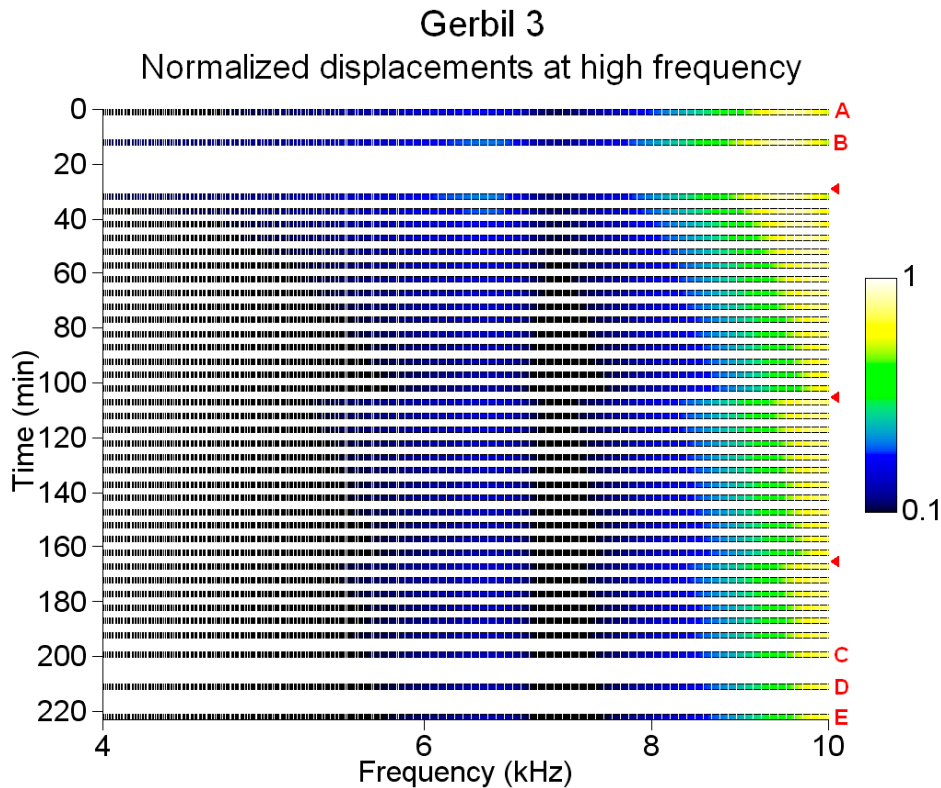


Figure 6.16: Tracking frequency shifts over time in gerbil 3 between 4 and 10 kHz. The colour scale is normalized to 75 nm/Pa.

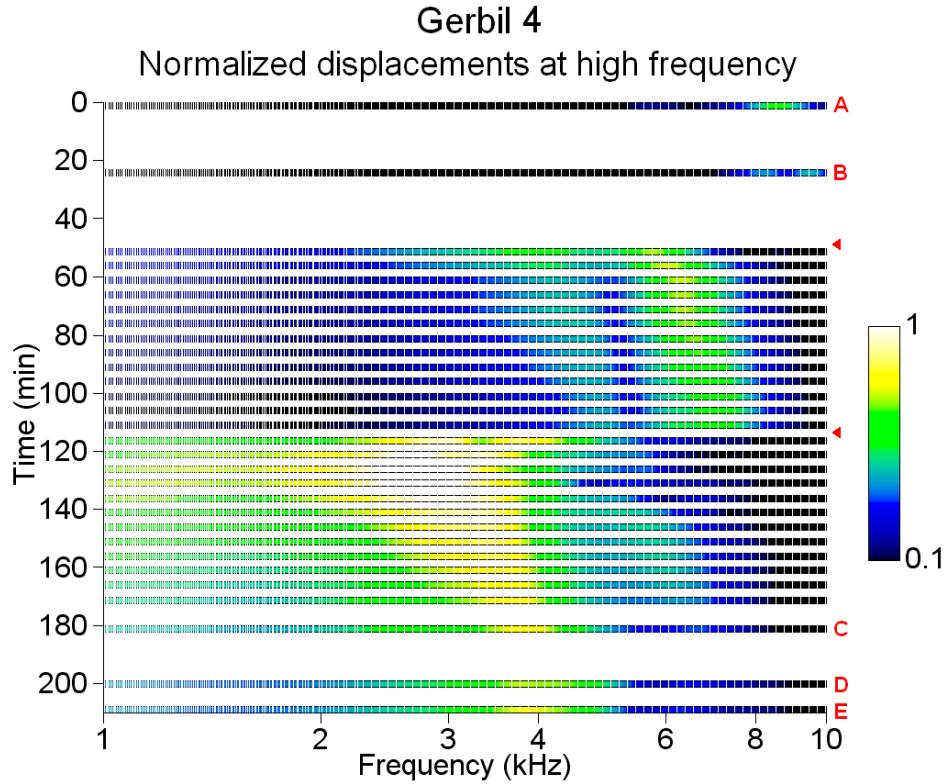


Figure 6.17: Tracking frequency shifts over time in gerbil 4 between 1 and 10 kHz. The colour scale is normalized to 150 nm/Pa.

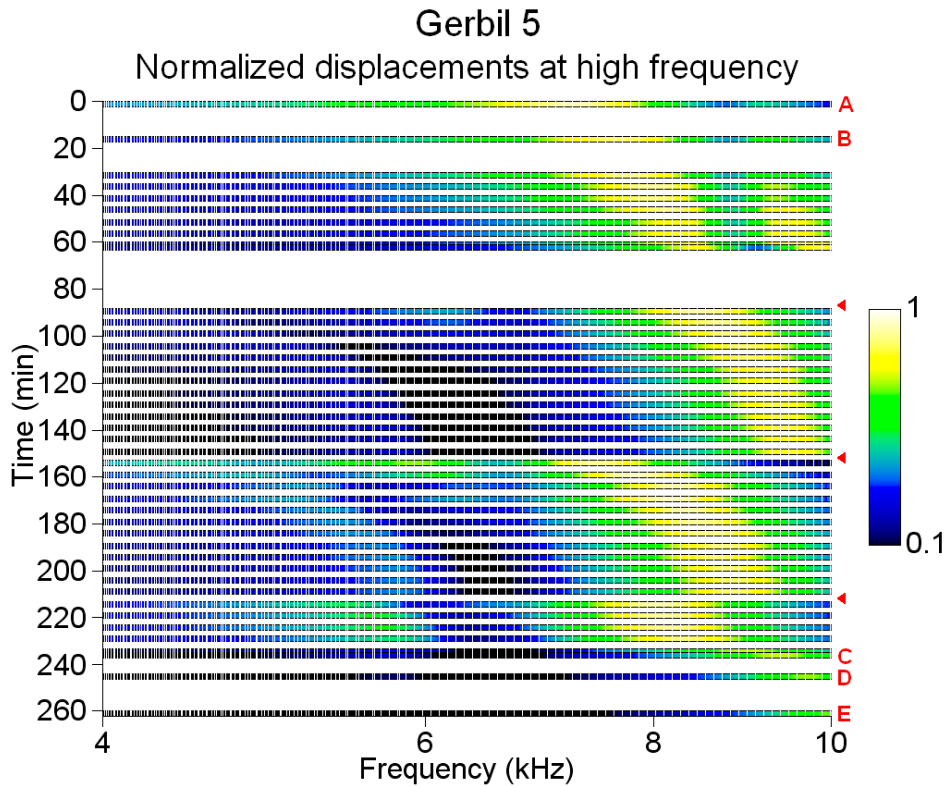


Figure 6.18: Tracking frequency shifts over time in gerbil 5 between 4 and 10 kHz. The colour scale is normalized to 90 nm/Pa.

6.4 Manubrial vibrations

Figures 6.19 to 6.23 present the displacements measured at different points along the manubrium in gerbils 1 to 5 respectively. For each measurement, the location and sequence, as outlined in Figure 5.13 in the previous chapter, are indicated with a schematic diagram next to the legend. A plot of the ratio of the displacement at each location to the displacement at the umbo is shown in the bottom portion of each figure. These plots help characterize the mode of vibration of the manubrium. Ignoring low-frequency noise, the average ratios are calculated at the lower frequencies, before the high-frequency peaks occur, and summarized in Table 6.4. An amplitude ratio smaller than 1 indicates that vibrations at the measured point are less than at the umbo.

Table 6.4: Summary of amplitude ratios at all points of measurement along the manubrium.

Amplitude ratio	Gerbil 1	Gerbil 2	Gerbil 3	Gerbil 4	Gerbil 5
Lateral process / umbo	0.35	0.51	0.50	-	0.44
Manubrium-sup. / umbo	0.60	0.68	-	0.60	-
Mid-manubrium / umbo	-	-	0.69	-	0.78
Manubrium-inf. / umbo	-	0.85	-	0.78	-

With a few exceptions at high frequencies in some specimens, the displacements maintain a similar shape over the frequency range studied. In all 5 specimens, a decrease in magnitude can be observed as we travel upward along the manubrium from the umbo to the lateral process of the malleus. The amplitude ratios maintain virtually constant values (less than 1) from low frequencies up to the frequencies where the high-frequency peaks occur. At high frequencies, changes are more or less complex and will be discussed next.

In gerbils 1, 2, 3 and 5, all of the high-frequency deviations from low-frequency amplitude ratios can presumably be attributed mainly to the drying-induced frequency shifts of the peaks as discussed in detail in Section 6.3.4. Even slight frequency shifts can cause large changes in the amplitude ratio.

In gerbil 4, changes occur as of approximately 3.5 kHz, with a small dip in the amplitude ratios between 3.5 and 5.5 kHz, followed by a significant increase: from around 0.70 to 0.87 for point 4 and from around 0.53 to 0.70 for point 9. Between 8 and 9 kHz, the displacements at the umbo are even lower than those at the next point along the manubrium (point 4), the amplitude ratio reaching a peak of 1.1 around 8.5 kHz. A rather subtle change of frequency-response shape is observed at high frequencies at point 9. This unexpected change was also seen in all subsequent measurements taken at other locations (measurements 9A, 10A, 11A, 1B, 2B, 3B, 4B, 5B, 6B) until another change brought the frequency response back to its original shape. The sharp dip observed in the amplitude ratio around 8 kHz at point 9 can be attributed to this temporal effect.

The similarity of the shapes of the frequency responses over most of the frequency range indicates that the motion of the manubrium follows a simple vibration pattern that fits the traditional concept of a rigid malleus-incus complex rotating around a fixed axis. Studies have suggested that there could be a frequency-dependent shifting of the axis of rotation, or a bending at the tip of the manubrium (cf. Section 3.2.2). These factors, often more pronounced at high frequencies, could lead to smaller vibrations at the umbo than at points higher up the manubrium. Nonetheless, temporal effects due to drying (cf. Section 6.3.4) also need to be taken into consideration. It is not possible to conclude from the plots presented here, especially in the absence of phase information, whether the changes we described in some specimens are due only to temporal effects or to a combination of these factors.

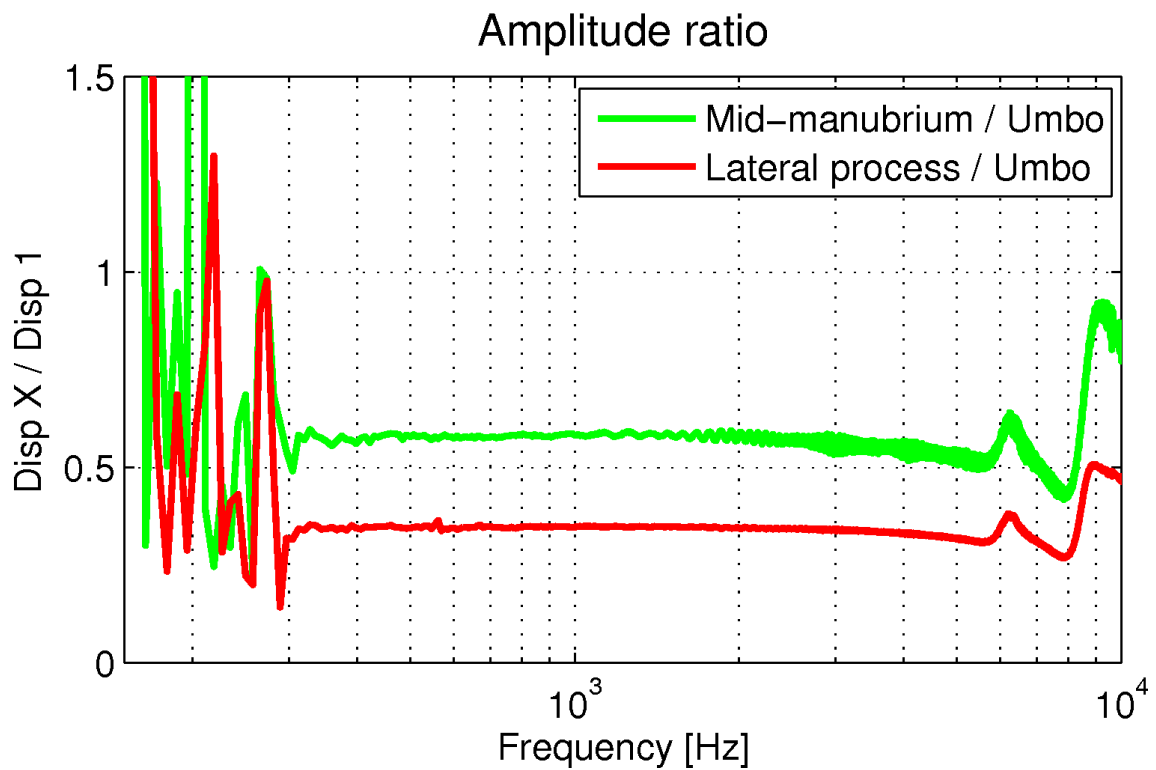
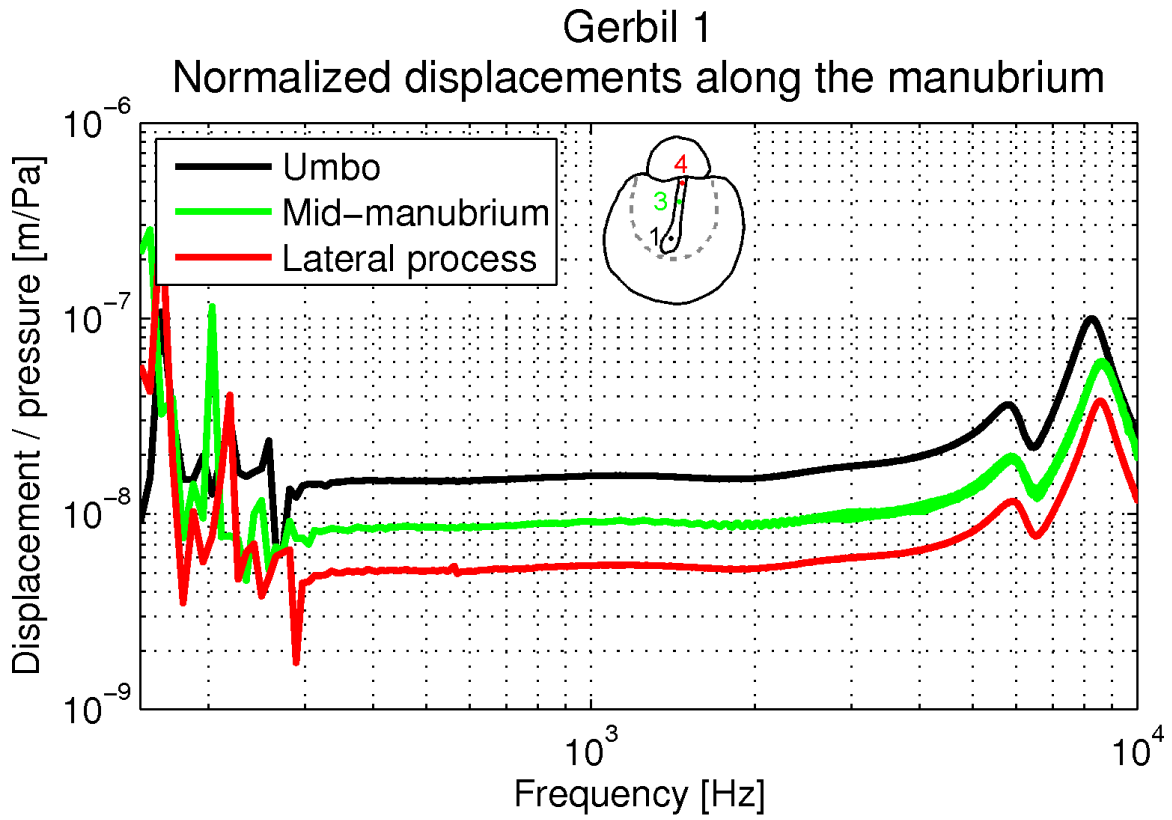


Figure 6.19: Manubrial displacements for Gerbil 1.

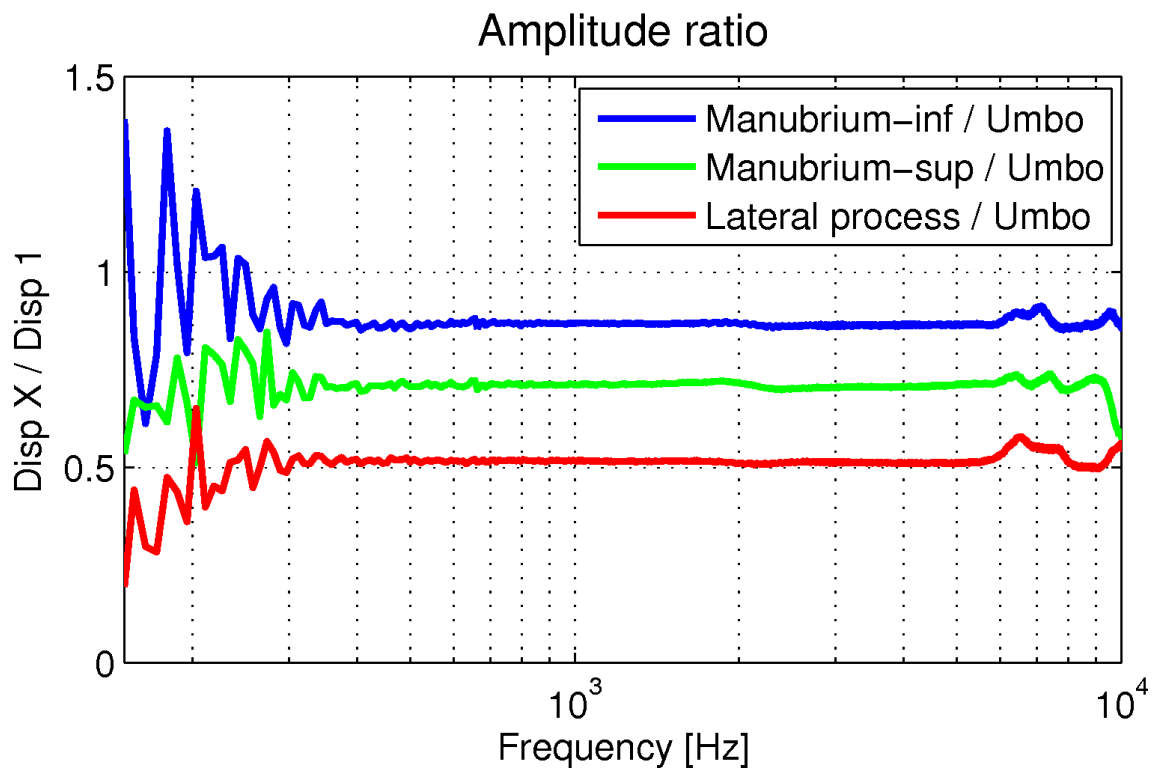
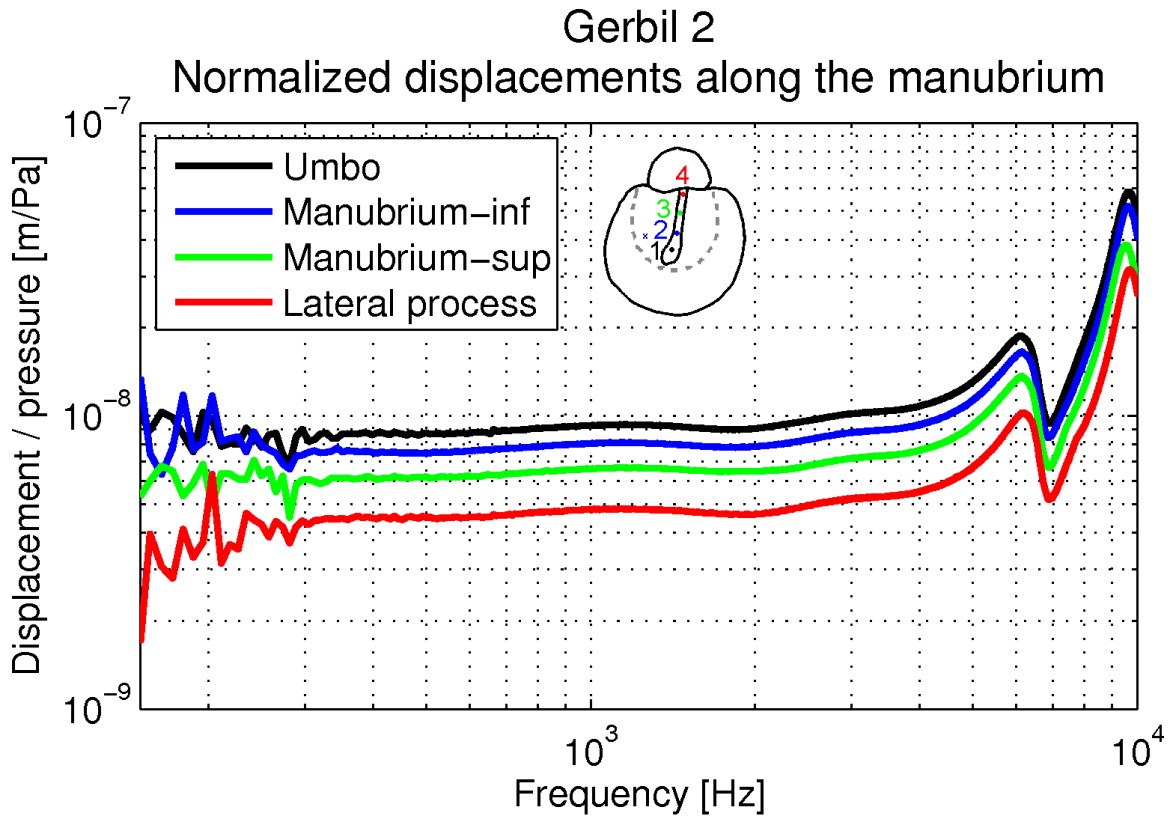


Figure 6.20: Manubrial displacements for Gerbil 2.

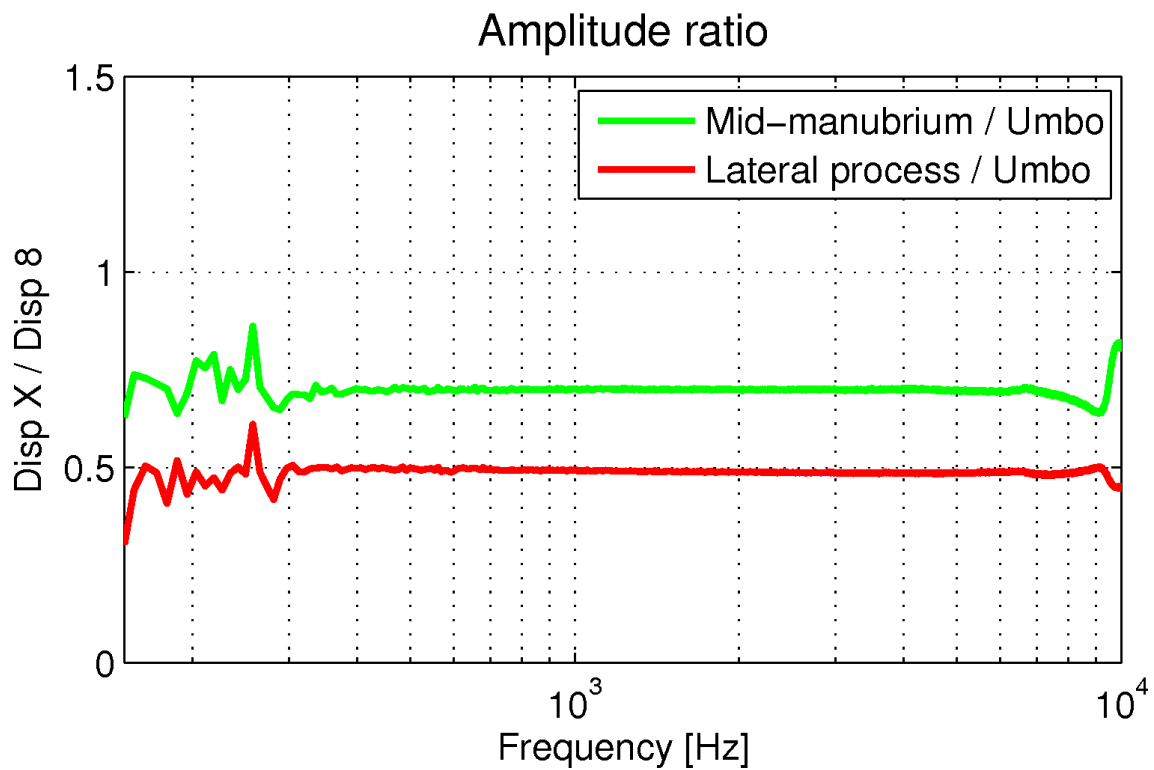
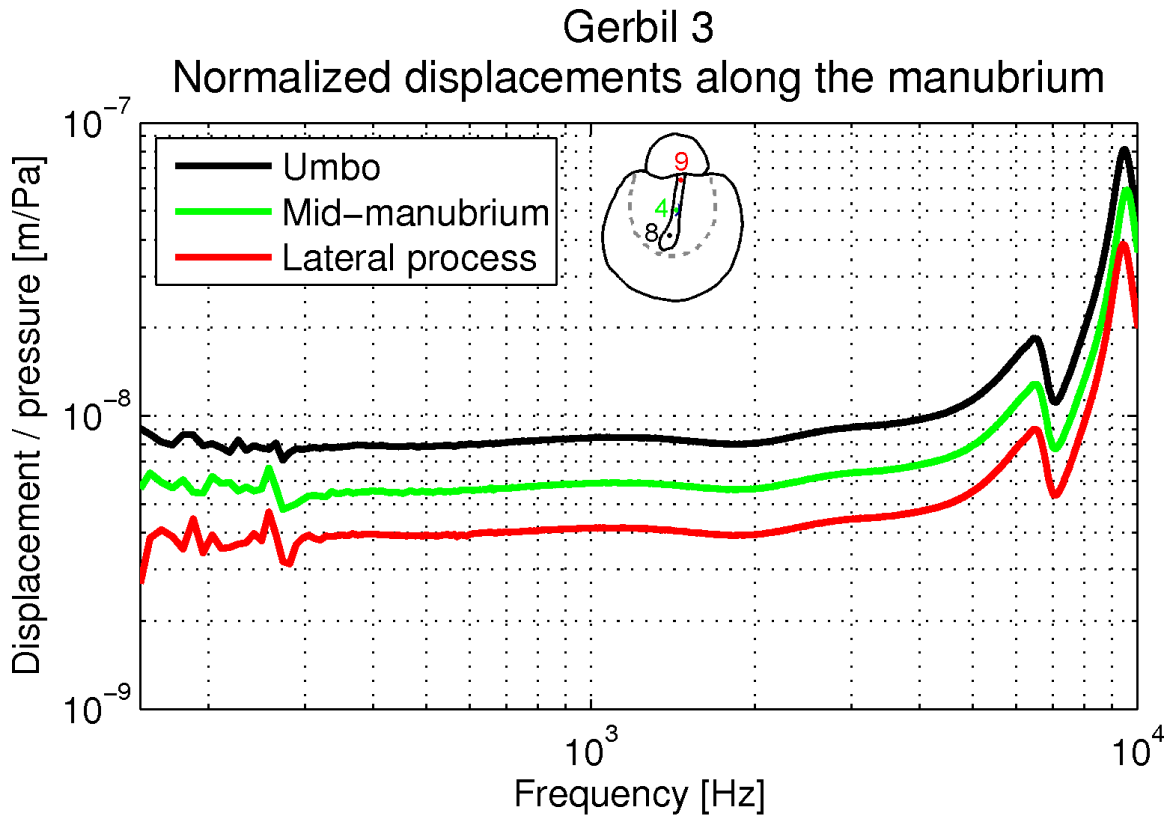


Figure 6.21: Manubrial displacements for Gerbil 3.

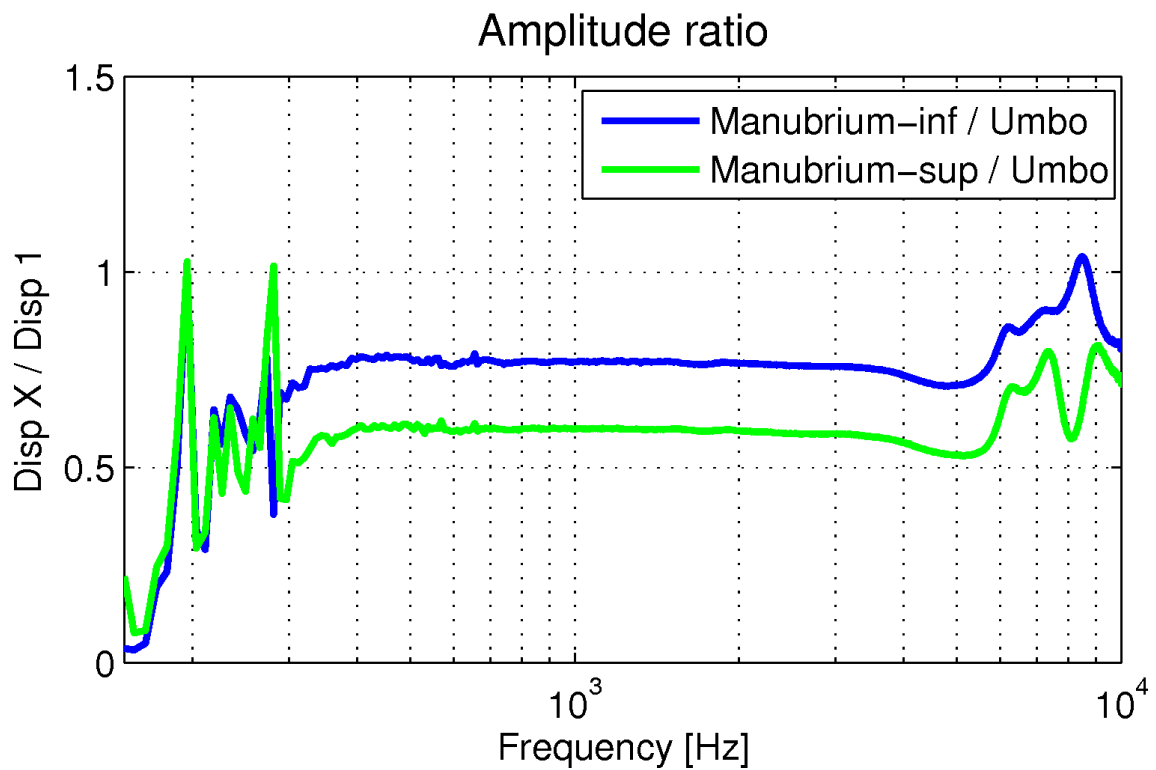
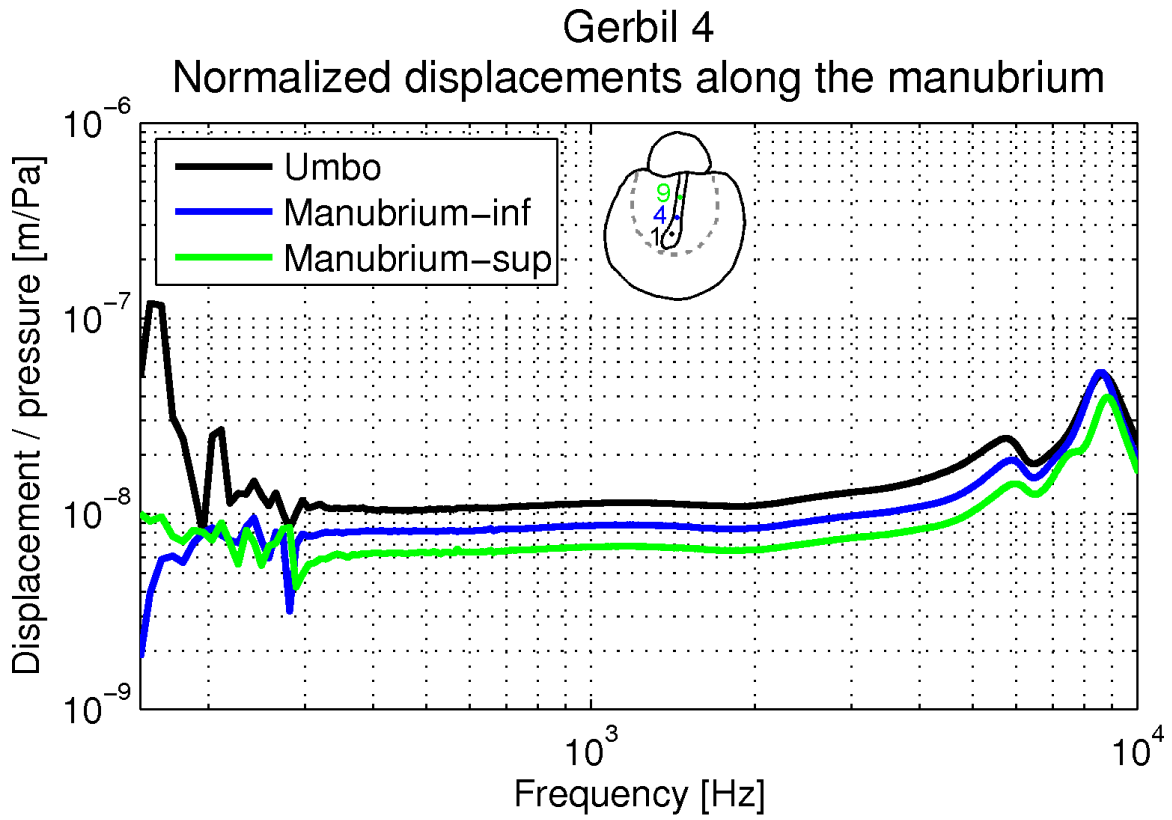


Figure 6.22: Manubrial displacements for Gerbil 4.

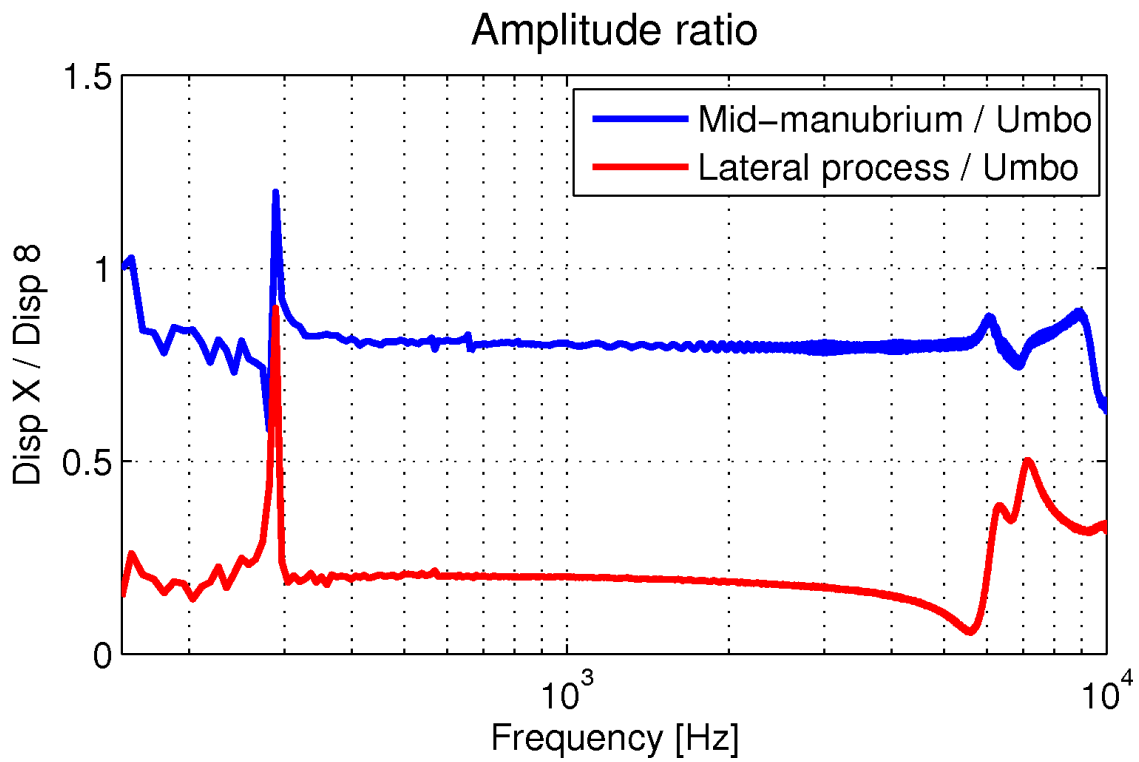
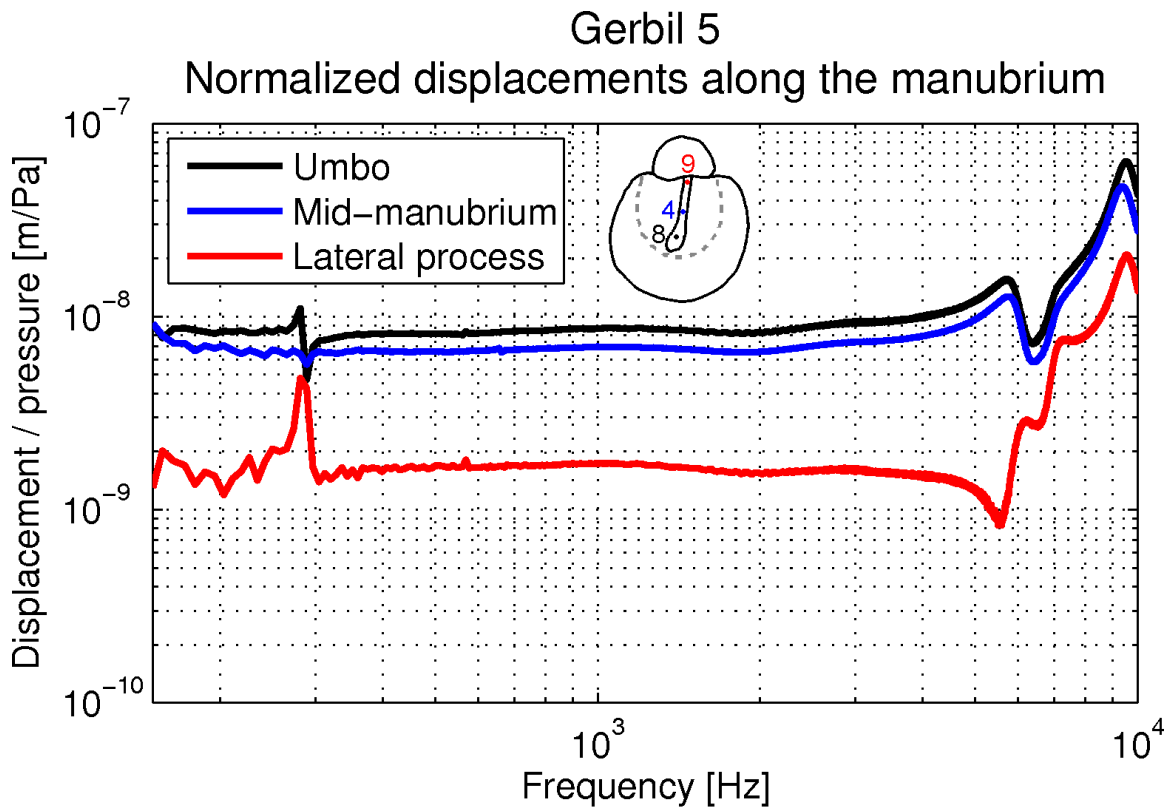


Figure 6.23: Manubrial displacements for Gerbil 5.

6.5 Tympanic-membrane vibrations

Displacements were measured at multiple points on the pars tensa of the tympanic membrane as shown in Figure 5.13 in the previous chapter. In Figures 6.24 to 6.28, we present the displacements at these points for all 5 specimens, along with measurements at nearby points on the manubrium. The arrangement of beads is shown schematically next to the legend in each figure. To the extent possible, we tried to maintain symmetry across the manubrium when placing the beads. Figure 6.27 contains 2 graphs for gerbil 4, one for each of the two horizontal lines of measurement points.

An arrangement of beads consisting of one bead in each quadrant was used in gerbils 1 and 2. In Figures 6.24 and 6.25 we note that displacements at all 4 points on the pars tensa are almost the same over the entire frequency range. In gerbil 1, the measurement at point 6 is noisier and slightly lower. For gerbil 2, as mentioned in Section 5.4.2, during the preparation of the specimen a small bone chip was accidentally deposited on the anterior side of the pars tensa close to the bead at point 5. This presumably explains the oddly shaped peak around 6 kHz and the somewhat lower amplitudes measured at point 5.

In gerbils 3 and 5 the beads were arranged to provide a profile of vibrations across the visible portion of the pars tensa on a line approximately normal to and midway along the manubrium. In gerbil 4, measurements were performed along both an inferior line and a superior line. The plots in Figures 6.26 to 6.28 show that as we travel away from the manubrium, the amplitudes of the displacements increase on each side. A comparison between symmetrically located points on each side of the manubrium reveals that displacements are essentially the same on the anterior and posterior sides. In gerbil 4, a somewhat complex behaviour is observed beyond 7.5 kHz in the supero-anterior displacements (at points 9, 10, and 11). These are not due to spatial effects but can rather be attributed to temporal effects as discussed already in the previous section for the manubrial displacements at point 9.

As an overall observation, we note that displacements measured on the pars tensa in all five specimens are, as expected, larger than those measured on the manubrium. We also note the great similarity in the shapes of the curves over the entire frequency range for each specimen, indicating that the motion of the gerbil eardrum follows a simple pattern and that we have not yet reached the frequencies where the pattern breaks up into sectional vibrations.

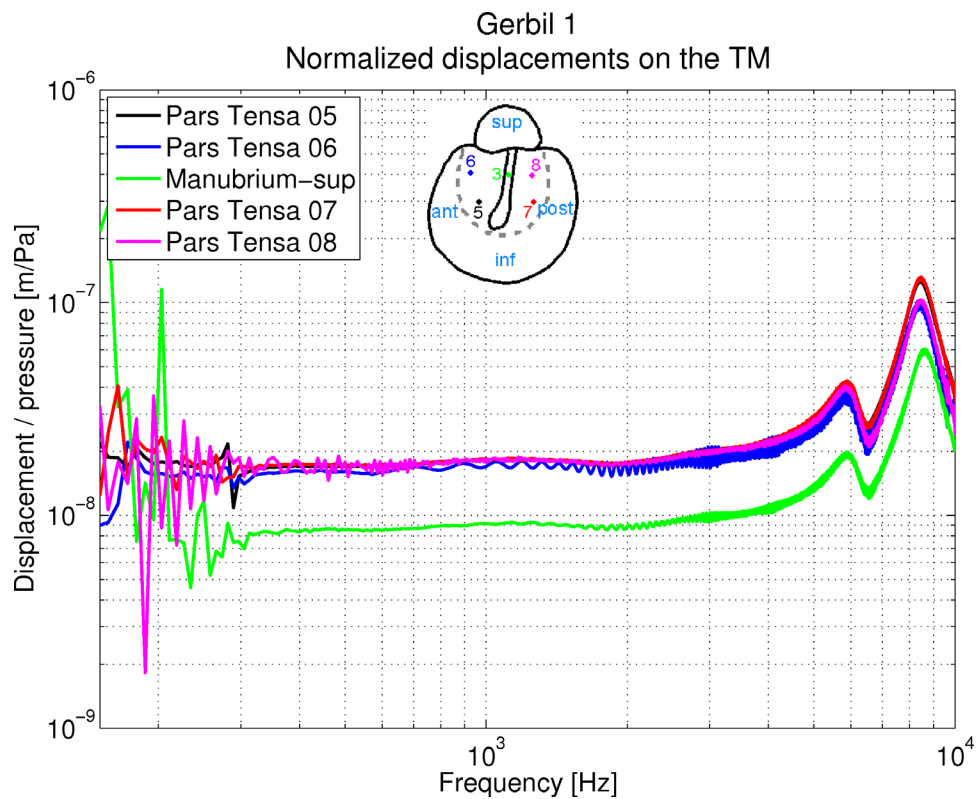


Figure 6.24: TM displacements for gerbil 1.

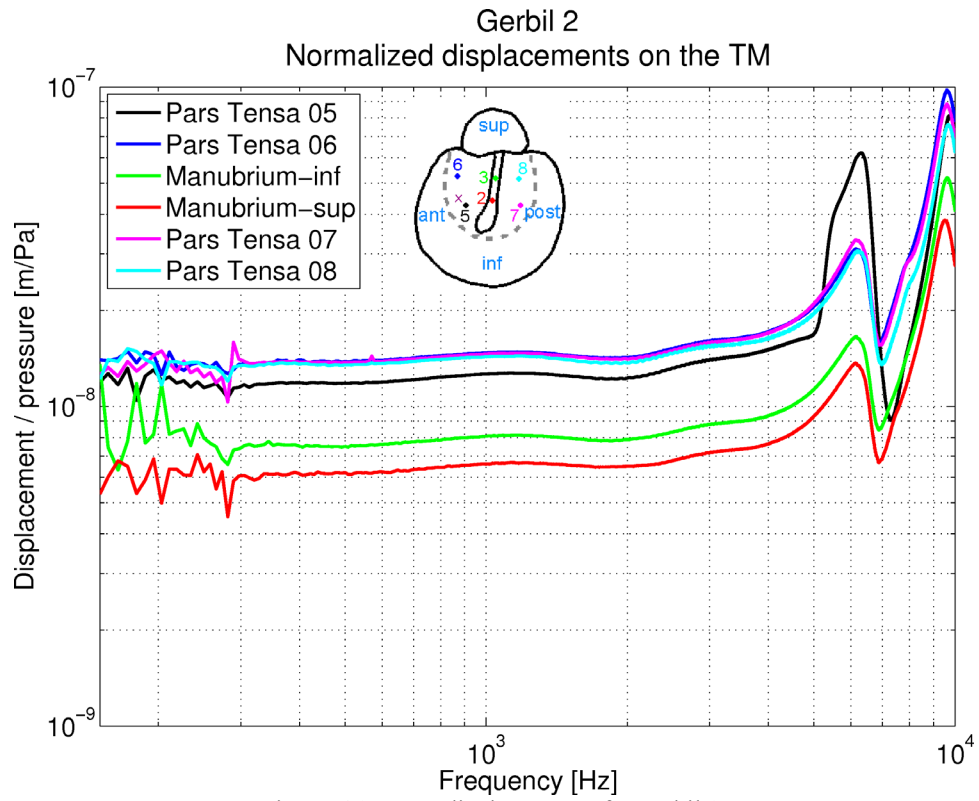


Figure 6.25: TM displacements for gerbil 2.

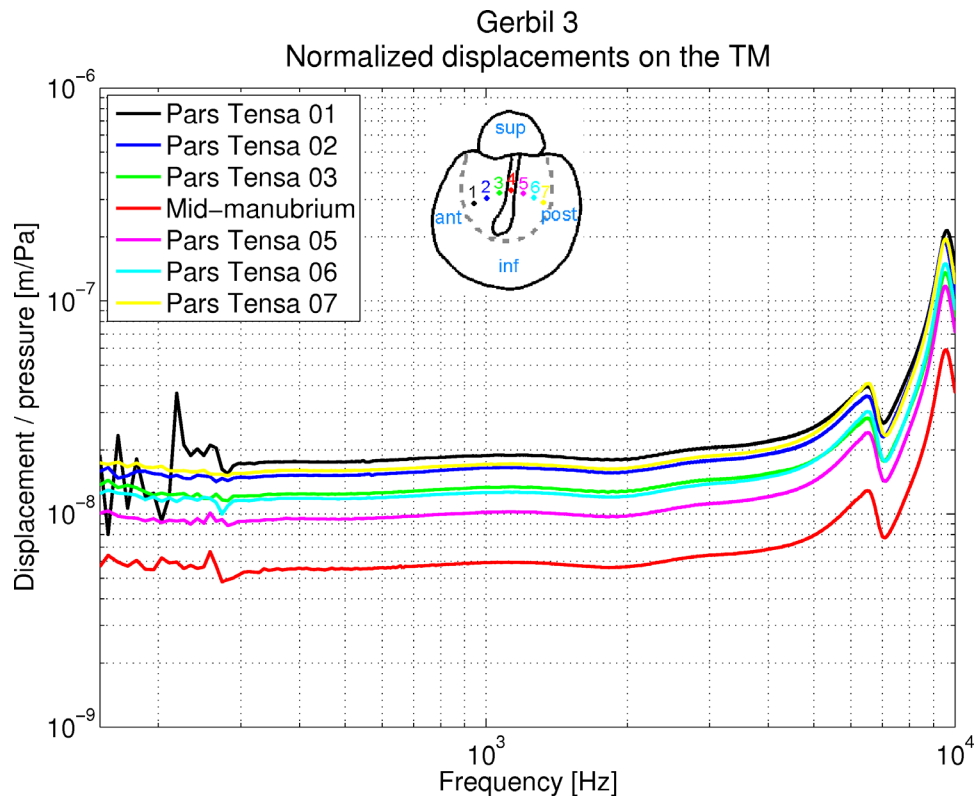


Figure 6.26: TM displacements for gerbil 3.

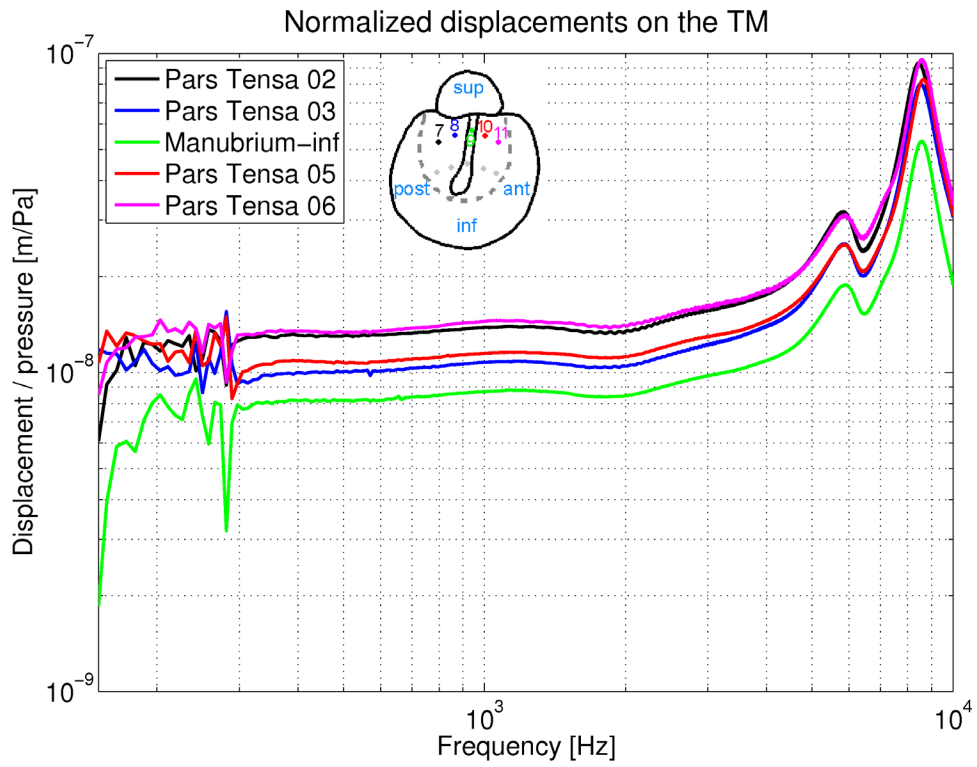
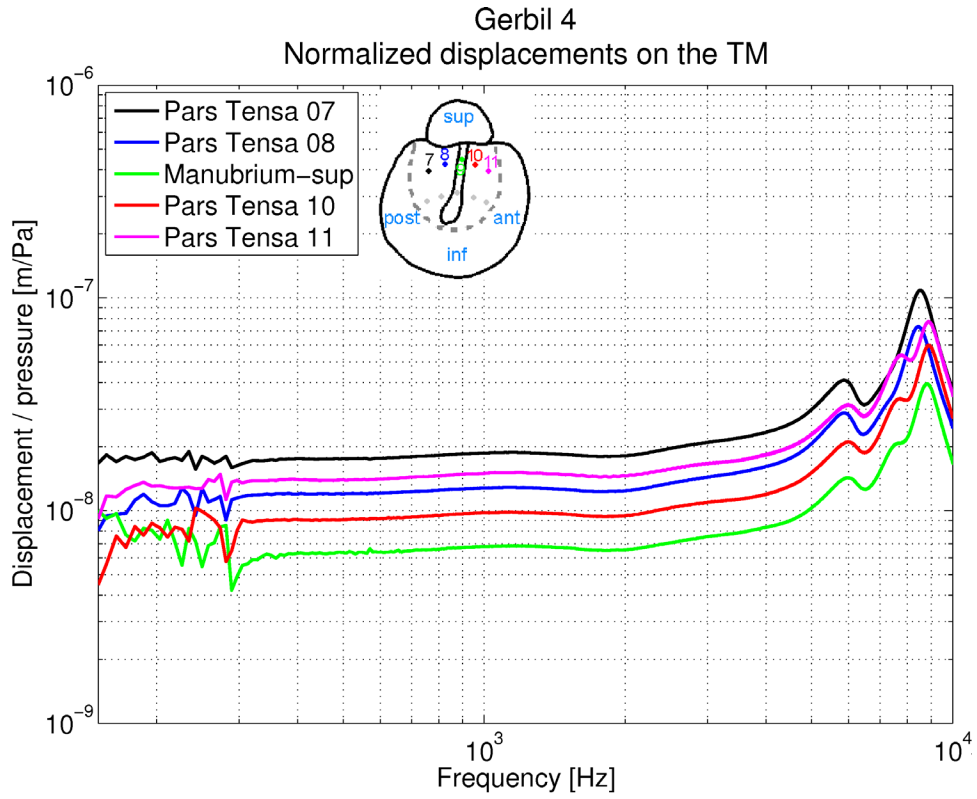


Figure 6.27: TM displacements for gerbil 4.
TOP: Measurement in superior half. BOTTOM: measurements in inferior half

Gerbil 5
Normalized displacements on the TM

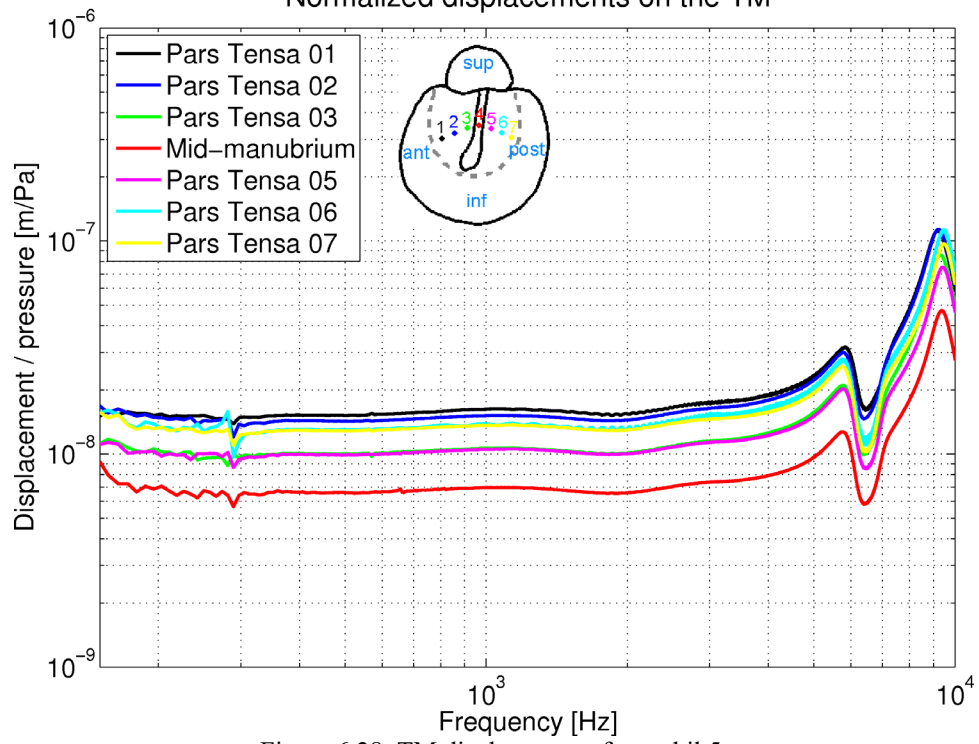


Figure 6.28: TM displacements for gerbil 5.

CHAPTER 7

CONCLUSION

7.1 Summary

In this work, we have presented two experimental studies of eardrum vibrations in the gerbil: a study of displacement measurements at multiple points on the eardrum, with the aim of enhancing our understanding of the mechanics of the gerbil middle ear; and a study of temporal effects due to drying of the middle ear, affecting the repeatability of measurements. *Post mortem* displacement frequency responses were acquired using laser Doppler vibrometry (LDV) and analyzed over the frequency range between 0.15 and 10 kHz.

7.1.1 Middle-ear mechanics

First, we have provided displacement frequency responses measured at the umbo in 5 gerbils. The shape and variability of the responses were studied and a comparison was conducted with previous measurements and simulation results by other groups. Discrepancies in the magnitudes of displacements and the shapes of the frequency response were discussed. Since our experiments were performed on ears with an open middle-ear cavity, the effects of opening the bulla were also investigated in one specimen.

We also studied the spatial vibration patterns along the manubrium of the malleus and at multiple points on the pars tensa of the tympanic membrane. Over most of the frequency range studied, measurements along the manubrium were found to be consistent with the traditional notion of a rigid rotation of the malleus-incus complex about a fixed axis. Some exceptions were observed at high frequencies in some specimens, suggesting possible frequency-dependent complexities. Simple vibration patterns typical of low-frequency behaviour were also observed on the eardrum. The shapes of the frequency responses were similar at all measurement locations and over the entire frequency range, showing that we have not yet reached the frequencies where the pattern breaks up into sectional vibrations. Characterizing manubrial and tympanic membrane vibration patterns provides important details which are not addressed by the single-point measurements commonly performed, thus helping in better understanding the function of the middle ear.

7.1.2 Drying and rehydration effects

An experimental protocol was designed to study temporal effects related to the drying of middle-ear structures, and to quantify the effects of rehydrating the middle ear. A substantial number of measurements were carried out on 4 specimens. For simplicity, the effects of drying were summarized as magnitude changes at low frequencies and frequency shifts at high frequencies. Magnitude changes also occur at high frequencies, but are more difficult to quantify due to the frequency shifts of the peaks. Consistent with the findings of Voss et al. (2000), we found that drying effects are highly variable among specimens, and that remoistening the middle ear can partially restore the shape and amplitude of the measured frequency response. The effects of drying were found to be gradual, and the effects of rehydration were found to be quite rapid.

7.2 Discussion

7.2.1 Comparison with previous measurements

In Section 6.3.2, we compared our frequency responses with those measured by Cohen et al. (1993) and Rosowski et al. (1997) and the simulation results of Elkhouri et al. (2006). We found that our measured displacements had lower magnitudes at low frequencies (cf. Table 6.2). We also found that our responses had 2 peaks at high frequencies, whereas measurements from other groups had a single peak at a lower frequency. We attributed these discrepancies mainly to *post mortem* (temporal) effects. Since our experimental setup was different from the other groups, we also investigated the effect of opening of the middle-ear cavity on the frequency responses.

When investigating the *post mortem* effects of drying and rehydration, we found that when a larger amount of saline was used in the rehydration steps in some specimens, the two peaks formerly observed at high frequencies merged into 1 peak and shifted to a lower frequency. In fact, in gerbil 4, the measurements following the second rehydration step reveal a single peak as low as 2.8 kHz, much closer to the peaks observed by Cohen et al. and by Rosowski et al. in live ears. This suggests that drying effects are responsible for the shifting (and possible breaking up) of the peak, and that an increased rehydration might make the *post mortem* ear behave more like a live one. Our rehydration technique was designed to avoid interference with middle-ear

vibrations by excess water, but the technique is apparently too conservative.

It should be noted that the responses with a single peak, namely the measurements after the second rehydration step (including measurements C and D) in gerbil 4, had amplitudes considerably higher than our other measurements. These amplitudes are more comparable to the ones measured by the two other groups in live ears. We could also speculate that the adult responses presented by Cohen et al. correspond to a dryer middle-ear state than in the experiments of Rosowski et al. In fact, the larger hole drilled in the bulla in their experiments might have accelerated the drying of the middle ear, thus leading to the lower magnitude and higher peak-frequency observed in their responses.

Our investigation of the effect of opening the bulla was not conclusive. Opening the middle-ear cavity is expected to reduce the load faced by the tympanic membrane, thus increasing the magnitude of its displacements. As we monitored the frequency response while opening the bulla, we observed a *decrease* in amplitude. However, this observation is not very reliable since the unaveraged measurements were noisy and very sensitive to relative motion of the experimental setup when opening the bulla. Since the first averaged and recorded open-bulla measurement was taken after the initial hydration of the absorbent tissue, the effect of opening the bulla observed in Figure 6.10 was combined with rehydration effects (cf. Section 6.3.3). However, when investigating the effect of a small hole in the bulla (cf. Figure 6.9), a magnitude increase was observed at frequencies below the anti-resonance, similar to what Rosowski et al. observed in their measurements (cf. Figure 6.3 in Section 6.3.2). Reliable measurements of the effect of gradually opening the bulla would be required to estimate the size of the increase that would result from a wide opening of the middle-ear cavity.

It is interesting to note that, despite the discrepancies between our measured frequency responses and those observed by the two other groups, the frequencies at which the peaks occur in our measurements (around 6 and 9 kHz) match the frequencies of the vocalizations recorded by Finck and Goehl (1968) as mentioned in Section 3.3.1.

7.2.2 Spatial vibration patterns

The vibration measurements presented in this work were taken along a single observation direction, and corrected to correspond to a direction normal to the plane of the tympanic ring surrounding the pars tensa. This rather arbitrary choice is useful to simplify the discussion of manubrial vibration patterns with the assumptions that the manubrium vibrates as a rigid body and that it rotates around a fixed axis. The previous studies presented in Section 3.2.2 have shown that (at least in some species) the manubrium tends to exhibit bending and that the motion of the malleus-incus complex consists of a combination of translational and rotational motion. Moreover, these studies suggest that, even when the motion is rotational, the axis of rotation is not fixed. Three-dimensional vibration measurements, such as the ones presented by Decraemer et al. (1994) and Decraemer & Khanna (1996 & 1997), are required to fully describe this complex motion. While we have observed simple vibration patterns over most of the frequency range, 3-dimensional measurements would be necessary to conclusively attribute the discrepancies described at high frequencies in some specimens to either spatial or temporal effects.

The measurements presented in this work only cover points on the pars tensa inside the area visible under the microscope (cf. Figure 5.11 in Section 5.3.2). Within this area, the simple vibration pattern observed is typical of the low-frequency patterns described in the holographic measurements in cats and humans (Tonndorf & Khanna, 1972; and Khanna & Tonndorf, 1972). Gerbil studies using moiré interferometry (von Unge et al. 1993; and Dirckx & Decraemer, 2001) and model simulations (Funnell et al., 2000; and Elkhouri et al., 2006) have also reported similar patterns, with a point of maximum displacement on each side of the pars tensa (anterior and posterior), generally closer to the manubrium than to the tympanic ring. It is difficult to find the exact location of the point of maximum displacement using discrete measurements with a spatial resolution limited by the possible effects of using too many micro-beads, and by the temporal effects that would result from long measurement times. We also do not know whether the maximum is within the visible area of the pars tensa. However, based on these studies, we can safely assume that the pattern remains simple outside this area. Since the tympanic membrane is clamped at its periphery, we expect the magnitude of displacements to eventually

decrease to zero as we travel closer towards the tympanic ring.

7.2.3 Drying and rehydration effects

Our experimental protocol was designed to track the effects of drying, and to correct for these effects by periodic remoistening of the middle ear. In their experiments on human cadavers, Voss et al. (2000) observed a drop in magnitude of stapes velocity over time which they attributed to drying effects. The magnitude drop varied from ear to ear, leading to a distinction between stable and unstable ears. They specifically noted that in some preparations the magnitude remained stable for several hours before dropping suddenly (cf. Section 3.4.2).

Our experiments dealing with the effects of drying and rehydration of the middle ear showed gradual magnitude drops and frequency shifts, both of which were variable between specimens and even between rehydration steps within the same experiment. Rehydration effects may be dependent on several factors, including how dry the middle ear was prior to rehydration, and the amount of saline used during rehydration. In one specimen (gerbil 4) a sudden change in the shape of the frequency was observed. The change persisted in subsequent measurements over a period of about 30 minutes, until another change brought the frequency response back to its original shape (cf. Section 6.4). There remain a lot of unknown characteristics of drying effects, and there could also be other *post mortem* effects, not related to drying, which can affect the material properties of middle-ear structures and contribute to the changes observed. Further efforts would be required to investigate this possibility, and also the changes which occur during the time between sacrificing the animal and the first measurements.

7.3 Future Work

There remain some aspects of middle-ear mechanics, and especially drying effects, that this study has not covered. In addition to advancing this work, we also foresee some long-term implications for future measurements of middle-ear vibrations in the gerbil in our lab.

Vibration measurements from 5 specimens were presented in this work. Extending the study to

include more specimens would inevitably help us draw more generalized conclusions concerning middle-ear vibrations in gerbils. Although efforts were made to minimize the relative motion of the specimen with respect to the measurement system, whether or not the gerbil head was vibrating as a whole during the measurements has not been verified experimentally. To confirm this, measurements need to be performed at a point where we would not expect vibrations, such as the ear-canal wall. The effect of opening the middle-ear cavity also needs to be further investigated, as discussed in Section 7.2.1. Additional experiments, similar to the one presented for gerbil 4 in this work, need to be performed, with reliable measurements of the frequency response while gradually opening the bulla.

Extending the study to include more measurement locations on the eardrum would help to better characterize the mechanics of the middle-ear and permit a more complete comparison with model simulations. This, however, would require a larger number of micro-beads to be placed on the eardrum, thus requiring a careful study of the effects of these beads. Some technical difficulties need to be considered, because the bead placement procedure is very delicate and time consuming. Some scenarios that we have envisioned involve taking repeated measurements on a single bead while sequentially adding beads at neighbouring locations on the eardrum. This needs to be done carefully to make sure not to disrupt the experimental setup, to maintain the accuracy of the measurements. The possibility of using the medial side of the eardrum (on the side of the middle-ear cavity) to place additional beads should also be investigated.

Further investigations of manubrial vibrations need to be carried out: performing vibration measurements from different observation angles, and deriving the 3-dimensional components of the vibrations, would be required to fully characterize the motion of the manubrium and address the issues of manubrial bending and shifting of the axis of rotation.

Further investigations of drying and, more importantly, rehydration effects need to be carried out to better explain their variability. Possible scenarios include: performing measurements at shorter time intervals (less than 5 minutes); studying the effects of using different amounts of saline

during rehydration; and performing 2 consecutive rehydration steps allowing little time for drying effects (just enough time to perform one measurement, for example). In addition to these scenarios, different methods for rehydration should be investigated. Many groups have rehydrated the ear by flooding with saline, then using gentle suction to remove the excess fluid and allowing some time for drying before making measurements (e.g., Voss et al., 2001; Chien et al., 2006). This would be another way of correcting for drying effects although undetected water within the cavity could affect middle-ear vibrations in unpredictable ways. An alternative would be to try to avoid these effects, at least during the time of specimen preparation: the use of a local humidifier while performing manipulations to keep a constant level of humidity has been recently discussed by Ladak et al. (2004) and Dirckx et al. (2006). The feasibility of these solutions needs to be investigated, taking into consideration the possible effects of humidity and condensation on the electronic and optical equipment attached to the experimental setup.

It will be interesting to investigate the feasibility of experiments involving manipulations of middle-ear structures, given the small size of the gerbil ear. Such experiments have been performed in gerbils using other measurement techniques (e.g., Dirckx and Decraemer, 2001), and find interesting applications in model validation, for example. It would also be interesting to use a finite-element model in order to understand certain features of the observed *post mortem* effects, by adjusting the model parameters to simulate drying and rehydration effects, and perhaps to simulate things like accidental bone fragments and water droplets on the TM.

Temporal effects between the time the animal is sacrificed and the first measurement need to be investigated. To this end, middle-ear input impedance measurements (e.g., tympanometry) and LDV measurements (at least at the umbo) could be performed before and after the dissection. Such experiments would require a new setup which allows fixing of the gerbil head under the tympanometer or the vibrometer head for reliable measurements. Finally, it is important that some future work be done on live specimens in order to study *post mortem* effects (and middle-ear mechanics) fully. LDV measurements, at least at the umbo, should be acquired in order to provide a baseline to compare with the *post mortem* measurements.

REFERENCES

- Akache F (2005): *An experimental study of middle-ear vibrations in rats*, Master's thesis, McGill University, Montreal.
- Akache F, Funnell WRJ & Daniel SJ (2007), *An experimental study of tympanic membrane and manubrium vibrations in rats*. *Audiol Neurotol* 12: 59–63.
- Békésy G v (1949): *The structure of the middle ear and the hearing of one's own voice by bone conduction*. *J Acoust Soc Am* 21: 217–232.
- Békésy (1960): *Experiments in hearing*, McGraw Hill, NY, 142.
- Bigelow DC, Swanson PB & Saunders JC (1996): *The effect of tympanic membrane perforation size on umbo velocity in the rat*. *Laryngoscope* 106(1): 71–76.
- Bigelow DC, David K & Saunders JC (1998): *Effect of healed tympanic-membrane perforations on umbo velocity in the rat*. *Ann Otol Rhinol Laryngol* 107: 928–934.
- Buunen TJF & Vlaming MSMG (1981): *Laser-Doppler velocity meter applied to tympanic membrane vibrations in cat*. *J Acoust Soc Am* 58: 223–228.
- Chien W, Ravicz ME, Merchant SN, Rosowski JJ (2006): *The effect of methodological differences in the measurement of stapes motion in live and cadaver ears*. *Audiol Neurotol* 11: 183–197.
- Cohen YE, Doan DE, Rubin DM & Saunders JC (1993): *Middle-ear development V: Development of umbo sensitivity in the gerbil*. *American Journal of Otolaryngology* 14(3): 191–198.

- Decraemer WF & Khanna SM (1994): *A method for determining three-dimensional vibration in the ear*. Hearing Research, 77, 19–37.
- Decraemer WF & Khanna SM (1996): *Malleus vibrations in the cat ear are three dimensional*. Proceedings of the Diversity in Auditory Mechanisms, Berkeley, California, 1996, pp. 115–121.
- Decraemer WF & Khanna SM (1997): *Vibrations on the malleus measured through the ear canal*. Proceedings of Middle ear mechanics in Research and Otosurgery. Dresden, September 19-22, 1996, Ed. K.B. Hüttenbrink, 32–39.
- Decraemer WF, Khanna SM & Funnell WRJ (1989): *Interferometric measurement of the amplitude and phase of tympanic membrane vibrations in cat*, Hearing Research 38: 1–18.
- Decraemer WF, Khanna SM & Funnell WRJ (1991): *Malleus vibration mode changes with frequency*, Hear Res, 54: 305–318.
- Decraemer WF, Khanna SM & Funnell WRJ (1994a): *Modelling the malleus vibration as a rigid body motion with one rotational and one translational degree of freedom*. Hearing Research, 72 1/2, 1–18.
- Decraemer WF, Khanna SM & Funnell WRJ (1994b): *Bending of the manubrium in cat under normal sound stimulation*. SPIE Proc. 2329: 74–84.
- de La Rochefoucauld O & Olson E (2007): *Exploring sound transmission through the middle ear by tracing middle ear delay*. 30th ARO MidWinter Mtg.
- Dirckx JJJ & Decraemer WF (1991): *Human tympanic membrane deformation under static*

pressure. Hearing Research, 51(1): 93–105.

Dirckx JJJ & Decraemer WF (2001): *Effect of middle ear components on eardrum quasi-static deformation*. Hearing Research, 157: 124–137.

Dirckx JJJ, Decraemer WF, von Unge M & Larsson Ch (1998): *Volume displacement of the gerbil eardrum pars flaccida as a function of middle ear pressure*. Hearing Research 118(1-2): 35–46.

Dirckx JJ, Buytaert J & Decraemer WF (2006): *Quasi-static transfer function of the rabbit middle ear, measured with a heterodyne interferometer with high-resolution position decoder*. Journal of the Association for Research in Otolaryngology, 7(4) pp. 339–351.

Doan DE, Igit PG & Saunders J (1996): *Middle-ear development VII: Umbo velocity in the neonatal rat*. J Acoust Soc Am 99 (3), 1566–1572.

Elkhouri N, Liu H & Funnell WRJ (2006): *Low-frequency finite-element modelling of the gerbil middle ear*. JARO 7: 399–411.

Farina A (2000): *Simultaneous measurement of impulse response and distortion with a swept-sine technique*. 108th AES Convention, Paris, 18–22 February 2000.

Feldman A.S. & Wilber L.A. (1976): *Acoustic Impedance and Admittance – The Measurement of Middle Ear Function*. (The Williams and Wilkins Company, Baltimore)

Fink A & Sofonglu (1966): *Auditory sensitivity of the Mongolian gerbil*. J. Aud. Res., 6, 313–319.

Finck A, & Goehl H (1968): *Vocal spectra and cochlear sensitivity in the Mongolian gerbil*. J Aud. Res., 8: 65–69.

- Fleischer G (1978): *Evolutionary Principles of the Mammalian middle ear*. Adv Anat Embryol Cell Biol 55: 1–70.
- Funnell WRJ (1975): *A theoretical study of eardrum vibrations using the finite-element method*. PhD thesis, McGill University.
- Funnell WRJ (1996): *Low-frequency coupling between eardrum and manubrium in a finite element model*. J Acoust Soc Am, 99: 3036–3043.
- Funnell WRJ & Laszlo CA (1978): *Modeling of the cat eardrum as a thin shell using the finite-element method*. J. Acoust. Soc. Am. 63(5): 1461–1467.
- Funnell WRJ & Laszlo CA (1982): *A critical review of experimental observations on ear-drum structure and function*, ORL 44(4):181–205.
- Funnell WRJ, Khanna SM & Decraemer WF (1992): *On the degree of rigidity of the manubrium in a finite-element model of the cat eardrum*. J. Acoust. Soc. Am. 91(4): 2082–2090.
- Funnell WRJ, Decraemer WFS, von Unge M & Dirckx JJJ (1999): *Finite-element modelling of the gerbil eardrum and middle ear*. 22nd Midwinter Res. Mtg., Assoc. Res. Otolaryngol., St. Petersburg Beach
- Funnell WRJ, Decraemer WFS, von Unge M & Dirckx JJJ (2000): *Finite-element modelling of the gerbil eardrum and middle ear*. 23rd Midwinter Res. Mtg., Assoc. Res. Otolaryngol., St. Petersburg Beach
- Funnell WRJ, Siah TH, McKee MD, Daniel SJ & Decraemer WF (2005): *On the coupling*

between the incus and the stapes in the cat. JARO 6(1): 9–18.

Goode RL, Ball G & Nishihara S (1993): *Measurement of umbo vibration in human subjects – method and possible clinical applications.* Am J Otol 14(3): 247–251.

Goode RL, Ball G & Nishihara S (1996): *Laser Doppler vibrometer (LDV) – A new clinical tool for the otologist.* Am J Otolaryngol 17: 813–822.

Gray H (2000): *Anatomy of the Human Body*, Philadelphia: Lea & Febiger, 1918; Bartleby.com, 2000. www.bartleby.com/107

Gulya AJ & Schuknecht HF (1995): *Anatomy of the temporal bone with surgical implications.* The Parthenon Publishing Group Inc., 2nd Edition, Pearl River, NY.

Gundersen T & Hogmoen K (1996): *Holographic vibration analysis of the ossicular chain.* Acta Otolaryngol, 82(1-2):16–25.

Gyo K, Arimoto H & Goode RL (1987): *Measurement of the ossicular vibration ratio in human temporal bones by use of a video measurement system.* Acta Otolaryngol, 103: 87–95.

Hagr AA, Funnell WRJ, Zeitouni AG & Rappaport JM (2004): *High-resolution x-ray computed tomographic scanning of the human stapes footplate.* J. Otolaryngol. 33(4): 217–221.

Hariharan P (2007): *Basics of Interferometry*, 2nd Ed. (Academic Press, Sydney)

Helmholtz HFL (1869): *Die Mechanik der Gehörknöchelchen und des Trommelfells*, Pflügers Archiv. Physiol. 1, 1–60. English translations — (1) Bucks AH, & Smith N (transl.) (1873) *The Mechanism of the Ossicles of the Ear and Membrana Tympani* (Woods, New York), 69 pp. (2) Hilton J (transl) (1874). *The Mechanism of the Ossicles and the Membrana*

Tympani, (New Sydenham Society, London), Vol. 62, pp. 97–155.

Helmholtz HLF (1877): *Die Lehre von den Tonempfindungen* (Verlag von Fr. Vieweg u. Sohn, Braunschweig), 4th ed. English translation — Ellis, AJ (transl.) (1885). *Sensations of Tone* (Longmans, Green & Co., London), 2nd ed. Reprinted (1954). (Dover, New York), pp. 134–135.

Henry KR, McGinn MD & Chole RA (1980): *Age-related Auditory Loss in the Mongolian Gerbil*. *Arch Otorhinolaryngol* 228, 233–238.

Henry KR, Chole RA & McGinn MD (1983): *Age-related increase of spontaneous aural cholesteatoma in the Mongolian Gerbil*. *Arch Otolaryngol Head Neck Surg* 109, 19–21.

Henson OW Jr. & Henson MM (2000): *The tympanic membrane: highly developed smooth muscle arrays in the annulus fibrosus of mustached bats*. *JARO*, 1, 25–32.

Henson MM, Rask-Andersen H, Madden VJ & Henson OW (2001a): *The human tympanic membrane: Smooth muscle in the region of the annulus fibrosus*. 24th ARO MidWinter Meeting, St. Petersburg Beach.

Henson OW, Henson MM & Cannon J (2001b): *Comparative study of smooth muscle and collagen fibers in the attachment zone of the tympanic membrane*. 24th ARO MidWinter Meeting, St. Petersburg Beach.

Huber A, Ball G, Asai M & Goode R (1997): *The vibration pattern of the tympanic membrane after placement of a total ossicular replacement prosthesis*. In: Huttenbrink K, ed. *Middle-ear mechanics in research and Otosurgery*. Baalsdorf, Germany: UniMedia GmbH, 82–88.

Huber AM, Schwab C, Linder T, Stoeckli SJ, Ferrazzini M, Dillier N & Fisch U (2001):

Evaluation of eardrum laser Doppler interferometry as a diagnostic tool. Laryngoscope 111: 501–507.

Huber AM, Ma F, Felix H & Linder T (2003): *Stapes Prosthesis Attachment: The effect of crimping on sound transfer in otosclerosis surgery.* Laryngoscope 113: 853–858.

Hüttenbrink KB (1992): *The mechanics and function of the middle ear. Part 1: The ossicular chain and middle ear muscles.* Laryngorhinootologie, 71(11):545-51. (In German)

Khanna SM & Tonndorf J (1972): *Tympanic membrane vibrations in cats studied by time-averaged holography.* J. Acoust. Soc. Am. 51, 1904–1920.

Kohllöffel LUE (1984): *Notes on the comparative mechanics of hearing. III. On Shrapnell's Membrane.* Hearing Research 13: 83–88.

Koike T, Wada H & Kobayashi T (2002): *Modeling of the human middle ear using the finite-element method.* J Acoust Soc Am, 111: 1306–1317.

Kuijpers W, Peters TA & Tonnaer ELGM (1999): *Nature of the tympanic membrane insertion into the tympanic bone of the rat.* Hearing Research, 128: 80–88

Ladak H, Decraemer WF, Dirckx JJ & Funnell WRJ (2004): *Response of the cat eardrum to static pressures: Mobile versus immobile malleus.* J. Acoust. Soc. Am., 116 (5), pp. 3008–3021.

Lay DM (1972): *The Anatomy, Physiology, Functional Significance and Evolution of Specialized Hearing Organs of Gerbilline Rodents.* J. Morph., 138: 41–120.

Legoux JP & Wisner A (1955): *Role fonctionnel des bulles tympaniques geantes de certains*

rongeurs (Meriones). *Acoustica*. 5: 208–216.

Lim DJ (1968): *Tympanic membrane. Electron microscopic observation. Part 1. Pars tensa*. *Acta Otolaryngol*, 66: 181–198.

Lim DJ (1968): *Tympanic membrane. Electron microscopic observation. Part 2. Pars flaccida*. *Acta Otolaryngol*, 66: 515–532.

Lim DJ (1970): *Human tympanic membrane. An ultrastructural observation*. *Acta Otolaryngol*, 70: 176–186.

Lynch TJ, Nedzelnitsky V & Peak WT (1982): *Input impedance of the cochlea in cat*. *J. Acoust. Soc. Am.* 72(1): 108–130.

Lynch TJ, Peake WT & Rosowski JJJ (1994): *Measurements of the acoustic input impedance of cat ears: 10 Hz to 20 kHz*. *J. Acoust. Soc. Am.* 96 (4) 2184–2209.

Masterton B, Heffner H & Rovizza R (1969): *The evolution of Human Hearing*. *J. Acoust. Soc. Am.*, 45, 966–985.

Mateljan I & Ugrinovic K (2003): *The Comparison of Room Impulse Response Measuring Systems*. Proceedings of the First Congress of Alps Adria Acoustics Association, Portorož, Slovenia, ISBN 961-6238-73-6 (pozvano predavanje).

Merchant SN, Ravicz ME & Rosowski JJ (1996): *Acoustic input impedance of the stapes and cochlea in human temporal bones*. *Hearing Research* 97: 30–45

Mikhael CS (2005): *Finite-element modeling of the human middle ear*. Master's thesis, McGill University, Montreal.

- Müller S & Massarani P (2001): *Transfer-function measurement with sweeps*. Journal of the Audio Engineering Society, 2001 June, P.443–5471.
- Nakajima HH, Ravicz ME, Rosowski JJ, Peake WT & Merchant SN (2005): *Experimental and Clinical Studies of Malleus Fixation*. Laryngoscope 115: 147–154.
- Nishihara S & Goode RL (1997): *Measurement of tympanic membrane vibration in 99 human ears*. In: Proceedings of the international workshop on middle-ear mechanics in research and otosurgery, Dresden, Germany, 91–94.
- Oaks E (1967): *Structure and function of inflated middle ears of rodents*. University Microfilms, Inc., Ann Arbor, Michigan.
- Olson ES (1998): *Observing middle and inner ear mechanics with novel intracochlear pressure sensors*. J. Acoust. Soc. Am. 103: 3445–3463.
- Olson E & Cooper N (2000): *Stapes motion and scala vestibuli pressure in gerbil*. 23rd ARO MidWinter Meeting.
- Overstreet EH & Ruggero MA (2002): *Development of a wide-band middle-ear transmission in the Mongolian gerbil*. J Acoust Soc Am, 111 (1): 261–270.
- Overstreet EH, Richter CP, Temchin AN, Cheatham MA & Ruggero MA (2003): *High-frequency sensitivity of the mature gerbil cochlea and its development*. Audiol Neurootol, 8: 19–27.
- Ravicz ME, Rosowski JJ & Voigt HF (1992): *Sound-power collection by the auditory periphery of the Mongolian gerbil Meriones unguiculatus. I: Middle-ear input impedance*. J. Acoust Soc. Am. 92(1) 157–177.

- Ravicz ME & Rosowski JJ (1997): *Sound-power collection by the auditory periphery of the Mongolian gerbil Meriones unguiculatus. III. Effect of variations in middle-ear volume on power collection.* J Acoust Soc Am, 101: 2135–2147.
- Ravicz ME & Rosowski JJ (2004): *High-frequency sound transmission through the gerbil middle ear.* 27th ARO MidWinter Mtg.
- Rosowski JJ, Davis PJ, Merchant SN, Donahue KM & Coltrera MD (1990): *Cadaver middle ears as models for living ears: Comparisons of middle-ear input immittance.* Ann Otol Rhinol Laryngol, 99:403–412.
- Rosowski JJ, Teoh SW & Flandermeyer DT (1997): *The effect of pars flaccida on the sensitivity to sound;* in Lewis ER, Long GR, Lyon RF, Narins PM, Steele CR, Hecht-Poinar E (eds): *Diversity in Auditory Mechanics.* Singapore, World Scientific, pp 129–135.
- Rosowski JJ, Ravicz ME, Teoh SW & Flandermeyer D (1999): *Measurements of middle-ear function in the Mongolian gerbil, a specialized mammalian ear.* Audiol Neurootol 4(3-4): 129–136.
- Rosowski JJ, Brinsko KM, Tempel BI & Kujawa KG (2003a): *The aging of the middle ear in 129S6/SvEvTac and CBA/CAJ mice: measurements of umbo velocity, hearing function, and the incidence of pathology.* JARO 04: 371–383.
- Rosowski JJ, Mehta RP & Merchant SN (2003b): *Diagnostic utility of laser-Doppler vibrometry in conductive hearing loss with normal tympanic membrane,* Otolology & Neurotology, 24:165–175.
- Rosowski JJ, Huber AM, Ravicz ME & Goode RL (2004): *Are temporal bones useful models of human middle-ear mechanics?,* 27th ARO Midwinter Meeting, Daytona Beach, FL, USA.

- Rosowski JJ, Rodgers MT, Ravicz ME & Furlong C (2007): *Preliminary Analyses of Tympanic-Membrane Motion from Holographic Measurements*, 30th ARO Midwinter Meeting, Denver, Colorado, USA.
- Ruggero MA & Temchin AN (2003): *Middle-ear transmission in humans: wide-band, not frequency-tuned?* Acoustic Research Letters Online 4(2): 53–58.
- Ryan A (1976): *Hearing sensitivity of the mongolian gerbil, Meriones unguiculatis*, J. Acoust. Soc. Am., 59 (5): 1222–1226.
- Siah (2002): *Finite-element modelling of the mechanics of the coupling between the incus and the stapes in the middle ear*. Master's Thesis, McGill University, Montreal, Canada.
- Songer JE, Brinsko KM & Rosowski JJ (2004): *Superior semicircular canal dehiscence and bone conduction in chinchilla*. In: K. Gyo, H. Wada, H. Hato and T. Koike, Editors, The Proceedings of the Third International Symposium on Middle Ear Research and Oto-Surgery, World Scientific, Singapore.
- Tonndorf J & Khanna SM (1972): *Tympanic-membrane vibrations in human cadaver ears studied by time-averaged holography*, J. Acoust. Soc. Am., 52: 1221–1233.
- Vander AJ, Sherman JH & Luciano DS (2004): *HUMAN PHYSIOLOGY: The Mechanisms of Body Function*. Ninth Edition (McGraw Hill, Sydney)
- Vlaming MSMG & Feenstra L (1986): *Studies on the mechanics of the normal human middle ear*. Clin Otolaryngol, 11(5):353–363.
- Vogel U, Zahnert T, Hofmann G, Offergeld C & Hüttenbrink KB (1996): *Laser vibrometry of*

the middle ear: opportunities and limitations, in *Middle ear mechanics in research and otosurgery*, edited by K.B. Hüttenbrink (UniMedia GmbH, Dresden), pp. 128–133.

von Unge M, Bagger-Sjöback D & Borg E (1991): *Mechanoacoustic properties of the tympanic membrane: a study on isolated Mongolian gerbil temporal bones*. *Am. J. of Otology*, 12(6) 407–419.

von Unge M, Decraemer WF, Bagger-Sjöback D & Dirckx JJ (1993): *Displacement of the gerbil tympanic membrane under static pressure variations measured with a real-time differential moiré interferometer*. *Hearing Research*, 70, p. 229–242.

von Unge M, Decraemer WF, Dirckx JJ & Bagger-Sjöback D (1995): *Shape and displacement patterns of the gerbil tympanic membrane in experimental otitis media with effusion*. *Hearing Research*, 82: 184–196.

von Unge M, Decraemer WF, Dirckx JJ & Bagger-Sjöback D (1999): *Tympanic membrane displacement patterns in experimental cholesteatoma*. *Hearing Research*, 128(1-2): 1–15.

Voss SE, Rosowski JJ, Merchant SN & Peake WT (2000): *Acoustic responses of the human middle ear*. *Hearing Research* 150: 43–69.

Voss SE, Rosowski JJ, Merchant SN & Peake WT (2001): *Middle-ear function with tympanic-membrane perforations. II. A simple model*. *J. Acoust. Soc. Am.* 110: 1445–1452.

Weber M (1927): *Die Säugetiere*. Vol. 1, p.202. Jena: Fischer 1927

Webster D & Webster M (1972): *Kangaroo rat auditory thresholds before and after middle ear reduction*. *Brain Behav. Evol.*, 5, 41–53.

Wever EG & Lawrence M (1954): *Physiological acoustics*. Princeton University Press,

Princeton, NJ.

Yang X & Henson OW Jr. (2002): *Smooth muscle in the annulus fibrosus of the tympanic membrane: physiological effects on sound transmission in the gerbil*. *Hearing Research* 164: 105–114.

Zimmer WM, Deborah FR & Saunders JC (1994): *Middle-ear development VI: Structural maturation of the rat conducting apparatus*. *Anatomical Record* 239: 475–484

oafccd.com: *Speech and Language Terms and Abbreviations* (Ontario Association for Families of Children with Communication Disorders), Retrieved March 1, 2007
<http://www.oafccd.com/factshee/fact59.htm>

polytec.com: *Polytec Vibrometer University*, Retrieved April 1, 2007
http://www.polytec.com/usa/158_463.asp?highlightSubMenu=Vibrometer%20University

rp-photonics.com: *Encyclopedia of Laser Physics and Technology*, Retrieved June 7, 2007
http://www.rp-photonics.com/laser_safety.html

thfc.ca: *The Hearing Foundation of Canada | Homepage*, Retrieved March 1, 2007
<http://www.thfc.ca/home.asp>

International Electrotechnical Commission (IEC) in Geneva, Switzerland, origin of the international laser safety standards: IEC 60825-1: "*Safety of laser products - Part 1: Equipment classification, requirements and user's guide*."